On the Control Aspects of Semiactive Suspensions for Automobile Applications

by

Emmanuel D. Blanchard

Thesis submitted to the Faculty of the

Virginia Polytechnic Institute and State University

in partial fulfillment of the requirements for the degree of

Master of Science

in

Mechanical Engineering

Approved:

_____
Mehdi Ahmadian, Chairman

_____ _____
Harry H. Robertshaw Donald J. Leo

June 2003
Blacksburg, Virginia

Keywords: Semiactive, Skyhook, Groundhook, Hybrid, Suspensions,

Vehicle Dynamics, H2

On the Control Aspects of Semiactive Suspensions for Automobile Applications

by

Emmanuel D. Blanchard

Mehdi Ahmadian, Chairman

Mechanical Engineering

Abstract

This analytical study evaluates the response characteristics of a two-degree-of freedom quarter-car model, using passive and semi-active dampers, along with a seven-degree-of-freedom full vehicle model. The behaviors of the semi-actively suspended vehicles have been evaluated using skyhook, groundhook, and hybrid control policies, and compared to the behaviors of the passively-suspended vehicles. The relationship between vibration isolation, suspension deflection, and road-holding is studied for the quarter-car model. Three main performance indices are used as a measure of vibration isolation (which can be seen as a comfort index), suspension travel requirements, and road-holding quality. After performing numerical simulations on a seven-degree-of-freedom full vehicle model in order to confirm the general trends found for the quarter-car model, these three indices are minimized using H_2 optimization techniques.

The results of this study indicate that the hybrid control policy yields better comfort than a passive suspension, without reducing the road-holding quality or increasing the suspension displacement for typical passenger cars. The results also indicate that for typical passenger cars, the hybrid control policy results in a better compromise between comfort, road-holding and suspension travel requirements than the skyhook and groundhook control policies. Finally, the numerical simulations performed on a seven-degree-of-freedom full vehicle model indicate that the motion of the quarter-car model is not only a good approximation of the heave motion of a full-vehicle model, but also of the pitch and roll motions since both are very similar to the heave motion.

Acknowledgements

I would like to thank my advisor Dr. Mehdi Ahmadian for his guidance and support throughout my time as a Master's student in the Mechanical Engineering Department, as well as his encouragement. Working at the Advanced Vehicle Dynamics Laboratory was truly a great experience. I would also like to thank Dr. Donald J. Leo and Dr. Harry H. Robertshaw for serving on my graduate committee. I am also thankful to the Mechanical Engineering Department for the financial support of a graduate teaching assistantship. I would also like to thank Ben Poe and Jamie Archual. Working for them was also a great experience.

I would also like to thank all my current labmates, Fernando Goncalves, Jeong-Hoi Koo, Mohammad Elahinia, Michael Seigler, Jesse Norris, Christopher Boggs, Akua Ofori-Boateng, as well as those who have already left Virginia Tech, Paul Patricio, John Gravatt, Walid El-Aouar, Jiong Wang, and Johann Cairou, for their companionship and for their help. Each of them has contributed to this work, at least by making the AVDL such an enjoyable place to work. I am truly grateful for their assistance. I would especially like to thank Fernando for also having been such a great roommate and such a great friend to have, as well as for having helped me so much from the beginning to the end of my time as a Master's student.

I would also like to thank all the friends I have made here at Virginia Tech for their companionship and memories. Finally, I would like to thank my family for their love and support. I would especially like to thank my parents and grandparents for their love, care, and financial support during my time as a student. Their help has made this achievement possible.

Contents

List of Figures

List of Tables

1 Introduction

The purpose of this chapter is to provide the reader with an introduction to the research conducted throughout the course of this study. First, an overview of vehicle suspensions is provided and the motivation for the work is presented. The research objectives and approach to this research are then discussed. Finally, an outline of the remaining chapters is provided.

1.1 Motivation

A typical vehicle suspension consists of a spring and a damper. The role of the spring is to support the static weight of the vehicle. The spring is therefore chosen based on the weight and ride height of the vehicle. The role of the damper is to dissipate energy transmitted to the vehicle system by road surface irregularities. In a conventional passive suspension, both components are fixed at the design stage. The choice of the damper is affected by the classic trade off between vehicle safety and ride comfort. Ride comfort is linked to the amount of energy transmitted through the suspension. Car passengers are especially sensitive to the acceleration of the sprung mass of the car. The safety of a vehicle, as well as the road holding and the stability, is linked to the vertical motion of the tires (wheel hop). A low suspension damping provides good isolation of the sprung mass at the cost of large tire displacements, while a high suspension damping provides poor isolation of the sprung mass but reduced tire displacements. Therefore, a low damping provides good road holding and stability at the cost of little comfort, while a high damping results in good comfort at the cost of poor road holding quality. Luxury cars are usually lightly damped and sports cars are heavily damped.

The need to reduce the effects of this compromise has led to the development of active and semiactive suspensions. Active suspensions use force actuators. Unlike a passive damper, which can only dissipate energy, a force actuator can generate a force in any direction regardless of the relative velocity across it. Using a good control policy, it

can reduce the compromise between comfort and stability. However, the complexity and large power requirements of active suspensions make them too expensive for wide spread commercial use. Semiactive dampers are capable of changing their damping characteristics by using a small amount of external power. Semiactive suspensions are less complex, more reliable, and cheaper than active suspensions. They are becoming more and more popular for commercial vehicles.

1.2 Objectives

This study focuses on two primary objectives. The first is to analytically evaluate various control techniques that can be effectively applied to automobile suspensions. The second objective is to provide a comparison between selected semiactive control techniques and passive suspensions that are commonly used in vehicles. The semiactive techniques include the skyhook, groundhook and hybrid control policies. Performance indices need to be defined in order to evaluate the benefits and the drawbacks of the different control techniques.

1.3 Approach

The first step in accomplishing the objectives of this research was to develop the vehicle models used in this research, along with the passive damping and semiactive damping control models. Two vehicle models are used for this research: a two-degree-of-freedom "quarter-car" model and a seven-degree-of-freedom full car model. The two models use passive representations of the semiactive suspension modeling the ideal skyhook, groundhook, and hybrid configurations. Using a quarter car model provides the opportunity to compute mean square responses to random road disturbances and define performance indices that are simple enough to interpret and optimize after developing the necessary mathematical models. It, therefore, provides a good understanding of how each model parameter affects the behavior of the vehicle. Numerical simulations as well as parametric studies have been performed using the quarter car model. However, the

pitch and the roll responses can only be studied with a full car model. A numerical model has been developed to study the full vehicle ride response to both periodic road inputs and discrete road inputs.

1.4 Outline

Chapter 2 provides the necessary background information to understand skyhook, groundhook, and hybrid semiactive control of suspension systems before describing the actual passive representation of semiactive dampers that will be used in this study. It also contains an introduction to H_2 optimization techniques and a literature search on semiactive suspensions and policies, as well as H_2 optimization techniques. In Chapter 3, the relationship between vibration isolation, suspension deflection, and road holding for both passive and semiactive suspensions is studied based on a quarter car model. The results obtained for the skyhook, the groundhook, and the hybrid semiactive control policies are compared to the results obtained for a passive suspension. In Chapter 4, a numerical model of a full vehicle is used to study the pitch and roll motion of the car for the passive and semiactive configurations. Periodic and discrete road inputs are used. The heave response is also simulated to confirm the general results found for the simplified quarter car model used in Chapter 3. It is shown that working on a simplified quarter-car model gives a good estimation of the behavior of a full-vehicle. Then, Chapter 5 introduces H_2 optimization techniques to optimize the vibration isolation, the suspension deflection, and the road holding for the quarter-car model. Finally, Chapter 6 summarizes the results of the study and provides recommendations for future research.

The main contributions of this research are:

- A parametric study of the relationship between three performance indices for different semiactive configurations applied to the quarter-car model, and a comparison with the results obtained for the passive configuration. These three

performance indices are used as a measure of the vibration level, the rattlespace requirement, and road-holding quality.

- The derivation of closed-form solutions minimizing the three performance indices for a quarter-car model in which all the components except the damper are fixed. It is performed using H_2 optimization techniques.
- A numerical simulation of the full vehicle model's response to periodic heave, pitch, and roll inputs for different semiactive control policies, as well as a comparison with the results obtained for a passive suspension. The cross coupling effects are also computed.
- A numerical simulation of the full vehicle model's response to a discrete road input for different semiactive control policies, as well as a comparison with the results obtained for a passive suspension.

2 Background

The purpose of this chapter is to provide the background for the research conducted in this study. The first part of this chapter will present an overview of vehicle suspensions. The second part of this chapter will introduce the reader to a two-degree-of-freedom (2DOF) quarter-car model and the third part will present three different theoretical semiactive control schemes for the two-degree-of-freedom (2DOF) suspension system. Following this, the passive representation of semiactive dampers that will be used in this study is finally presented. Next, the H_2 optimization technique will be introduced. The chapter will conclude with a literature search on past research done in areas relating to this work.

2.1 Overview of Vehicle Suspensions

The primary suspension of a vehicle connects the axle and wheel assemblies to the frame of the vehicle. Typical vehicle primary suspensions consist of springs and dampers. The role of the springs is to support the static weight of the vehicle. The springs are therefore chosen based on the weight and ride height of the vehicle and the dampers are the only variables remaining to specify. The role of the dampers is to dissipate energy transmitted to the vehicle system by road surface irregularities. Three common types of vehicle suspension damping are passive, active, and semiactive damping. As illustrated on Figure 2.1, automobile suspensions can therefore be divided into three categories: passive, active, and semiactive suspensions.

The characteristics of the dampers used in a passive suspension are fixed. The choice of the damping coefficient is made considering the classic trade off between ride comfort and vehicle stability. A low damping coefficient will result in a more comfortable ride, but will reduce the stability of the vehicle. A vehicle with a lightly damped suspension will not be able to hold the road as well as one with a highly damped suspension. When negotiating sharp turns, it becomes a safety issue. A high damping

coefficient yields a better road holding ability, but also transfers more energy into the vehicle body, which is perceived as uncomfortable by the passengers of the vehicle. As shown on the next part of this chapter with the 2DOF quarter car model, a high damping coefficient results in good resonance control at the expense of high frequency isolation. The vehicle stability is improved, but the lack of isolation at high frequencies will result in a harsher vehicle ride. The need to reduce the effect of this compromise has given rise to new types of vehicle suspensions.

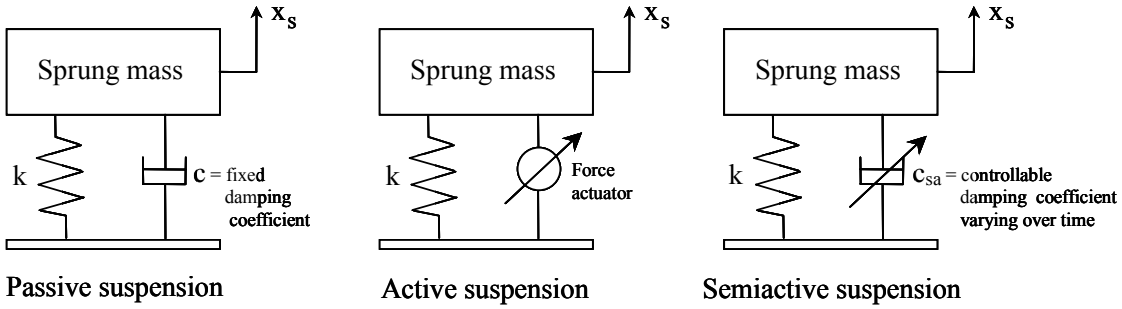

Figure 2.1: Passive, Active, and Semiactive Suspensions

In an active suspension, the damper is replaced by a force actuator. The advantage is that the force actuator can generate a force in any direction, regardless of the relative velocity across it, while a passive damper can only dissipate energy. A good control scheme can result in a much better compromise between ride comfort and vehicle stability compared to passive suspensions [1, 2]. Active suspensions can also easily reduce the pitch and the roll of the vehicle. However, active suspensions have many disadvantages and are too expensive for wide spread commercial use because of their complexity and large power requirements. Also, a failure of the force actuator could make the vehicle very unstable and therefore dangerous to drive.

In semiactive suspensions, the passive dampers are replaced with dampers capable of changing their damping characteristics. These dampers are called semiactive dampers. An external power is supplied to them for purposes of changing the damping level. This damping level is determined by a control algorithm based on the information

the controller receives from the sensors. Unlike for active dampers, the direction of the force exerted by a semiactive damper still depends on the relative velocity across the damper. But the amount of power required for controlling the damping level of a semiactive damper is much less than the amount of power required for the operation of an active suspension. Semiactive suspensions are more expensive than passive suspensions, but much less expensive than active suspensions and are therefore becoming more and more popular for commercial vehicles.

2.2 2DOF Suspension Systems

A typical vehicle primary suspension can be modeled as shown in Figure 2.2. Since the model represents a single suspension from one of the four corners of the vehicle, this 2DOF system is often referred to as the "quarter-car" model.

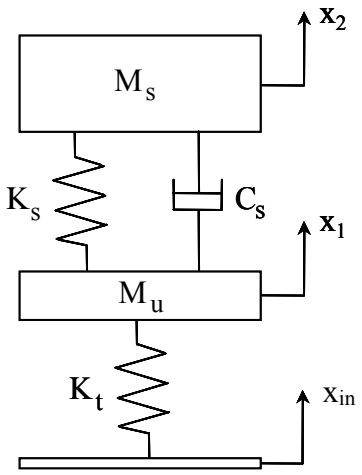

Figure 2.2: 2DOF Quarter-Car Model

The parameters used in the simulation of this model, which represent actual vehicle parameters, are shown in Table 2.1.

Table 2.1: System Parameters

Parameter	Value
Sprung Body Weight (M_S)	950 lbs
Unsprung Body Weight (M_U)	100 lbs
Suspension Stiffness (K_S)	200 lb/in
Tire Stiffness (K_t)	1085 lb/in

The input to this model is a displacement input which is representative of a typical road profile. The input excites the first degree of freedom (the unsprung mass of a quarter of the vehicle, representing the wheel, tire, and some suspension components) through a spring element which represents the tire stiffness. The unsprung mass is connected to the second degree of freedom (the sprung mass, representing the body of the vehicle) through the primary suspension spring and damper. The transmissibility of the 2DOF system, if all the elements of the quarter-car are passive, is shown in Figure 2.3 for various damping coefficients. The first plot shows the displacement of the sprung mass (x_2) with respect to the input (x_{in}), while the second plot shows the displacement of the unsprung mass (x_1) with respect to the input (x_{in}).

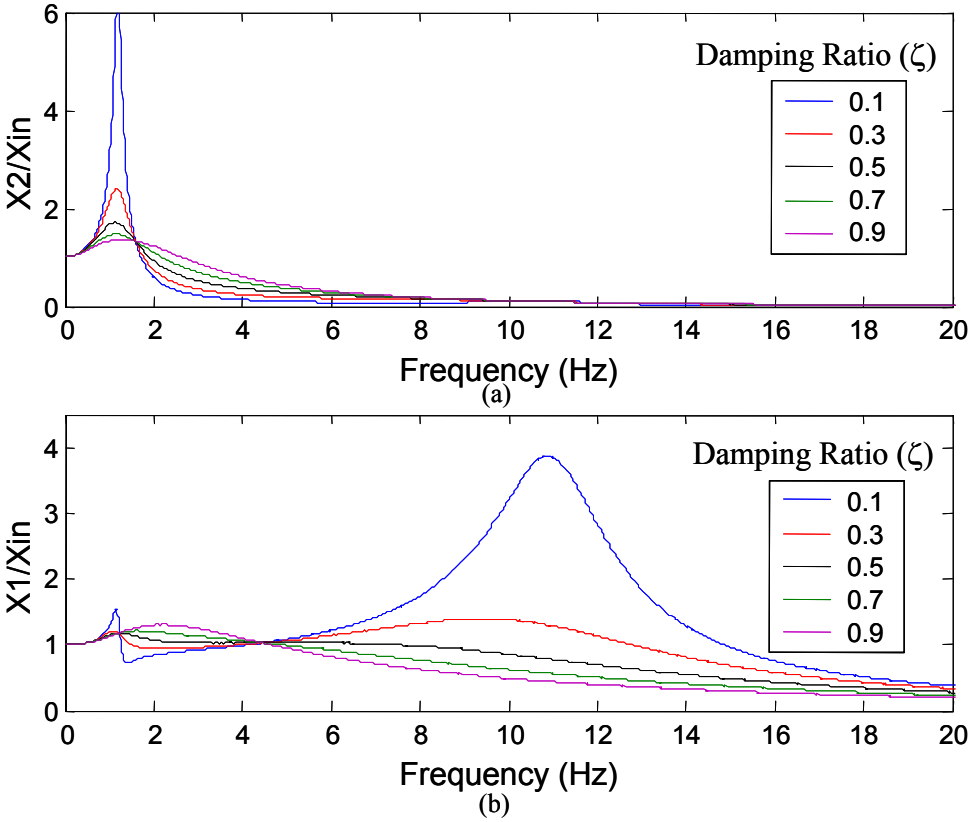

Figure 2.3: Passive Suspension Transmissibility:
(a) Sprung Mass Transmissibility; (b) Unsprung Mass Transmissibility

Notice that at low passive damping, the resonant transmissibility (near $\omega = \omega_{n1}$) or 1.5 Hz and $\omega = \omega_{n2}$ or 10.5Hz) is relatively large, while the transmissibility at higher frequencies is quite low. As the damping is increased, the resonant peaks are attenuated, but isolation is lost both at high frequency and at frequencies between the two natural frequencies of the system. The lack of isolation between the two natural frequencies is caused by the increased coupling of the two degrees of freedom with a stiffer damper. The lack of isolation at higher frequencies will result in a harsher vehicle ride. These transmissibility plots graphically illustrate the inherent tradeoff between resonance control and high frequency isolation that is associated with the design of passive vehicle suspension systems.

The equations of motion for the 2DOF system can be written in matrix form as

$$\begin{bmatrix} M_s & 0 \\ 0 & M_u \end{bmatrix}\begin{Bmatrix} \ddot{x}_2 \\ \ddot{x}_1 \end{Bmatrix}+\begin{bmatrix} C_S & -C_S \\ -C_S & C_S \end{bmatrix}\begin{Bmatrix} \dot{x}_2 \\ \dot{x}_1 \end{Bmatrix}+\begin{bmatrix} K_S & -K_S \\ -K_S & K_S+K_t \end{bmatrix}\begin{Bmatrix} x_2 \\ x_1 \end{Bmatrix}=\begin{bmatrix} 0 \\ K_t \end{bmatrix} x_{in} \tag{2.1}$$

Knowing the physical parameters of the 2DOF system, we can approximate the damping ratio for each mode. In order to make this approximation, we have to assume that the system can be decoupled. We will treat the system as two SDOF systems. In order to present the transmissibility plots as a function of damping ratio rather than damping coefficient, we can decouple the equations of motion by neglecting the off-diagonal terms, and then estimate the damping ratio for each mass as

$$\zeta_S = \frac{C_S}{2\sqrt{K_S M_S}} \tag{2.2}$$

$$\zeta_u = \frac{C_S}{2\sqrt{(K_S + K_t) M_U}} \tag{2.3}$$

While this method of calculating the damping ratio is only valid at low damping, the intent is not to precisely define the damping ratio, but rather to show the effects of increased damping on transmissibility.

2.3 Control Schemes for a 2DOF System

This section will introduce the three 2DOF control schemes of interest in this study. Skyhook, groundhook, and hybrid semiactive control will be presented and compared with a typical 2DOF passive suspension.

2.3.1 Skyhook Control

As the name implies, the skyhook configuration shown in Figure 2.4 has a damper connected to some inertial reference in the sky. With the skyhook configuration [3, 4], the tradeoff between resonance control and high-frequency isolation, common in passive suspensions, is eliminated [5]. Notice that skyhook control focuses on the sprung mass;

as C_{sky} increases, the sprung mass motion decreases. This, of course, comes at a cost. The skyhook configuration excels at isolating the sprung mass from base excitations, at the expense of increased unsprung mass motion.

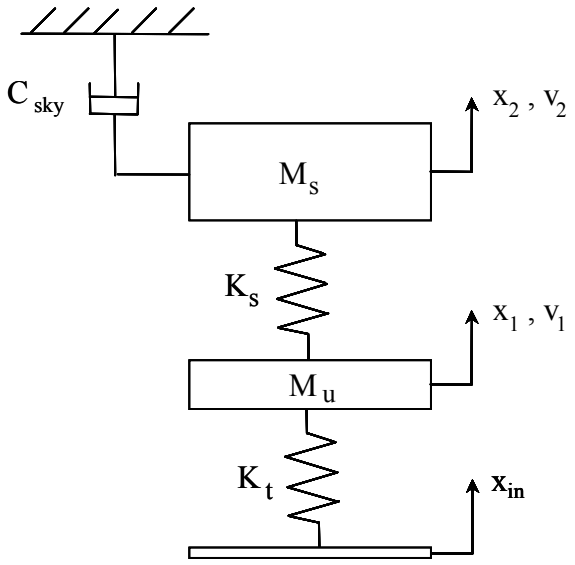

Figure 2.4: Skyhook Damper Configuration

The transmissibility for this system is shown in Figure 2.5 for different values of the skyhook-damping coefficient C_{sky}. Notice that as the skyhook damping ratio increases, the resonant transmissibility near ω_{n1} decreases, even to the point of isolation, but the transmissibility near ω_{n2} increases. In essence, this skyhook configuration is adding more damping to the sprung mass and taking away damping from the unsprung mass. The skyhook configuration is ideal if the primary goal is isolating the sprung mass from base excitations [6], even at the expense of excessive unsprung mass motion. An additional benefit is apparent in the frequency range between the two natural frequencies. With the skyhook configuration, isolation in this region actually increases with increasing C_{sky}.

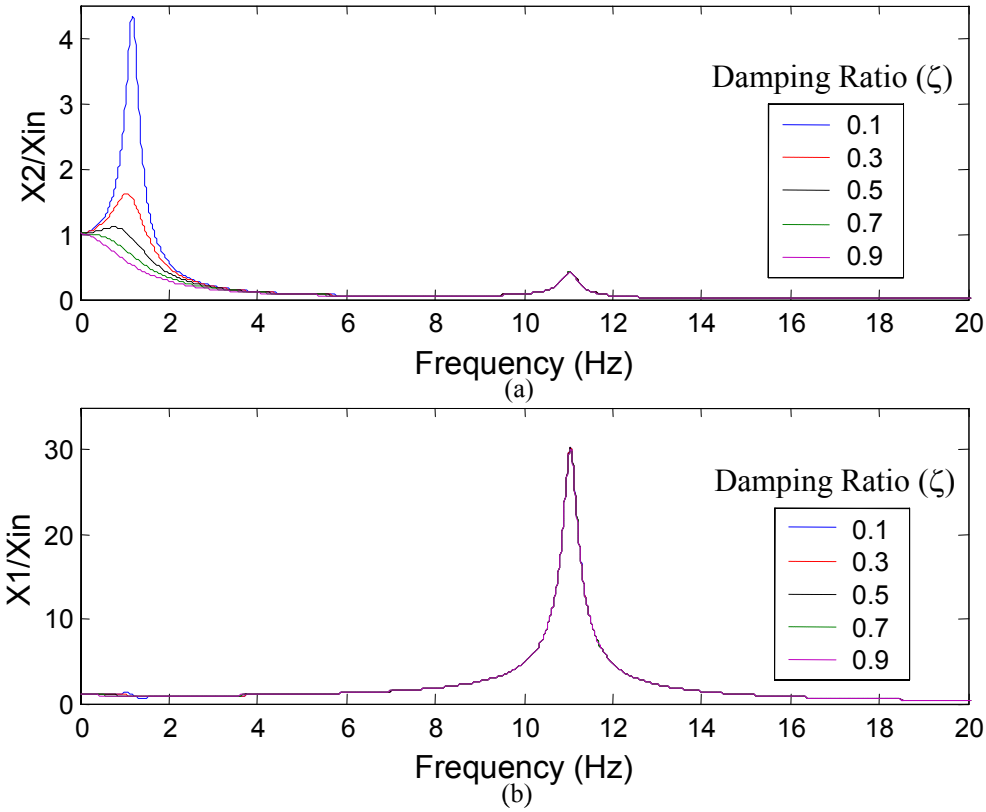

Figure 2.5: Skyhook Configuration Transmissibility:
(a) Sprung Mass Transmissibility; (b) Unsprung Mass Transmissibility

Because this damper configuration is not possible in realistic automotive applications, a controllable damper is often used to achieve a similar response to the system modeled in Figure 2.4. The semiactive damper is commanded such that it acts like a damper connected to an inertial reference in the sky. Figure 2.6 shows the semiactive equivalent model with the use of a semiactive damper.

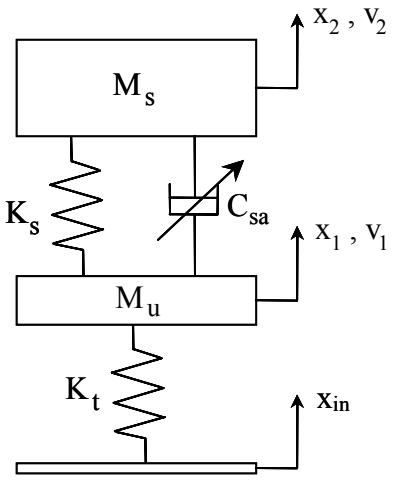

Figure 2.6: Semiactive Equivalent Model

Several methods exist for representing the equivalent skyhook damping force with the configuration shown in Figure 2.6. Perhaps the most comprehensive way to arrive at the equivalent skyhook damping force is to examine the forces on the sprung mass under several conditions. First, let us define certain parameters and conventions that will be used throughout controller development. Referring to Figure 2.6, the relative velocity v_{21} is defined as the velocity of the sprung mass (M_S) relative to the unsprung mass (M_U). When the two masses are separating, v_{21} is positive. For all other cases, up is positive and down is negative.

Now, with these definitions, let us consider the case when the sprung mass is moving upwards and the two masses are separating. Under the ideal skyhook configuration we find that the force due to the skyhook damper is

$$F_{sky} = -C_{sky} v_2 \tag{2.4}$$

where F_{sky} is the skyhook damping force. Next we examine the semiactive equivalent model and find that the damper is in tension and the damping force due to the semiactive damper is

$$F_{sa} = -C_{sa} v_{21} \tag{2.5}$$

where F_{sa} is the semiactive damping force. Now, in order for the semiactive equivalent model to perform like the skyhook model, the damping forces must be equal, or

$$F_{sky} = -C_{sky} v_2 = -C_{sa} v_{21} = F_{sa} \tag{2.6}$$

We can solve for the semiactive damping in terms of the skyhook damping (2.7) and use this to find the semiactive damping force needed to represent skyhook damping when both v_2 and v_{21} are positive (2.8).

$$C_{sa} = \frac{C_{sky} v_2}{v_{21}} \tag{2.7}$$

$$F_{sa} = C_{sky} v_2 \tag{2.8}$$

Next, let us consider the case when both v_2 and v_{21} are negative. Now the sprung mass is moving down and the two masses are coming together. In this scenario, the skyhook damping force would be in the positive direction, or

$$F_{sky} = C_{sky} v_2 \tag{2.9}$$

Likewise, because the semiactive damper is in compression, the force due to the semiactive damper is also positive, or

$$F_{sa} = C_{sa} v_{21} \tag{2.10}$$

Following the same procedure as the first case, equating the damping forces reveals the same semiactive damping force as the first case. Thus, we can conclude that when the product of the two velocities is positive, the semiactive force is defined by equation (2.8).

Now consider the case when the sprung mass is moving upwards and the two masses are coming together. The skyhook damper would again apply a force on the sprung mass in the negative direction. In this case, the semiactive damper is in compression and cannot apply a force in the same direction as the skyhook damper. For this reason, we would want to minimize the damping, thus minimizing the force on the sprung mass.

The final case to consider is the case when the sprung mass is moving downwards and the two masses are separating. Again, under this condition the skyhook damping force and the semiactive damping force are not in the same direction. The skyhook damping force would be in the positive direction, while the semiactive damping force would be in the negative direction. The best that can be achieved is to minimize the damping in the semiactive damper.

Summarizing these four conditions, we arrive at the well-known semiactive skyhook control policy:

$$\begin{Bmatrix} v_2 v_{21} \geq 0 & F_{sa} = C_{sky} v_2 \\ v_2 v_{21} < 0 & F_{sa} = 0 \end{Bmatrix} \tag{2.11}$$

It is worth emphasizing that when the product of the two velocities is positive that the semiactive damping force is proportional to the velocity of the sprung mass. Otherwise, the semiactive damping force is at a minimum. The semiactive skyhook control policy is illustrated and compared to the ideal skyhook configuration in Figure 2.7.

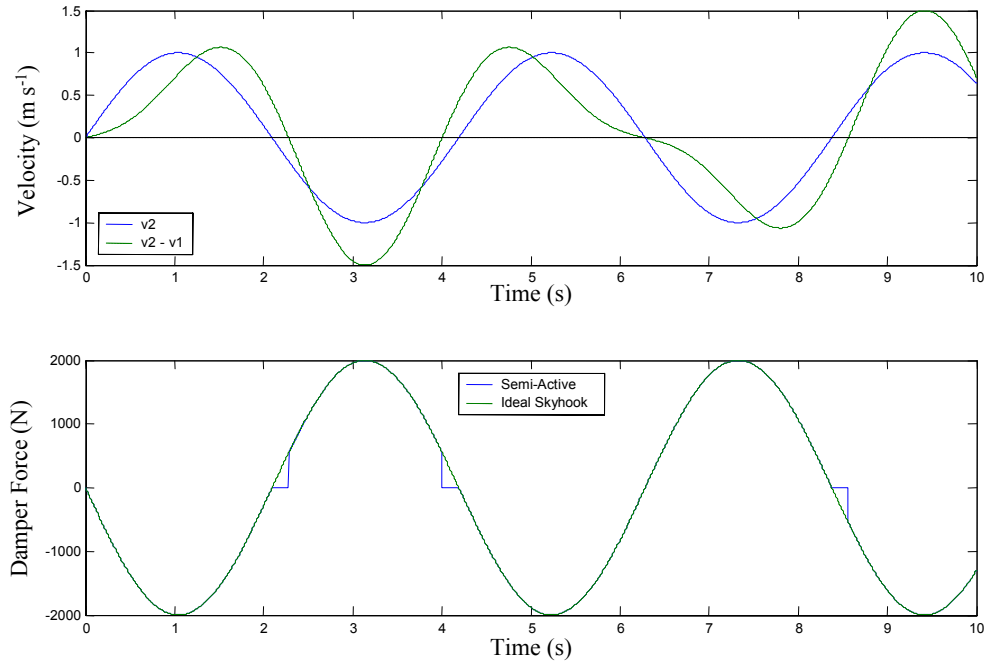

Figure 2.7: Skyhook Control Illustration

2.3.2 Groundhook Control

The groundhook model differs from the skyhook model in that the damper is now connected to the unsprung mass rather than the sprung mass. This modified configuration is shown in Figure 2.8.

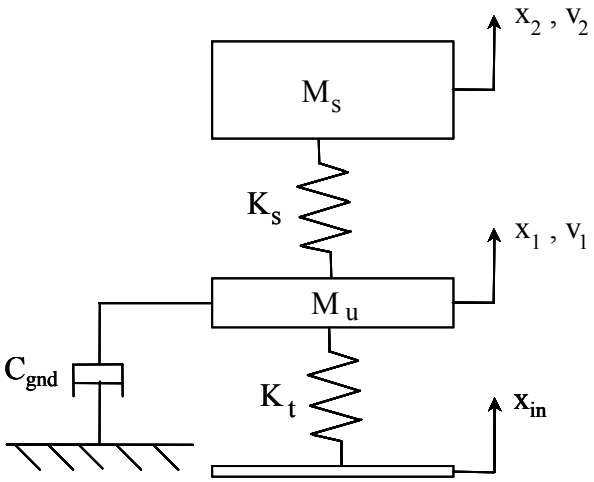

Figure 2.8: Groundhook Damper Configuration

Under the groundhook configuration, the focus shifts from the sprung mass to the unsprung mass. As skyhook control excelled at isolating the sprung mass from base excitations, groundhook control performs just as well at isolating the unsprung mass from base excitations. Again, this performance comes at the cost of excessive sprung mass motion. The groundhook configuration effectively adds damping to the unsprung mass and removes it from the sprung mass as shown in the transmissibility plots in Figure 2.9.

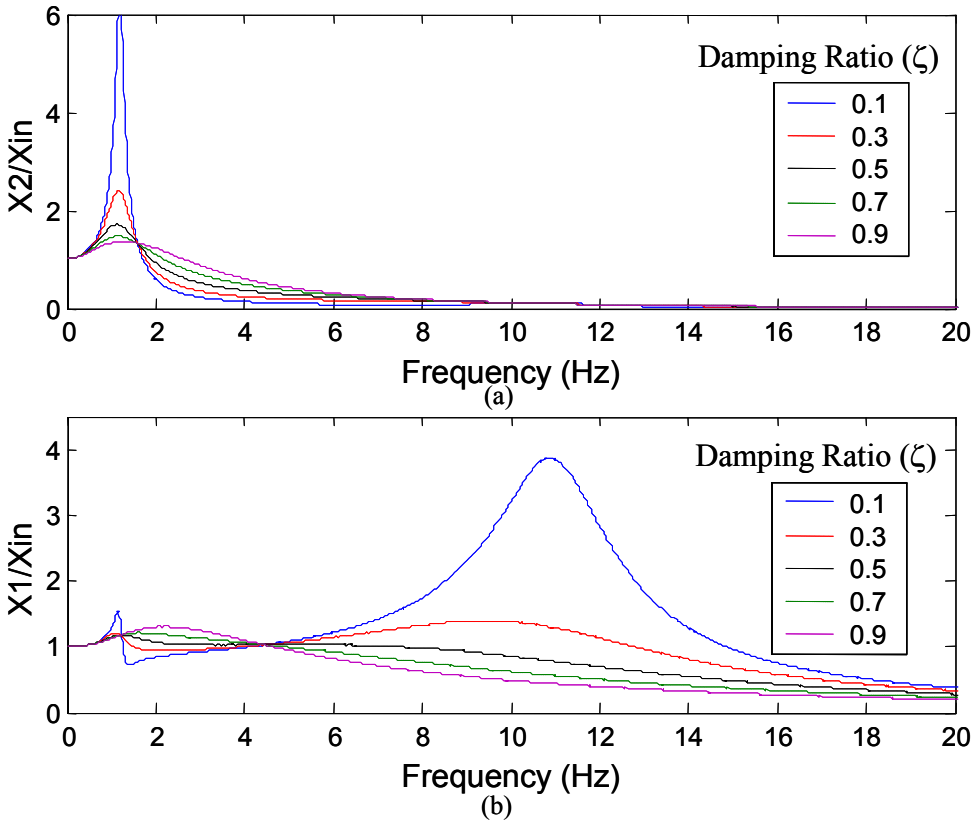

Figure 2.9: Groundhook Configuration Transmissibility:
(a) Sprung Mass Transmissibility; (b) Unsprung Mass Transmissibility

Through the same reasoning used for skyhook control, it can easily be shown that the groundhook semiactive control policy reduces to:

$$\begin{Bmatrix} -v_1 v_{21} \geq 0 & F_{sa} = C_{gnd} v_1 \\ -v_1 v_{21} < 0 & F_{sa} = 0 \end{Bmatrix} \tag{2.12}$$

2.3.3 Hybrid Control

An alternative semiactive control policy known as hybrid control has been shown to take advantage of the benefits of both skyhook and groundhook control [7]. With hybrid control, the user has the ability to specify how closely the controller emulates skyhook or

groundhook. In other words, hybrid control can divert the damping energy to the bodies in a manner that eliminates the compromise that is inherent in passive dampers. The hybrid configuration is shown in Figure 2.10.

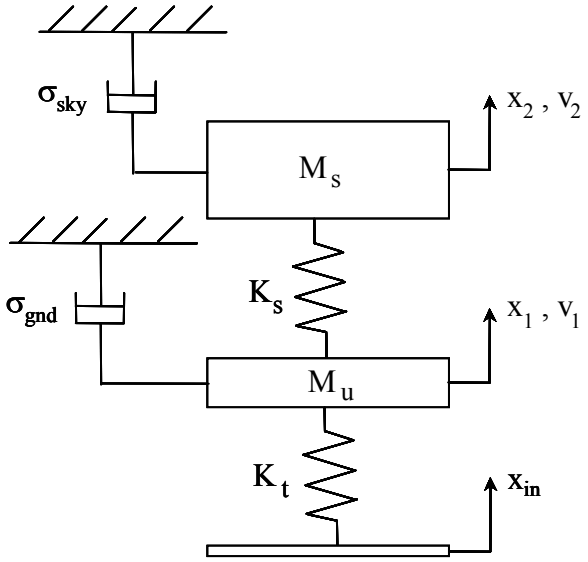

Figure 2.10: Hybrid Configuration

Using hybrid control, the user can specify how closely the controller resembles skyhook or groundhook. Combining the equations (2.11) and (2.12) we arrive at the semiactive hybrid control policy:

$$\begin{Bmatrix} v_2 v_{21} \geq 0 & \sigma_{sky} = v_2 \\ v_2 v_{21} < 0 & \sigma_{sky} = 0 \end{Bmatrix}$$

$$\left\{ F_{sa} = G\left[\alpha\,\sigma_{sky} + (1-\alpha)\sigma_{gnd}\right] \right\} \tag{2.13}$$

$$\begin{Bmatrix} -v_1 v_{21} \geq 0 & \sigma_{gnd} = v_1 \\ -v_1 v_{21} < 0 & \sigma_{gnd} = 0 \end{Bmatrix}$$

where σ_{sky} and σ_{gnd} are the skyhook and groundhook components of the damping force. The variable α is the relative ratio between the skyhook and groundhook control, and G is a constant gain. As the transmissibility plots in Figure 2.11 show, when α is 1, the

control policy reduces to pure skyhook, whereas when α is 0, the control is purely groundhook. These transmissibilities were generated with a damping ratio of 0.3.

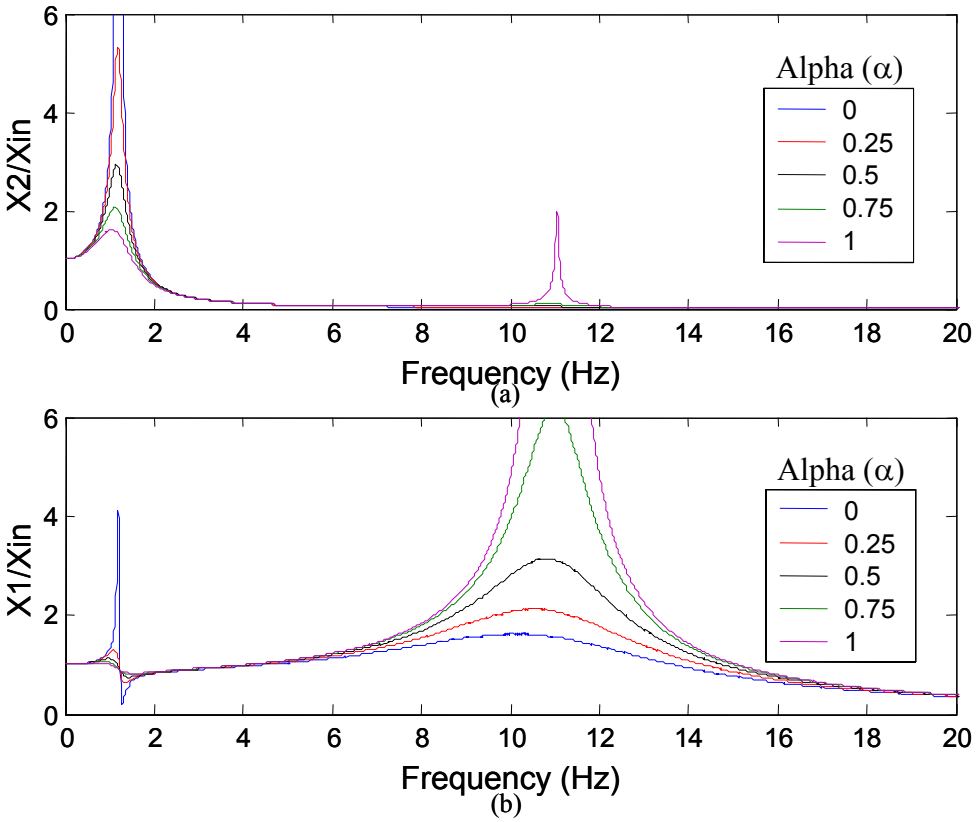

Figure 2.11: Hybrid Configuration Transmissibility:
(a) Sprung Mass Transmissibility; (b) Unsprung Mass Transmissibility

2.3.4 Passive vs. Semiactive Dampers

The previously mentioned benefits of semiactive dampers over passive dampers are clearly evident if we compare the transmissibilities for passive, skyhook, groundhook, and hybrid damping. Figure 2.12 shows the transmissibility of each at a damping ratio of 0.3. The hybrid control transmissibility is shown with an alpha of 0.5.

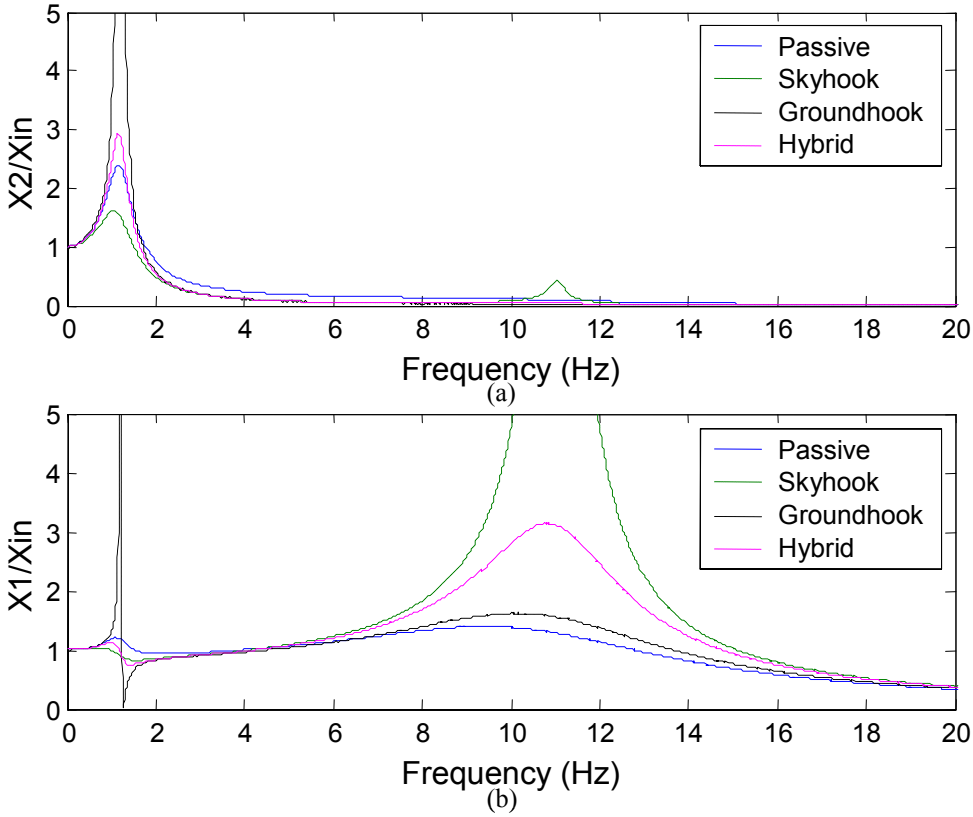

Figure 2.12: Transmissibility Comparison of Passive and Semiactive Dampers: (a) Sprung Mass Transmissibility; (b) Unsprung Mass Transmissibility

2.4 Actual Passive Representation of Semiactive Suspensions

The passive representations of the semiactive suspensions shown in Figures 2.4, 2.8, and 2.10 assume that the damping coefficient C_{sa} of a semiactive suspension (see Figure 2.6) can bet set equal to zero when it is needed for applying the skyhook, groundhook or hybrid control policy. In reality, it is not possible to completely eliminate any amount of damping in the suspension, and it can even be undesirable [8]. Therefore, the passive representation of the semiactive dampers controlled by the hybrid policy appears as shown in Figure 2.13. The off-state damping C_{off} is a small portion of the on-state damping C_{on}. The passive representation of the semiactive dampers controlled by the skyhook policy is obtained by setting α equal to 1, and the passive representation of the

semiactive dampers controlled by the groundhook policy is obtained by setting α equal to 0.

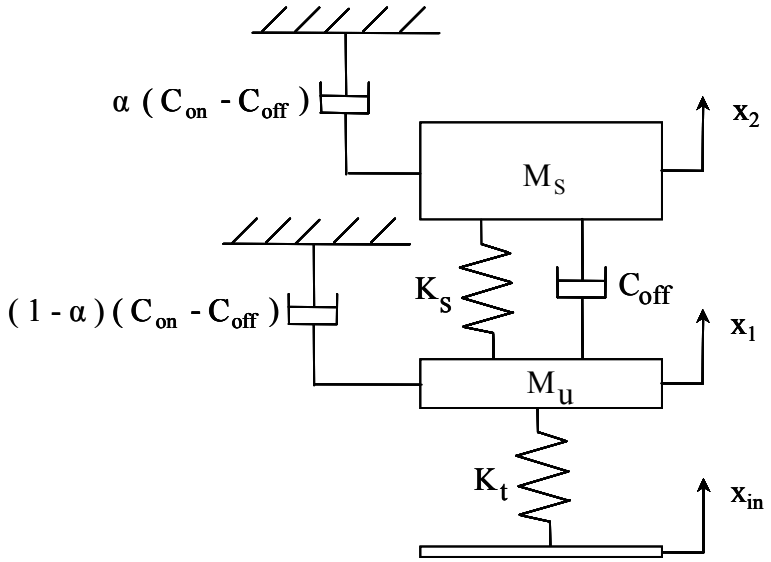

Figure 2.13: Actual Passive Representation of Semiactive Suspension – Hybrid Configuration

2.5 H_2 Optimization Method

The objective of H_2 optimization is to reduce the total vibration energy of the system for overall frequencies [9]. It is achieved by minimizing the H_2 norm of the corresponding transmibility, which is the square root of the area under the frequency response curve for a white-noise input. For instance, if the objective is to minimize the energy transmitted from the road displacement to the sprung mass, the H_2 norm that needs to be minimized is:

$$\sqrt{\int_{-\infty}^{\infty} \left| \frac{x_2}{x_{in}} \right|^2 d\omega} \tag{2.14}$$

H_2 optimization techniques are presented in § 5.2.1. They can be used to minimize other H_2 norms. For instance, since the road profile can be approximated by an integrated

white-noise input [1], the H_2 norm that needs to be minimized is order to reduce the acceleration of the sprung mass (i.e., the acceleration felt by the driver and the passengers) for overall frequencies is:

$$\sqrt{\int_{-\infty}^{\infty} \left| \frac{\ddot{x}_2}{\dot{x}_{in}} \right|^2 d\omega} \tag{2.15}$$

It is equivalent to minimizing $\int_{-\infty}^{\infty} \left| \frac{\ddot{x}_2}{\dot{x}_{in}} \right|^2 d\omega$, which can therefore be used as a comfort index for the driver and the passengers since the human body is mostly affected by acceleration it is subjected to [10].

Two other important indices can be minimized using H_2 optimization techniques as well:

- $\int_{-\infty}^{\infty} \left| \frac{x_2 - x_1}{\dot{x}_{in}} \right|^2 d\omega$, which can used as a measure of the rattlespace requirement
- $\int_{-\infty}^{\infty} \left| \frac{x_1 - x_{in}}{\dot{x}_{in}} \right|^2 d\omega$, which can be used as a measure of the road-holding quality since reducing the deflection of the tire increases the road-holding quality

These performance indices are minimized after assuming fixed values for the sprung mass, the unsprung mass, and the springs. The objective is therefore to find the expressions of the damping coefficients that minimize the performance indices as a function of M_S, M_U, K_S and K_t. Indeed, the dampers are often the only parts of the suspension system one would like to change in order to modify the behavior of the suspension system, because the main role of the springs is to balance the static load of the vehicle. Also, not assuming fixed values for M_S, M_U, K_S and K_t would yield trivial solutions that are not possible to use in real life. For instance, Chapter 5 shows that for a passive suspension:

$$\int_{-\infty}^{\infty} \left| \frac{\ddot{x}_2}{\dot{x}_{in}} \right|^2 d\omega = \pi \frac{(C_S{}^2 K_t + K_S{}^2 (M_S + M_U))}{C_S M_S{}^2} \tag{2.16}$$

Taking both K_S and K_t as small as possible would therefore minimize the performance index associated with comfort. But taking $K_S \approx 0$ or $K_t \approx 0$ is not possible in real life. The role of the springs is to support the static weight of the vehicle; they are therefore chosen based on the weight of the vehicle. A tire with a very low stiffness could never be used either. Fixing only M_S, M_U, K_t, and not K_S would still yield solutions that are not acceptable for real life applications. For instance, (2.16) shows that minimizing the performance index associated with comfort yields $K_S = 0$ and $C_S = 0$. Having a stiffness equal to zero is certainly not a real life solution. Damping coefficients can have a large range of values, but it is not possible to completely eliminate any amount of damping and obtain exactly $C_S = 0$. Assuming fixed values for M_S, M_U, K_S and K_t, minimizing the expression shown in (2.16) yields a non trivial solution: $C_S = K_S \sqrt{\frac{M_S + M_U}{K_t}}$, and is what would be done for real life applications. These performance indices will therefore be optimized by fixing the values of M_S, M_U, K_S and K_t, and then finding the expressions of the damping coefficients minimizing the performance indices as a function of M_S, M_U, K_S and K_t.

2.6 Literature Review

The work shown in this thesis is mainly an extension of [1] and [2] to semi-active suspensions. In the first part of a two-part paper [1], Chalasani uses a two-degree-of-freedom quarter car model to study the relationship between ride comfort, suspension travel, and road holding for random road inputs. His work involves passive suspensions and active suspensions based on linear-full-state feedback control laws. It is shown that an active suspension can result in a reduction of the rms acceleration of the sprung mass, i.e., a more comfortable ride, for approximately the same level of suspension travel and

tire displacement (which is linked to road holding). In [2], an active suspension is designed as a full-state, optimal, linear regulator, using a seven-degree-of-freedom full vehicle model. The comparison with a passive suspension for a seven-degree-of-freedom model yields similar results to the ones obtained with the quarter-car model.

The work of Chalasani has led to an increased interest in active suspensions. Ikenaga *et al.* [11] used similar control loops on a full-vehicle model and blended them with an 'input decoupling transformation' to reduce the motion of the sprung mass.

Studying the relationship between ride comfort, suspension travel, and road holding for semi-active suspensions systems with an approach similar to the one used in [1] and [2] is interesting since active suspensions are too expensive for wide spread commercial use because of their complexity and large power requirements.

Semiactive suspensions results in important improvements, as compared with passive suspensions. Ahmadian [8] shows that for a sufficiently large damping ratio, a semiactive damper can provide isolation at all frequencies, while a passive damper can isolate only isolate at frequencies larger than $\sqrt{2}$ times the natural frequency of the suspension, regardless of the magnitude of damping. His actual passive representation of the semiactive suspension will be used in this thesis. Ahmadian and Pare [12] have conducted an experimental study of three semiactive control policies: skyhook, groundhook and hybrid. Their results indicate that skyhook control can significantly improve the ride comfort and that groundhook control can significantly reduce the wheel hop, and hybrid control can yield a better compromise between vehicle stability and ride comfort. These three on-off control techniques (skyhook, groundhook, hybrid) will be studied analytically in this thesis.

Other semiactive control techniques include fuzzy logic control. Lieh and Li [13] discuss the benefits of an adaptive fuzzy control compared to simple on-off and variable semiactive suspensions. The intent of their work is to apply a fuzzy logic concept to control semiactive damping that is normally nonlinear with stochastic disturbances. A quarter-car model was used to validate their fuzzy control design.

Jalili [14] reviews the theoretical concepts for semiactive control design and implementation.

Finally, the work shown in this research applies H_2 optimization control techniques to vehicle suspensions. The techniques used in this thesis are similar to the techniques used by Asami and Nishihara [9] on dynamic vibration absorbers. The objective of H_2 optimization is to minimize the vibrations for overall frequencies. H_2 optimization is probably more desirable than H_∞ optimization in case of random inputs. The objective of H_∞ optimization is to minimize peak transmibilities.

H_∞ optimization has been used extensively for dynamic vibration absorbers as well as for vehicle suspensions. Asami *et al.* [15] found analytical solutions to the H_∞ and H_2 optimization problems of the Voigt type dynamic vibration absorbers. Jeong *et al.* [16] designed a robust H_∞ controller for semi-active suspension systems. Ohsaku *et al.* [17] designed a damping control system based on nonlinear H_∞ control theory and showed that it results in better ride comfort than a linear H_∞ state feedback controller. Haddad and Razavi [18] have used mixed H_2/H_∞ techniques applied to passive isolators and absorbers.

3 Quarter Car Modeling

The work shown in this chapter is based on a quarter car model. The work of Chalasani [1] for passive and active suspensions is extended to semiactive suspensions using the skyhook, groundhook, and hybrid configurations. The results for the passive case are shown for the purpose of comparison, and the figures dealing with passive suspensions are very similar to the figures in [1]. The objective of this chapter is to study the mean square responses to a white noise velocity input for three motion variables: the vertical acceleration of the sprung mass, the deflection of the suspension, and the deflection of the tire. The three corresponding RMS values can be used respectively as a measure of the vibration level, a measure of the rattlespace requirement, and a measure of the road-holding quality. After deriving the expressions of interest, the relationship between vibration isolation, suspension deflection, and road holding is studied.

3.1 Model Formulation

The model of the quarter-car suspension system used in this analysis is an extension of the passive suspension model used in [1] to semiactive suspensions. As shown in Figure 3.1, the model uses the actual passive representation of the semiactive suspension, as discussed in § 2.4, for the skyhook, groundhook, and hybrid configurations. The model consists of a single sprung mass (M_S) free to move in the vertical direction, connected to an unsprung mass (M_U) free to bounce vertically with respect to the sprung mass. The tire is modeled as a spring of stiffness K_U. The tire damping is small enough to be neglected. The suspension between the sprung mass M_s and the unsprung mass M_U is modeled as a linear spring of stiffness K_S, and a linear damper with a damping coefficient of C_{off}. A linear damper with a damping rate of $\alpha(C_{on} - C_{off})$ connects the sprung mass to some inertial reference in the sky and a linear damper with a damping rate of $(1-\alpha)(C_{on} - C_{off})$, connects the unsprung mass to some inertial reference in the sky.

When α is 1, the control policy reduces to pure skyhook, whereas when α is 0, the control is purely groundhook.

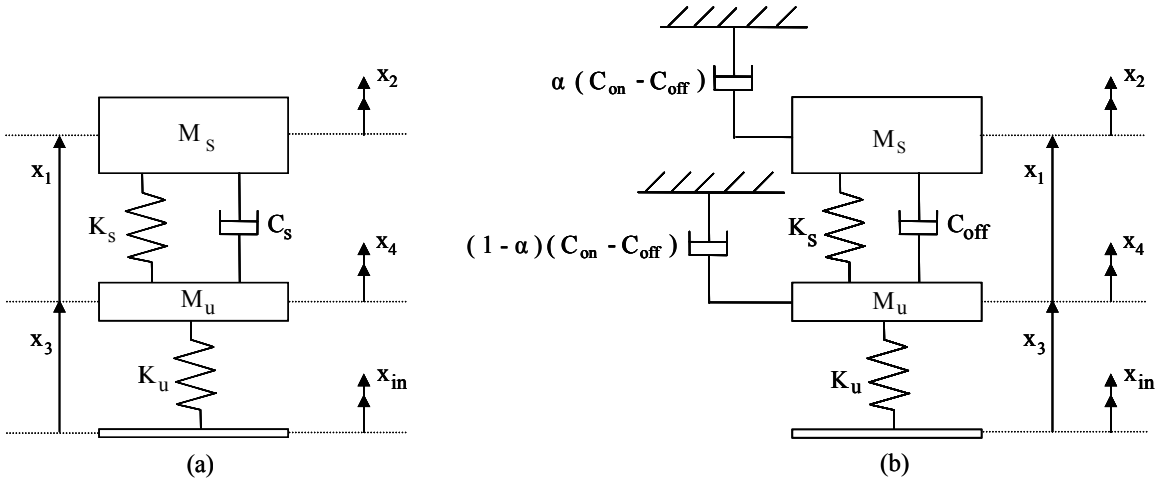

Figure 3.1: Quarter-Car Suspension System: (a) Passive Configuration; (b) Semiactive Configuration

The states of the model are:

- The deflection of the suspension (x_1)
- The velocity of the sprung mass (x_2)
- The deflection of the tire (x_3)
- The velocity of the unsprung mass (x_4)

Road measurements have shown that, the road profile, i.e., the vertical displacement of the road surface, can be reasonably well approximated by an integrated white-noise input, except at very low frequencies [1]. In this analysis, the velocity input $\dot{x}_{in}$ will therefore be modeled as a white noise input.

All the results obtained in [1] for the quarter-car model can be re-derived by taking the results obtained for the semiactive model and replacing C_{off} by C_S and C_{on} by C_S (then $C_{on} - C_{off}$ is replaced by 0).

3.2 Mean Square Responses of Interest

The mean square response of any motion variable *y* can be computed using the relationship

$$E[y^2] = S_0 \int_{-\infty}^{\infty} \left| H_y(\omega) \right|^2 d\omega \tag{3.1}$$

where S_0 is the spectral density of the white-noise input, and $H_y(\omega)$ is the transfer function relating the response variable *y* to the white-noise input [1].

Like in [1], we are interested in the vibration isolation, suspension travel, and road-holding quality. The motion variables of interest in this analysis are: the vertical acceleration of the sprung mass $\dot{x}_2$, the deflection of the suspension x_1, and the deflection of the tire x_3.

The following expressions will therefore be computed:

- $E[\dot{x}_2{}^2] = S_0 \int_{-\infty}^{\infty} \left| H_{\dot{x}_2}(\omega) \right|^2 d\omega$, used as a measure of the vibration level
- $E[x_1{}^2] = S_0 \int_{-\infty}^{\infty} \left| H_{x_1}(\omega) \right|^2 d\omega$, used as a measure of the rattlespace requirement
- $E[x_3{}^2] = S_0 \int_{-\infty}^{\infty} \left| H_{x_3}(\omega) \right|^2 d\omega$, used as a measure of the road-holding quality

The system can be fully described with the 4 state - variable equations of motion below:

$$\dot{x}_1 = x_2 - x_4 \tag{3.2}$$

$$\dot{x}_2 = -\frac{K_S}{M_S}x_1 - \frac{C_{off}}{M_S}(x_2 - x_4) - \frac{\alpha\,(C_{on} - C_{off})}{M_S}x_2 \tag{3.3}$$

$$\dot{x}_3 = x_4 - v_{in} \tag{3.4}$$

$$\dot{x}_4 = \frac{K_S}{M_U}x_1 + \frac{C_{off}}{M_U}(x_2 - x_4) - \frac{K_U}{M_U}x_3 - \frac{(1-\alpha)\,(C_{on} - C_{off})}{M_U}x_4 \tag{3.5}$$

Using a Matrix form, it can be rewritten as:

$$\begin{bmatrix} \dot{x}_1 \\ \dot{x}_2 \\ \dot{x}_3 \\ \dot{x}_4 \end{bmatrix} = \begin{bmatrix} 0 & 1 & 0 & -1 \\ -\frac{K_S}{M_S} & -\frac{C_{off} + \alpha\,(C_{on} - C_{off})}{M_S} & 0 & \frac{C_{off}}{M_S} \\ 0 & 0 & 0 & 1 \\ \frac{K_S}{M_U} & \frac{C_{off}}{M_U} & -\frac{K_U}{M_U} & -\frac{(1-\alpha)\,(C_{on} - C_{off}) + C_{off}}{M_U} \end{bmatrix} \begin{bmatrix} x_1 \\ x_2 \\ x_3 \\ x_4 \end{bmatrix} + \begin{bmatrix} 0 \\ 0 \\ -1 \\ 0 \end{bmatrix} v_{in} \tag{3.6}$$

In the Laplace domain, Equation (3.6) becomes:

$$\begin{bmatrix} s & -1 & 0 & 1 \\ \frac{K_S}{M_S} & s + \frac{C_{off} + \alpha\,(C_{on} - C_{off})}{M_s} & 0 & -\frac{C_{off}}{M_s} \\ 0 & 0 & s & -1 \\ -\frac{K_S}{M_U} & -\frac{C_{off}}{M_U} & \frac{K_U}{M_U} & s + \frac{(1-\alpha)\,(C_{on} - C_{off}) + C_{off}}{M_U} \end{bmatrix} \begin{bmatrix} x_1 \\ x_2 \\ x_3 \\ x_4 \end{bmatrix} = \begin{bmatrix} 0 \\ 0 \\ -1 \\ 0 \end{bmatrix} v_{in} \tag{3.7}$$

The 3 transfer functions $H_{x_1}(s) = \frac{x_1}{v_{in}}(s)$, $H_{\dot{x}_2}(s) = \frac{\dot{x}_2}{v_{in}}(s)$, and $H_{x_3}(s) = \frac{x_3}{v_{in}}(s)$ can be derived from Equation (3.7).

The transfer function for the vertical acceleration of the sprung mass is:

$$H_{\dot{x}_2}(s) = \frac{s\,Ku\,(K_S + C_{off}\,s)}{D_{SA}(s)} \tag{3.8}$$

where $D_{SA}(s) = d_{sa4}\,s^4 + d_{sa3}\,s^3 + d_{sa2}\,s^2 + d_{sa1}\,s + d_{sa0}$

with $d_{sa4} = M_S\,M_U$

$$d_{sa3} = M_S(C_{off} + (1-\alpha)(C_{on} - C_{off})) + M_U\,(C_{off} + \alpha(C_{on} - C_{off}))$$

$$d_{sa2} = K_S\,(M_S + M_U) + K_U\,M_S + C_{off}\,(C_{on} - C_{off}) + \alpha(1-\alpha)(C_{on} - C_{off})^2$$

$$d_{sa1} = K_S\,(C_{on} - C_{off}) + K_U\,(C_{off} + \alpha(C_{on} - C_{off}))$$

$$d_{sa0} = K_S\,K_U$$

The transfer function for the deflection of the suspension is:

$$H_{x_1}(s) = \frac{-K_U\,(M_S\,s + \alpha(C_{on} - C_{off}))}{D_{SA}(s)} \tag{3.9}$$

The transfer function for the deflection of the tire is:

$$H_{x_3}(s) = \frac{-h_{x3}\,s^3 - h_{x2}\,s^2 - h_{x1}\,s - h_{x0}}{D_{SA}(s)} \tag{3.10}$$

where $h_{x3} = M_S\,M_U$

$$h_{x2} = M_S\,(1-\alpha)(C_{on} - C_{off}) + M_U\,\alpha(C_{on} - C_{off}) + C_{off}\,(M_S + M_U)$$

$$h_{x1} = K_S\,(M_S + M_U) + C_{off}\,(C_{on} - C_{off}) + \alpha(1-\alpha)(C_{on} - C_{off})^2$$

$$h_{x0} = (C_{on} - C_{off})\,K_S$$

Replacing s by $j\omega$ in Equations (3.8) through (3.10) yield the transfer functions in the frequency domain.

Using the formula shown in (3.11), the three expressions for the mean square responses of interest can be derived from the three transfer functions shown in Equations (3.8) to (3.10). The formula shown in (3.11) is obtained using the techniques explained in Chapter 5.

$$\int_{-\infty}^{\infty} \left| \frac{a_3 s^3 + a_2 s^2 + a_1 s + a_0}{b_4 s^4 + b_3 s^3 + b_2 s^2 + b_1 s + b_0} \right|^2 ds =$$

$$\int_{-\infty}^{\infty} \left| \frac{-a_3 j\omega^3 - a_2 \omega^2 + a_1 j\omega + a_0}{b_4 \omega^4 - b_3 j\omega^3 - b_2 \omega^2 + b_1 j\omega + b_0} \right|^2 d\omega = \tag{3.11}$$

$$\pi \frac{a_3^2 b_0 (-b_1 b_2 + b_0 b_3) + 2 a_1 a_3 b_0 b_1 b_4}{b_0 b_4 (-b_1 b_2 b_3 + b_0 b_3^2 + b_1^2 b_4)} +$$

$$\pi \frac{b_4(-a_2^2 b_0 b_1 - a_1^2 b_0 b_3 + 2 a_0 a_2 b_0 b_3 - a_0^2 b_2 b_3 + a_0^2 b_1 b_4)}{b_0 b_4 (-b_1 b_2 b_3 + b_0 b_3^2 + b_1^2 b_4)}$$

The three mean square responses of interest can be expressed as:

$$E[\dot{x}_2^2] = f_{12}(M_S, M_U, K_S, K_U, C_{on}, C_{off}, \alpha) \tag{3.12}$$

$$E[x_1^2] = f_{13}(M_S, M_U, K_S, K_U, C_{on}, C_{off}, \alpha) \tag{3.13}$$

$$E[x_3^2] = f_{14}(M_S, M_U, K_S, K_U, C_{on}, C_{off}, \alpha) \tag{3.14}$$

These three expressions are shown in detail in Appendix 1.

Dimensionless parameters can provide better insight into how the three mean square responses are influenced by the vehicle model parameters. The dimensionless parameters

below will therefore be used to illustrate the effects of the parameters on the response of the quarter car.

These parameters are:

- The Mass Ratio: $r_m = \frac{M_U}{M_S}$ (3.15)
- The Stiffness Ratio: $r_k = \frac{K_U}{K_S}$ (3.16)
- The Off-State Damping Ratio of the Sprung Mass: $\zeta_{off} = \frac{C_{off}}{2\sqrt{K_S M_S}}$ (3.17)
- The On-State Damping Ratio of the Sprung Mass: $\zeta_{on} = \frac{C_{on}}{2\sqrt{K_S M_S}}$ (3.18)
- The Natural Frequency of the Unsprung Mass: $\omega_u = \sqrt{\frac{K_U}{M_U}}$ (3.19)

Using the parameters shown above, the dimensionless expressions for the rms vertical acceleration of the sprung mass, the rms deflection of the suspension, and the rms deflection of the tire can be derived and expressed as:

$$\left(\frac{E[\dot{x}_2^{\,2}]}{\pi S_0 \omega_u^{\,3}} \right)^{1/2} = f_{20}(r_m, r_k, \zeta_{off}, \zeta_{on}, \alpha) \tag{3.20}$$

$$\left(\frac{E[x_1^{\,2}]}{\pi S_0} \omega_u \right)^{1/2} = f_{21}(r_m, r_k, \zeta_{off}, \zeta_{on}, \alpha) \tag{3.21}$$

$$\left(\frac{E[x_3^{\,2}]}{\pi S_0} \omega_u \right)^{1/2} = f_{22}(r_m, r_k, \zeta_{off}, \zeta_{on}, \alpha) \tag{3.22}$$

These three expressions are also expressed in detail in Appendix 1.

3.3 Relationship Between Vibration Isolation, Suspension Deflection, and Road-Holding

Plotting the frequency responses of the different transmibilities first will prove to be useful in order to explain the relationship between the mean square responses quantities. Figure 3.2, Figure 3.3, and Figure 3.4 show the effects of varying the damping coefficients on the sprung mass acceleration response, the suspension deflection, and the tire deflection respectively. Each figure shows the effect of the varying the damping coefficients for four configurations: passive, groundhook, hybrid (with $\alpha = 0.5$) and skyhook. The same masses and springs will be used for every configuration. Their numerical values are shown in Table 3.1.

Table 3.1: Model Parameters

Parameter	Value
Sprung Body Weight (M_S)	240 Kg
Unsprung Body Weight (M_u)	36Kg
Suspension Stiffness (K_S)	16000 N / m
Tire Stiffness (K_U)	160000 N / m

The sprung mass natural frequency is $\omega_S = \sqrt{\frac{K_S}{M_S}} = 8.165 \text{ rad/s}$ (or 1.3 Hz)

The unsprung mass natural frequency is $\omega_u = \sqrt{\frac{K_U}{M_U}} = 66.666 \text{ rad/s}$ (or 10.6 Hz)

No damping values are shown in Table 3.1 because the passive configuration involves a different suspension system than the groundhook, hybrid, and skyhook configurations. Also, several damping level will be used for each configuration.

For the passive case, the three figures will each be obtained for three different values of damping:

- $C_S = 196\ \mathrm{N \cdot s/m}$: the corresponding damping ratio is $\zeta_S = 0.050$, which means the suspension is lightly damped
- $C_S = 980\ \mathrm{N \cdot s/m}$: the corresponding damping ratio is $\zeta_S = 0.250$, which is a typical value for passenger cars
- $C_S = 3920\ \mathrm{N \cdot s/m}$: the corresponding ratio is $\zeta_S = 1.000$, which means the suspension is heavily damped

Typical semiactive damping coefficients are chosen using the two relationships $C_{on} = 2.2\,C_S$ and $C_{off} = 0.2\,C_S$. These relationships also yield $(C_{on} - C_{off}) = 2\,C_S$.

For the groundhook, hybrid, and skyhook configurations, the pairs of damping coefficients used for plotting the frequency responses will therefore be:

- $C_{on} = 431.2\ \mathrm{N \cdot s/m}$, $C_{off} = 39.2\ \mathrm{N \cdot s/m}$ (i.e., $\zeta_{on} = 0.110$ and $\zeta_{off} = 0.010$)
- $C_{on} = 2156\ \mathrm{N \cdot s/m}$, $C_{off} = 196\ \mathrm{N \cdot s/m}$ (i.e., $\zeta_{on} = 0.550$ and $\zeta_{off} = 0.050$)
- $C_{on} = 8624\ \mathrm{N \cdot s/m}$, $C_{off} = 784\ \mathrm{N \cdot s/m}$ (i.e., $\zeta_{on} = 2.200$ and $\zeta_{off} = 0.200$)

Having $\zeta_S = 0.050$ for the passive suspension or $(\zeta_{on}, \zeta_{off}) = (0.110, 0.010)$ for the semiactive suspension will correspond to the curves or to the points denoted as 'A' in this chapter. Similarly, 'B' will denote either $\zeta_S = 0.250$ or $(\zeta_{on}, \zeta_{off}) = (0.550, 0.050)$ and 'C' will denote either $\zeta_S = 1.000$ or $(\zeta_{on}, \zeta_{off}) = (2.200, 0.200)$.

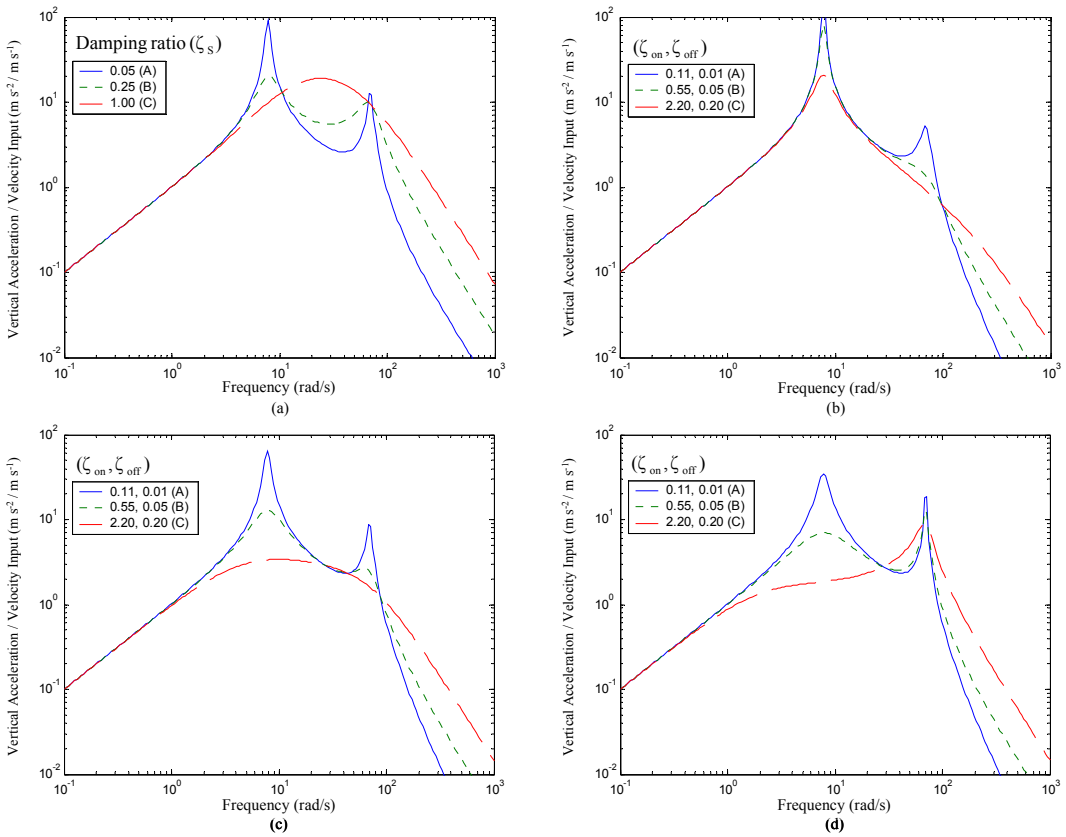

Figure 3.2: Effect of Damping on the Vertical Acceleration Response: (a) Passive; (b) Groundhook; (c) Hybrid; (d) Skyhook

Figure 3.2 shows that increasing the damping reduces the value of the vertical acceleration at the sprung mass natural frequency ω_s, which is the peak value for every configuration (passive, groundhook, hybrid and skyhook) unless the damping is too high. It also reduces the value of the vertical acceleration at the unsprung mass natural frequency ω_u. However, the area under the curve does not necessarily decrease with a reduced peak value of the acceleration. It means that the measure of the vibration level $E[\dot{x}_2^2]$ cannot be deducted from the peak value of the acceleration. It can be noted that the skyhook configuration is the one that needs to be chosen in order to minimize the vertical acceleration at the sprung mass natural frequency. However, the skyhook control policy may not be the best one for minimizing $E[\dot{x}_2^2]$.

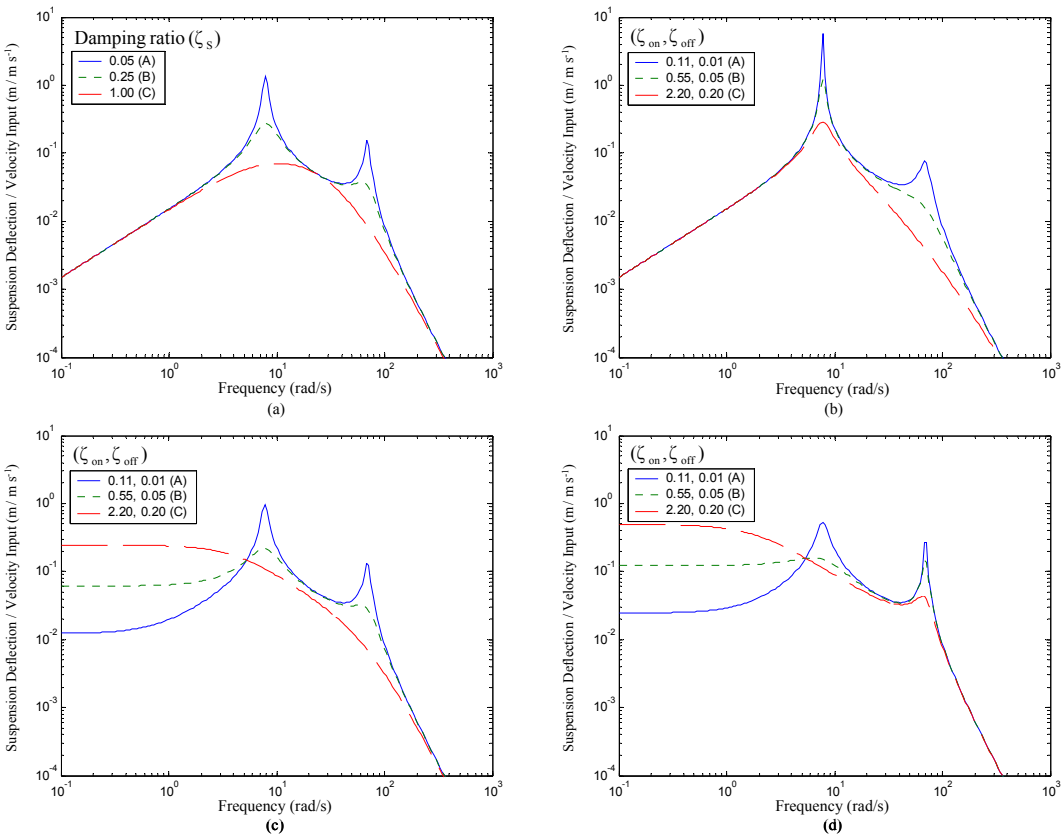

Figure 3.3: Effect of Damping on Suspension Deflection Response: (a) Passive; (b) Groundhook; (c) Hybrid; (d) Skyhook

Figure 3.3 shows that increasing the damping reduces the value of the suspension displacement at the sprung mass natural frequency ω_S, which is the peak value for every configuration (passive, groundhook, hybrid and skyhook) unless the damping is too high. It also reduces the value of the suspension displacement at the unsprung mass natural frequency ω_u. However, the area under the curve does not necessarily decrease with a reduced peak value of the suspension displacement for the skyhook and the hybrid configuration. It means that the measure of the rattlespace requirement $E[x_1^2]$ cannot be deducted from the peak value of the suspension displacement. It can be noted that the skyhook configuration is the one that needs to be chosen in order to minimize the suspension displacement at the sprung mass natural frequency. However, the skyhook control policy may not be the best one for minimizing $E[x_1^2]$.

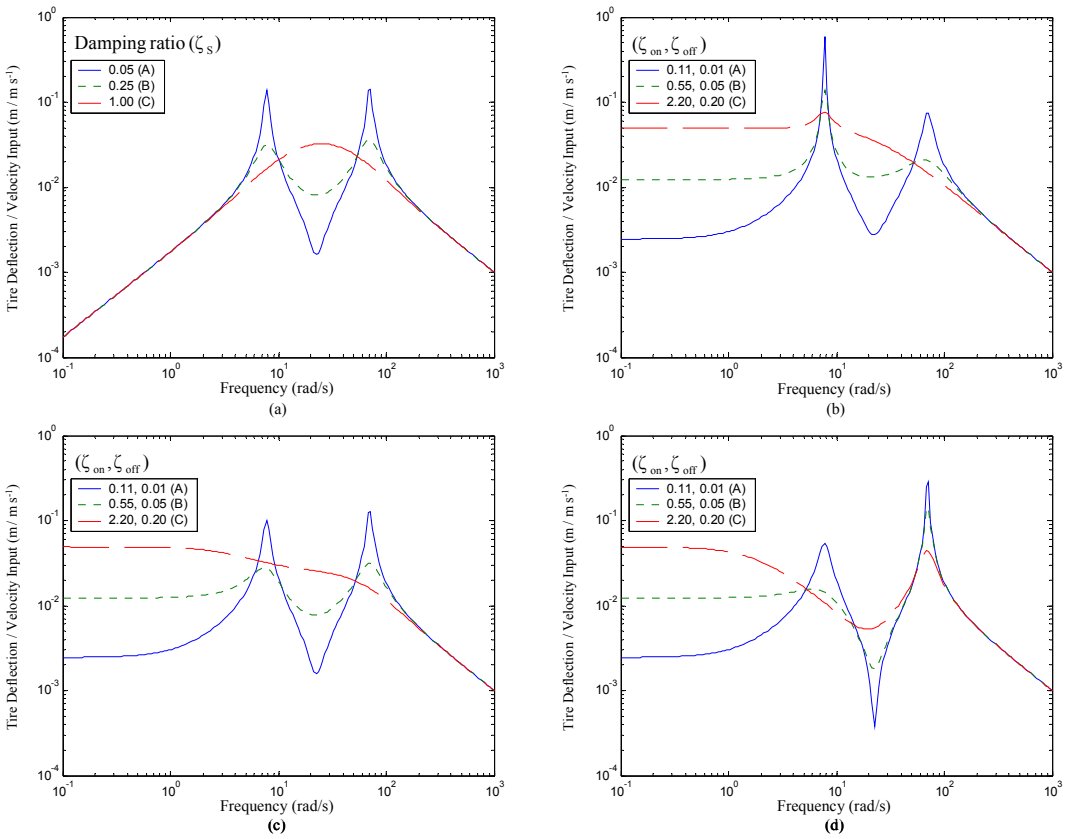

Figure 3.4: Effect of Damping on Tire Deflection Response: (a) Passive; (b) Groundhook; (c) Hybrid; (d) Skyhook

Figure 3.4 shows that increasing the damping reduces the value of the tire displacement at the sprung mass natural frequency ω_S, which is the peak value for every configuration (passive, groundhook, hybrid and skyhook) unless the damping is too high. It also reduces the value of the tire displacement at the unsprung mass natural frequency ω_u. However, the area under the curve does not necessarily decrease with a reduced peak value of the tire displacement. It means that the measure of the road-holding quality $E[x_3^2]$ cannot be deducted from the peak value of the tire displacement. It can be noted that the skyhook configuration is the one that needs to be chosen in order to minimize the tire displacement at the sprung mass natural frequency. However, the skyhook control policy may not be the best one for minimizing $E[x_3^2]$.

Figure 3.5 shows the influence of the damping and the suspension's stiffness on the relationship between vibration isolation and suspension travel, using the dimensionless expressions shown in Equations (3.20) and (3.21), which are shown in detail in Appendix 1. The vehicle is supposed to travel at a constant speed on a random road surface.

The mass ratio is chosen to be $r_m = 0.15$ so that it matches the model parameters of Table 3.1. The variables are the stiffness ratio r_k (for both passive and semiactive suspensions) and the damping ratio of the sprung mass ζ_S for the passive configuration. For the semiactive suspensions, ζ_S is replaced by the pair $(\zeta_{off}, \zeta_{on})$ using the relationship $(\zeta_{off}, \zeta_{on}) = (0.2\ \zeta_S,\ 2.2\ \zeta_S)$. The stiffness ratios will be ranging from $r_k = 5$ to $r_k = 20$. A stiffness ratio of 5 corresponds to a softly sprung car and a smaller stiffness ratio would raise serious safety issues. A stiffness ratio of 20 corresponds to a stiffly sprung sports car. Figure 3.5 draws one curve per stiffness ratio. For each curve, the damping ratio ζ_S will be ranging from 0.05 to 1 for the passive configuration, which means that the pair $(\zeta_{off}, \zeta_{on})$ will be ranging from (0.010, 0.110) to (0.200, 2.200) for the semiactive configurations. The figures of § 5.4 will plot results with independent values of ζ_{off} and ζ_{on} for $r_k = 10$.

The points A, B, and C in Figure 3.5 are obtained for a stiffness ratio $r_k = 10$ with respectively $\zeta_S = 0.250$, $\zeta_S = 0.050$, and $\zeta_S = 1.000$ for the passive configuration, and with $(\zeta_{off}, \zeta_{on}) = (0.010, 0.110)$, $(0.050, 0.550)$, $(0.200, 2.200)$ respectively for the semiactive configurations. The points A, B, and C can therefore be related to curves of Figures 3.2, 3.3, and 3.4. For those three figures, the curves using the low damping correspond to A, the curves using the middle damping correspond to B, and curves using the high damping correspond to C.

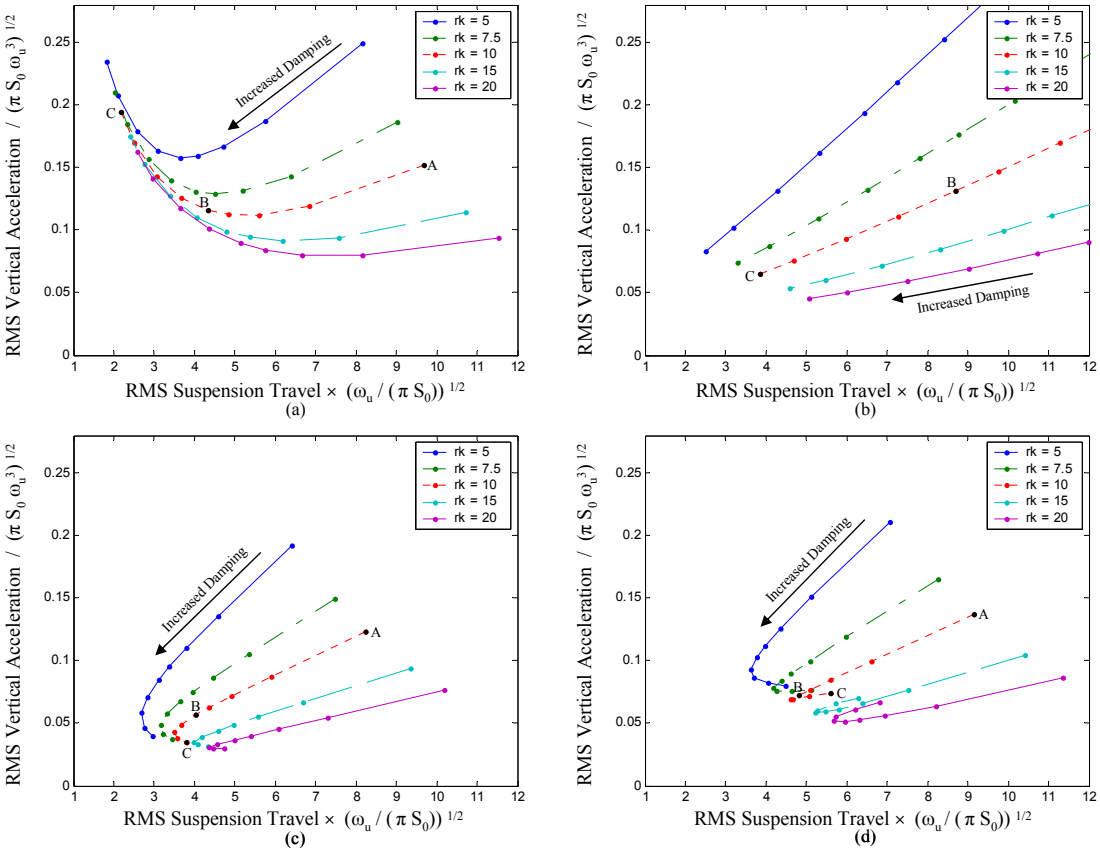

Figure 3.5: Relationship Between RMS Acceleration and RMS Suspension Travel (Mass Ratio 0.15): (a) Passive; (b) Groundhook; (c) Hybrid; (d) Skyhook

Figure 3.5 shows that for the passive suspension, increasing the damping from a low value (A for $r_k = 10$) to a midrange value (B for $r_k = 10$) results in both a lower rms suspension deflection and in a lower rms vertical acceleration. Increasing the damping even more until a high value is reached (C for $r_k = 10$) results in a lower rms suspension deflection, but in a higher rms vertical acceleration.

The influence of the damping on the rms suspension travel can be better understood by looking at Figure 3.2, which displays the frequency response for the vertical acceleration for $r_k = 10$ and three damping ratios corresponding to A, B, and C. For the passive configuration, increasing the damping reduces the suspension displacement at frequencies

close to ω_S and ω_u, and does not increase it at any frequency. The rms suspension travel is therefore always reduced when damping increases. The influence of the damping on the rms vertical acceleration can be better understood by looking at Figure 3.2, which displays the frequency response of the vertical acceleration for $r_k = 10$ and three damping ratios corresponding to A, B, and C. For the passive configuration, increasing the damping reduces the acceleration near ω_S. For a high damping ratio (C), there is no resonance anymore around the sprung mass natural frequency, but this reduction of the acceleration around ω_S is more than compensated by an increase at higher frequencies. An optimal damping ratio minimizing the rms acceleration can therefore be associated with any given suspension stiffness.

For a semiactive suspension, Figure 3.5 shows that increasing the damping always results in a lower rms vertical acceleration for the groundhook and hybrid configurations. For the skyhook configuration, increasing the damping always results in a lower rms vertical acceleration for lightly sprung suspensions, but for stiffly sprung suspensions, increasing the damping when the damping ratio is already high results in a higher rms vertical acceleration. Figure 3.5 also shows that increasing the damping always results in a lower rms suspension deflection for the groundhook configuration. For the skyhook and the hybrid configurations, increasing the damping from low values to midrange values results in a lower rms suspension deflection. As damping values gets high, this trend is reversed for the for the skyhook configuration, and then for the hybrid configuration as the damping gets even higher. Figure 3.2 and Figure 3.3 provide a better understanding of these effects for $r_k = 10$. An optimal damping ratio minimizing the rms suspension travel can therefore be associated with any given suspension stiffness for the hybrid configuration and the skyhook configuration.

It can be noted that the groundhook configuration is the one that always results in both a lower rms vertical acceleration of the sprung mass and a lower rms suspension displacement when the damping is increased. However, the rms vertical acceleration and

suspension displacement that result from a lightly damped suspension can be high. The hybrid configuration is the one that yields the best results for most of the stiffness and damping ratios when the objective is to minimize the rms vertical acceleration and the rms suspension displacement at the same time. Referring to Figure 3.5, it yields points on the bottom left hand corner. In this regard, skyhook control can be ranked as the second "best", among our control policies.

Figure 3.6 shows the relationship between the rms vertical acceleration and the rms tire deflection.

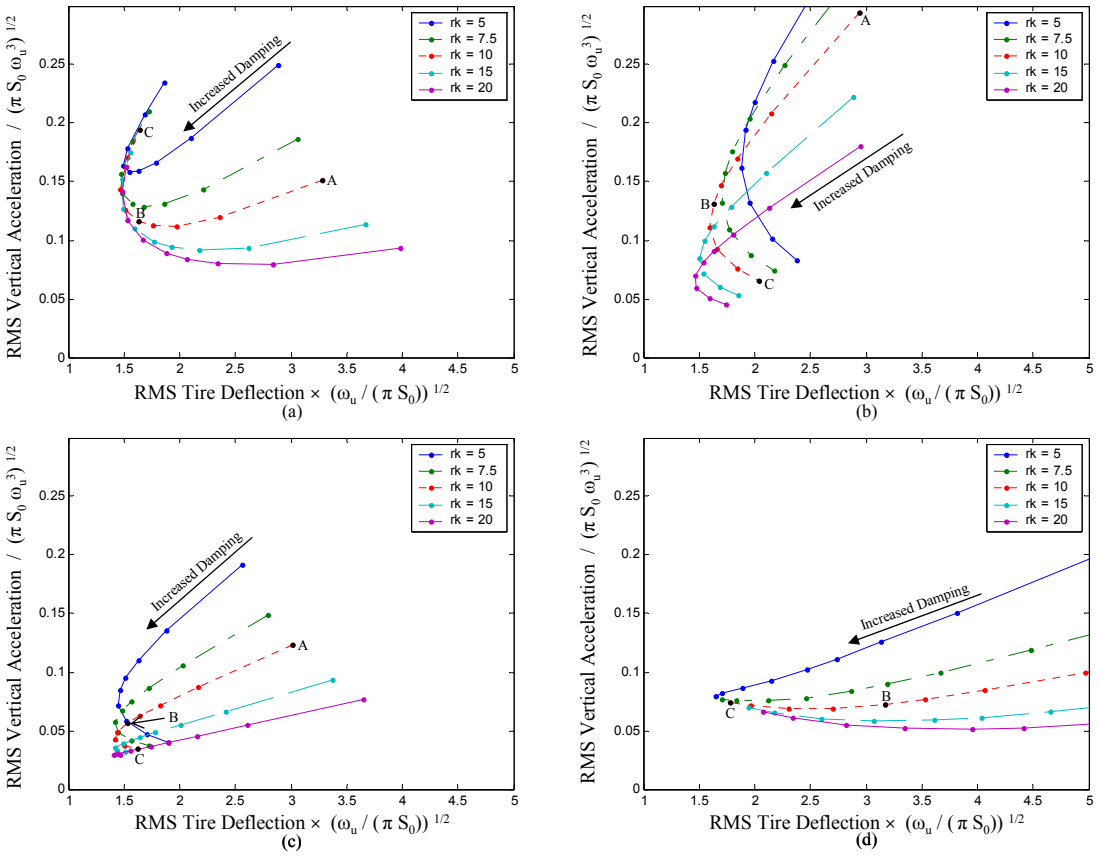

Figure 3.6: Relationship Between RMS Acceleration and RMS Tire Deflection (Mass Ratio 0.15): (a) Passive; (b) Groundhook; (c) Hybrid; (d) Skyhook

What was noted concerning the vertical acceleration can still be deducted from this Figure 3.6. For instance, it shows that for a semiactive suspension, the rms vertical acceleration is reduced when damping is increased, except at high damping levels for stiffly sprung cars using the skyhook control policy. The influence of damping on the rms tire deflection for the skyhook configuration is simple: increasing the damping decreases the rms tire deflection. The influence of damping on the rms tire deflection follows a similar pattern for the passive, groundhook and hybrid configurations. Increasing damping results in a lower rms tire deflection until a certain value is reached; then the rms tire deflection increases with the damping. These effects can be better explained by looking at Figure 3.4, which shows the frequency response of the vertical acceleration for $r_k = 10$. When damping is increased, the peaks at the sprung mass natural frequency ω_S and at the unsprung mass natural frequency ω_u are reduced. However, when damping is increased too much, it is more than compensated by the increase in tire deflection at low frequencies for the groundhook and hybrid configuration, and by the increase in tire deflection between ω_S and ω_u for the passive case. An optimal damping ratio minimizing the rms tire displacement can therefore be associated with any given suspension stiffness for the passive, hybrid, and groundhook configurations.

Figure 3.6 shows that the hybrid configuration is the one that yields the best results for most of the stiffness and damping ratios when the objective is to minimize both the rms acceleration and rms tire deflection at the same time. The groundhook and the skyhook policies would not be used for high damping ratios: the groundhook configuration yields very high accelerations, and the skyhook configuration yields very high tire deflections. Using the hybrid configuration will therefore result in a better compromise between comfort and road holding quality.

Figure 3.7 shows the relationship between the rms tire deflection and the rms suspension travel.

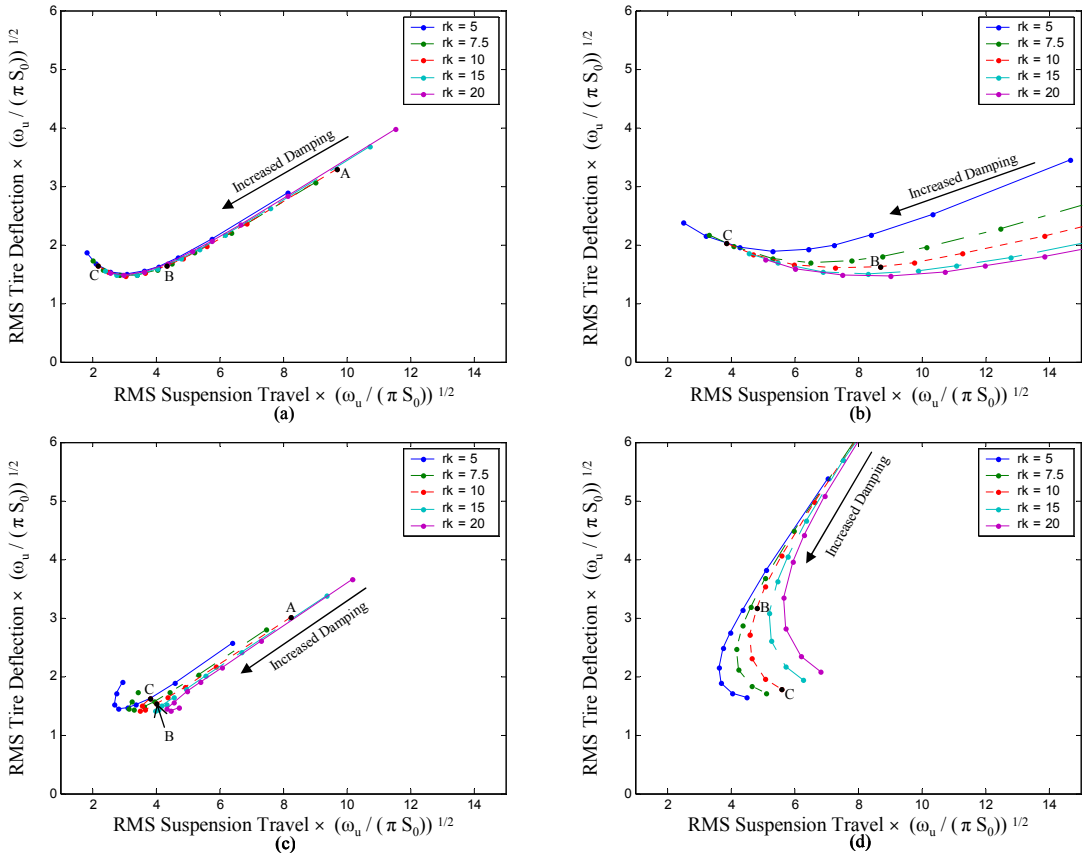

Figure 3.7: Relationship Between RMS Tire Deflection and RMS Suspension Travel (Mass Ratio 0.15): (a) Passive; (b) Groundhook; (c) Hybrid; (d) Skyhook

The influence of damping on the rms tire deflection and the rms suspension travel have already been described separately. Figure 3.7 confirms the trends already observed, and also show that relationship between rms tire deflection and rms suspension travel is not affected much by the stiffness ratio. Figure 3.7 also shows that the hybrid configuration is the one that yields the best results for most of the stiffness and damping ratios when the objective is to minimize both the rms tire deflection and rms suspension travel at the same time.

3.4 Performance of Semiactive Suspensions

Figures 3.5-3.7 show that the hybrid configuration clearly yields better results than skyhook and groundhook configurations when the objective is to minimize the rms vertical acceleration of the sprung mass, the rms tire deflection, and the rms suspension travel at the same time. Figure 3.8 compares the results obtained for hybrid semiactive suspension with the results obtained for passive suspension, for the stiffness ratio $r_k = 10$, which is a typical value for passenger cars. The mass ratio is still $r_m = 0.15$.

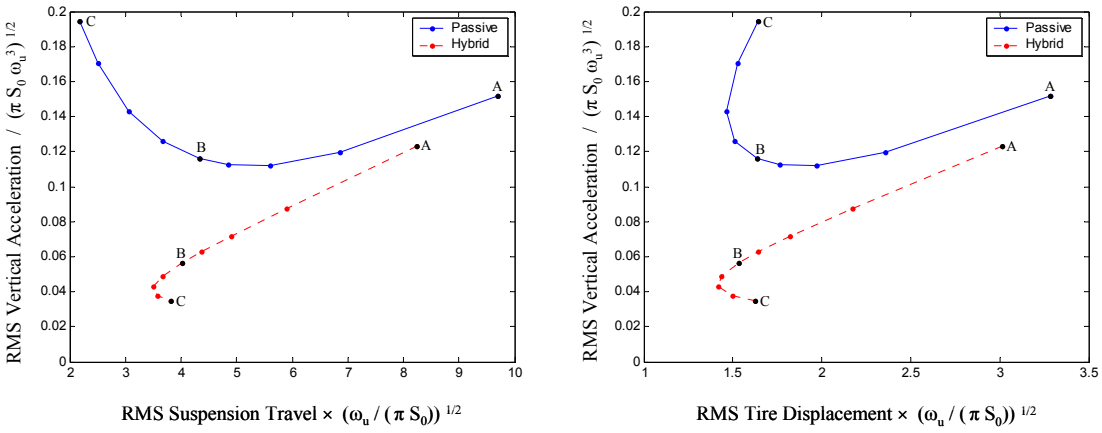

Figure 3.8: Comparison Between the Performances of a Passive Suspension and a Hybrid Semiactive Suspension (Mass Ratio: 0.15; Stiffness Ratio: 10)

For the configuration B, corresponding to a typical damping for passengers cars, the hybrid configuration ($\alpha = 0.5$) reduces the rms acceleration of the sprung mass by half, and also reduces the rms suspension travel and the rms tire displacements in smaller proportions. This is for a typical mass ratio ($r_m = 0.15$) and a typical stiffness ratio ($r_k = 10$) for passenger cars. Therefore, using semiactive suspensions with the hybrid configuration yields a much better comfort than a passive suspension, without reducing the road-holding quality or increasing the suspension displacement for most passenger cars.

4 Full Car Modeling

The work shown in this chapter is based on a full car model so that not only the heave response, but also the pitch and the roll responses can be studied. The work of Chalasani [2] for passive and active suspensions is extended to semiactive suspensions using the skyhook, groundhook, and hybrid configurations. Numerical models are developed to study the heave, pitch, and roll motions of the vehicle for periodic and discrete road inputs.

4.1 Model Formulation

The model of the full-vehicle suspension system used in this analysis is similar the one used by [2]. Instead of having a passive or active suspension, the model uses the actual passive representation of the semiactive suspension for the skyhook, groundhook, and hybrid configurations, as shown in Figure 4.1. The numerical values remain the same than in [2], except those related to the dampers used in the suspension system.

The vehicle is represented as a linearized seven-degree-of-freedom system, as shown in Figure 4.1. It consists of a single sprung mass (M_s) free to heave, pitch, and roll, connected to four unsprung masses (M_{U1}, M_{U2}, M_{U3} and M_{U4}) free to bounce vertically with respect to the sprung mass. All pitch and roll angles are assumed to be small.

The four tires are modeled as four springs of stiffness K_{U1}, K_{U2}, K_{U3} and K_{U4} respectively. The damping in each tire is small enough to be neglected. The suspensions between the sprung mass M_s and the unsprung masses M_{U1}, M_{U2}, M_{U3} and M_{U4} are modeled as four linear springs of stiffness K_{S1}, K_{S2}, K_{S3} and K_{S4} respectively, and four linear dampers with a damping coefficient of C_{off1}, C_{off2}, C_{off3} and C_{off4}. Four linear dampers with a damping rate of $\alpha(C_{on1} - C_{off1})$, $\alpha(C_{on2} - C_{off2})$, $\alpha(C_{on3} - C_{off3})$,

$\alpha(C_{on4} - C_{off4})$ connect the four corners of the sprung mass to some inertial reference in the sky and four linear dampers with a damping rate of $(1-\alpha)(C_{on1} - C_{off1})$, $(1-\alpha)(C_{on2} - C_{off2})$, $(1-\alpha)(C_{on3} - C_{off3})$, $(1-\alpha)(C_{on4} - C_{off4})$ connect the four unsprung masses to some inertial reference in the sky. The variable α is the relative ratio between the skyhook and groundhook control. When α is 1, the control policy reduces to pure skyhook, whereas when α is 0, the control is purely groundhook. Finally, the front and rear anti – roll bars are modeled as linear torsional springs of stiffness KF and KR respectively.

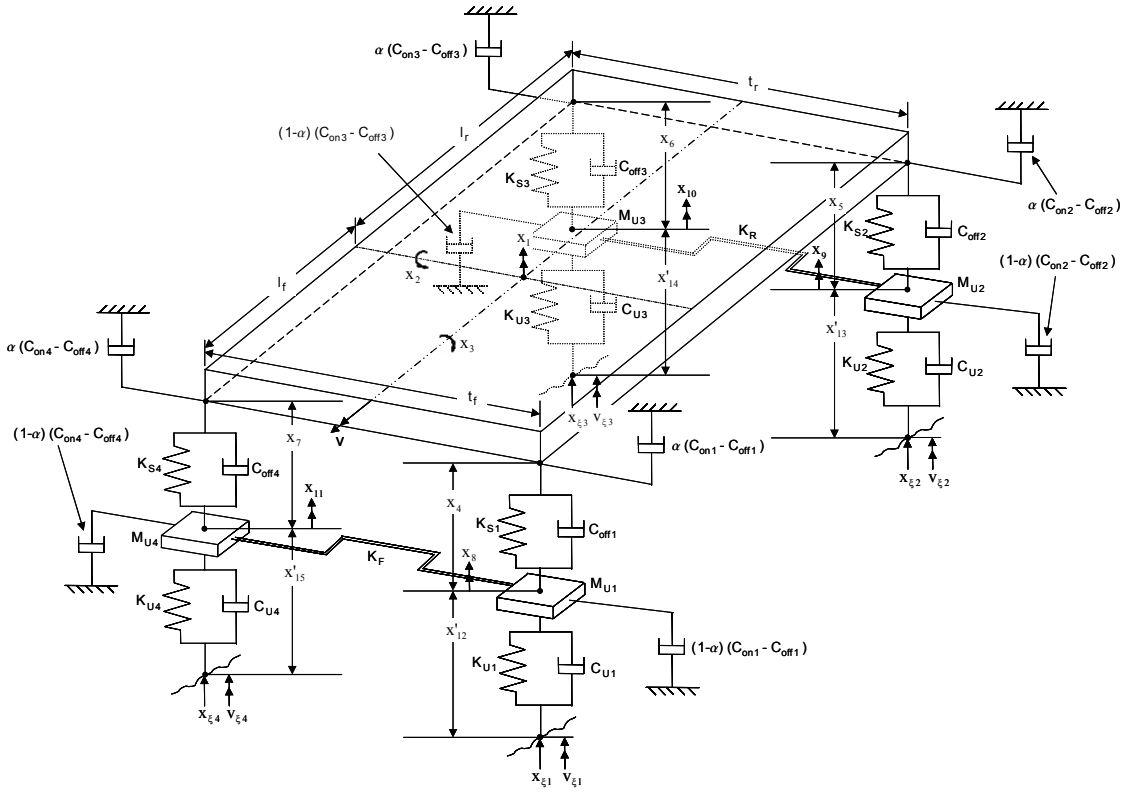

Figure 4.1: Full-Vehicle Diagram (adapted from [2])

The model parameters and their respective units are summarized in Table 4.1.

Table 4.1: Full Vehicle Model Parameters

Symbol	**Description**	**Numerical Value**
M_S	Sprung Mass	1460 Kg
M_{U1}, M_{U4}	Left and Right Front Unsprung Mass	40 Kg
M_{U2}, M_{U3}	Left and Right Rear Unsprung Mass	35.5 Kg
K_{S1}, K_{S4}	Left and Right Front Suspension Stiffness	19960 N / m
K_{S2}, K_{S3}	Left and Right Rear Suspension Stiffness	17500 N / m
K_{U1}, K_{U2}, K_{U3}, K_{U4}	Tire Vertical Stiffness	175500 N / m
C_{off1}, C_{off4}	Left and Right Front Off-State Damping	258 N · s / m
C_{off2}, C_{off3}	Left and Right Rear Off-State Damping	324 N · s / m
C_{on1}, C_{on4}	Left and Right Front On-State Damping	2838 N · s / m
C_{on2}, C_{on3}	Left and Right Rear On-State Damping	3564 N · s / m
I_{XX}	Roll Moment of Inertia	460 Kg · m^2
I_{YY}	Pitch Moment of Inertia	2460 Kg · m^2
KF	Front Auxiliary Roll Stiffness	19200 N · m / rad
KR	Rear Auxiliary Roll Stiffness	0 N · m / rad
t_f	Front Track Width	1.522 m
t_r	Rear Track Width	1.51 m
l_f	Longitudinal Distance From Sprung Mass c.g. to Front Axle	1.011 m
l_r	Longitudinal Distance From Rear Axle to Sprung Mass c.g.	1.803 m
x_d	Longitudinal Distance From Sprung Mass c.g. to Driver c.g.	- 0.32 m
y_d	Lateral Distance From Sprung Mass c.g. to Driver c.g.	- 0.38 m

The states and inputs of the model are described in Table 4.2.

Table 4.2: Full Vehicle Model States and Inputs

Symbol	**Description**	**Units**
x_1	Velocity of the sprung mass	Meters / sec
x_2	Pitch angular velocity	Rad / sec
x_3	Roll angular velocity	Rad / sec
x_4	Suspension deflection at the front – left corner	Meters
x_5	Suspension deflection at the rear – left corner	Meters
x_6	Suspension deflection at the rear – right corner	Meters
x_7	Suspension deflection at the front – right corner	Meters
x_8	Vertical velocity of the front – left unsprung mass	Meters / sec
x_9	Vertical velocity of the rear – left unsprung mass	Meters / sec
x_{10}	Vertical velocity of the rear – right unsprung mass	Meters / sec
x_{11}	vertical velocity of the front – right unsprung mass	Meters / sec
x'_{12}	Deflection of the front – left tire	Meters
x'_{13}	Deflection of the rear – left tire	Meters
x'_{14}	Deflection of the rear – right tire	Meters
x'_{15}	Deflection of the front – right tire	Meters
$x_{\xi 1}$	Displacement input at the front-left wheel	Meters
$x_{\xi 2}$	Displacement input at the rear – left wheel	Meters
$x_{\xi 3}$	Displacement input at the rear – right wheel	Meters
$x_{\xi 4}$	Displacement input at the front-right wheel	Meters
$v_{\xi 1} = x'_{\xi 1}$	Velocity input at the front-left wheel	Meters / sec
$v_{\xi 2} = x'_{\xi 2}$	Velocity input at the rear – left wheel	Meters / sec
$v_{\xi 3} = x'_{\xi 3}$	Velocity input at the rear – right wheel	Meters / sec
$v_{\xi 4} = x'_{\xi 4}$	Velocity input at the front-right wheel	Meters / sec

The displacement inputs, $x_{\xi i}$ $(i = 1,\ 2, \ldots 4)$, and the velocity inputs, $v_{\xi i}$ $(i = 1,\ 2, \ldots 4)$, have to be consistent, i.e., $v_{\xi i}(t) = \dfrac{dx_{\xi i}(t)}{dt}$. The values of $C_{off,i}$ and $C_{off,i}$ $(i = 1,\ 2, \ldots 4)$ were chosen knowing that for the passive suspension model used in [2], the left and right front suspension damping coefficients (C_{S1} and C_{S4}, respectively) were equal to $1290\ N \cdot s/m$ and the left and right rear suspension damping coefficients (C_{S2} and C_{S3}, respectively) were equal to$1620\ N \cdot s/m$ Typical values for semiactive suspensions are chosen using the relations $C_{off} = 0.2\, C_S$ and $C_{on} = 2.2\, C_S$.

Using the 15 system states described earlier, 15 equations of motion can be derived in a straightforward manner. However, only 14 equations are needed in order to describe our seven-degree-of-freedom system. The variable x'_{15} can be eliminated. Indeed, as explained in [2], the deflection of the front right tire can be related to the deflection of the three other tires and the four suspension deflections by:

$$x'_{15} = (x_4 + x_{12} - x_7) - \left((x_5 + x_{13}) - (x_6 + x_{14})\right) \frac{t_f}{t_r} + \frac{t_f}{4}\left(\frac{(x_{\xi 1} - x_{\xi 4})}{t_f} - \frac{(x_{\xi 2} - x_{\xi 3})}{t_r}\right) \quad (4.1)$$

where

$$x_{12} = x'_{12} + \frac{t_f}{4}\left(\frac{(x_{\xi 1} - x_{\xi 4})}{t_f} - \frac{(x_{\xi 2} - x_{\xi 3})}{t_r}\right) \quad (4.2)$$

$$x_{13} = x'_{13} - \frac{t_r}{4}\left(\frac{(x_{\xi 1} - x_{\xi 4})}{t_f} - \frac{(x_{\xi 2} - x_{\xi 3})}{t_r}\right) \quad (4.3)$$

$$x_{14} = x'_{14} + \frac{t_r}{4}\left(\frac{(x_{\xi 1} - x_{\xi 4})}{t_f} - \frac{(x_{\xi 2} - x_{\xi 3})}{t_r}\right) \quad (4.4)$$

Using the variables x_{12}, x_{13}, and x_{14} to replace the variables x'_{12}, x'_{13}, x'_{14}, and x'_{15}, a system of 14 equations of motion can be derived. These 14 equations of motion are shown in Appendix 2.

The system can be represented in a matrix form as:

$$\dot{\vec{x}} = A\,\vec{x} + L\,\vec{\xi} \tag{4.5}$$

where A is the 14×14 system matrix, L the 14×8 disturbance matrix.

The vector of the 14 states $\vec{x}$ is described by:

$$\vec{x} = \left[x_1 \;\; x_2 \;\; x_3 \;\; x_4 \;\; x_5 \;\; x_6 \;\; x_7 \;\; x_8 \;\; x_9 \;\; x_{10} \;\; x_{11} \;\; x_{12} \;\; x_{13} \;\; x_{14} \right]^T$$

Similarly, $\dot{\vec{x}}$ is defined by:

$$\dot{\vec{x}} = \left[\dot{x}_1 \;\; \dot{x}_2 \;\; \dot{x}_3 \;\; \dot{x}_4 \;\; \dot{x}_5 \;\; \dot{x}_6 \;\; \dot{x}_7 \;\; \dot{x}_8 \;\; \dot{x}_9 \;\; \dot{x}_{10} \;\; \dot{x}_{11} \;\; \dot{x}_{12} \;\; \dot{x}_{13} \;\; \dot{x}_{14} \right]^T$$

The vector of road disturbances $\vec{\xi}$ is defined by:

$$\vec{\xi} = \left[x_{\xi 1} \; x_{\xi 2} \; x_{\xi 3} \; x_{\xi 4} \; v_{\xi 1} \; v_{\xi 2} \; v_{\xi 3} \; v_{\xi 4} \right]$$

The matrices A and L are shown in Appendix 3.

4.2 Vehicle Ride Response to Periodic Road Inputs

The response of the vehicle to three different periodic inputs will be simulated: heave input, pitch input, and roll input. The amplitude of the velocity inputs $v_{\xi 1}$, $v_{\xi 2}$, $v_{\xi 3}$ and $v_{\xi 4}$ is 1 m/s, and the corresponding displacements inputs $x_{\xi i}$ $(i = 1, 2, 3, 4)$ verify the

relationship $v_{\xi i}(t) = \frac{dx_{\xi i}(t)}{dt}$. The inputs used for this simulation analysis are shown in Table 4.3. The steady-state amplitudes of the responses will be plotted for frequencies ranging from 0.1 rad/s to 200 rad/s and for four different configurations: passive (using the model described in [2]), skyhook, groundhook and hybrid with $\alpha = 0.5$. We are reminded that for the passive suspension model used by [2], the left and right front suspension damping coefficients (C_{S1} and C_{S4}, respectively) are equal to $1290\,N \cdot s/m$ and the left and right rear suspension damping coefficients (C_{S2} and C_{S3}, respectively) are equal to $1620\,N \cdot s/m$.

The damping ratios are in the medium range (for the passive case: $\zeta_{front} = 0.169$ and $\zeta_{rear} = 0.227$). The heave motion of the full vehicle model can therefore be compared with configuration (B) in Chapter 3. Figure 4.2 shows the heave response to the heave velocity input of amplitude 1 m/s obtained with the quarter car model of Chapter 3 using configuration (B) for a passive suspension, as well as for groundhook, hybrid, and skyhook semiactive control policies.

Figure 4.3 shows the heave response of the full vehicle model to the heave velocity input of amplitude 1 m/s (i.e., the amplitude of each of the four velocity inputs $v_{\xi 1}$, $v_{\xi 2}$, $v_{\xi 3}$ and $v_{\xi 4}$ is 1 m/s). The pitch response to the pitch input, and the roll response to the roll input are shown in Figures 4.4 and 4.5. The pitch response to the heave input and the heave response to the pitch input (i.e., the cross-coupling effects) are shown in Figures 4.6 and 4.7. The roll motion is completely decoupled from the heave and pitch motions since the right side and the left side of the full vehicle model are identical. A heave or pitch input yields no roll response, and similarly, a roll input yields no heave or pitch response. Therefore, no figure will deal with any of those four cases.

All the figures show the results obtained with the passive, groundhook, hybrid (with $\alpha = 0.5$), and skyhook configurations.

Table 4.3: Periodic Inputs Used to Simulate the Vehicle Ride Response

Type of Road Disturbances Input	**Corresponding Velocity Input**	**Corresponding Displacement Input**
Heave Input 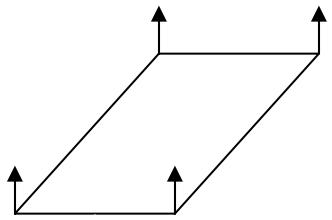	$v_{\xi 1} = \sin(\omega t)$ $v_{\xi 2} = \sin(\omega t)$ $v_{\xi 3} = \sin(\omega t)$ $v_{\xi 4} = \sin(\omega t)$	$x_{\xi 1} = -(1/\omega)\cos(\omega t)$ $x_{\xi 2} = -(1/\omega)\cos(\omega t)$ $x_{\xi 3} = -(1/\omega)\cos(\omega t)$ $x_{\xi 4} = -(1/\omega)\cos(\omega t)$
Pitch Input 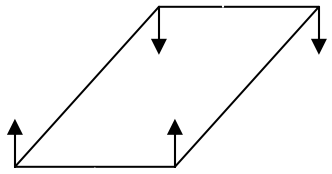	$v_{\xi 1} = \sin(\omega t)$ $v_{\xi 2} = -\sin(\omega t)$ $v_{\xi 3} = -\sin(\omega t)$ $v_{\xi 4} = \sin(\omega t)$	$x_{\xi 1} = -(1/\omega)\cos(\omega t)$ $x_{\xi 2} = (1/\omega)\cos(\omega t)$ $x_{\xi 3} = (1/\omega)\cos(\omega t)$ $x_{\xi 4} = -(1/\omega)\cos(\omega t)$
Roll Input 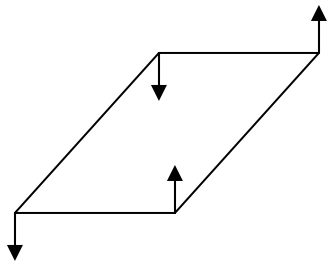	$v_{\xi 1} = \sin(\omega t)$ $v_{\xi 2} = \sin(\omega t)$ $v_{\xi 3} = -\sin(\omega t)$ $v_{\xi 4} = -\sin(\omega t)$	$x_{\xi 1} = -(1/\omega)\cos(\omega t)$ $x_{\xi 2} = -(1/\omega)\cos(\omega t)$ $x_{\xi 3} = (1/\omega)\cos(\omega t)$ $x_{\xi 4} = (1/\omega)\cos(\omega t)$

The figures corresponding to the heave response (i.e., Figures 4.3 and 4.7) will show:

- The vertical acceleration: $\dot{x}_1$
- The heave suspension deflection: $x_4 + x_5 + x_6 + x_7$
- The heave tire deflection: $x'_{12} + x'_{13} + x'_{14} + x'_{15}$

The figures corresponding to the pitch response (i.e., Figures 4.4 and 4.6) will show:

- The pitch angular acceleration: $\dot{x}_2$
- The pitch suspension deflection: $(x_4 + x_7) - (x_5 + x_6)$
- The pitch tire deflection: $(x'_{12} + x'_{15}) - (x'_{13} + x'_{14})$

The figure corresponding to the roll response (i.e., Figure 4.5) will show:

- The roll angular acceleration: $\dot{x}_3$
- The roll suspension deflection: $(x_4 + x_5) - (x_6 + x_7)$
- The roll tire deflection: $(x'_{12} + x'_{13}) - (x'_{14} + x'_{15})$

For Figure 4.2, the suspension deflection and the tire deflection obtained with the quarter car model are multiplied by four in order to match the definitions of the heave suspension deflection and the heave tire deflection for the full vehicle model.

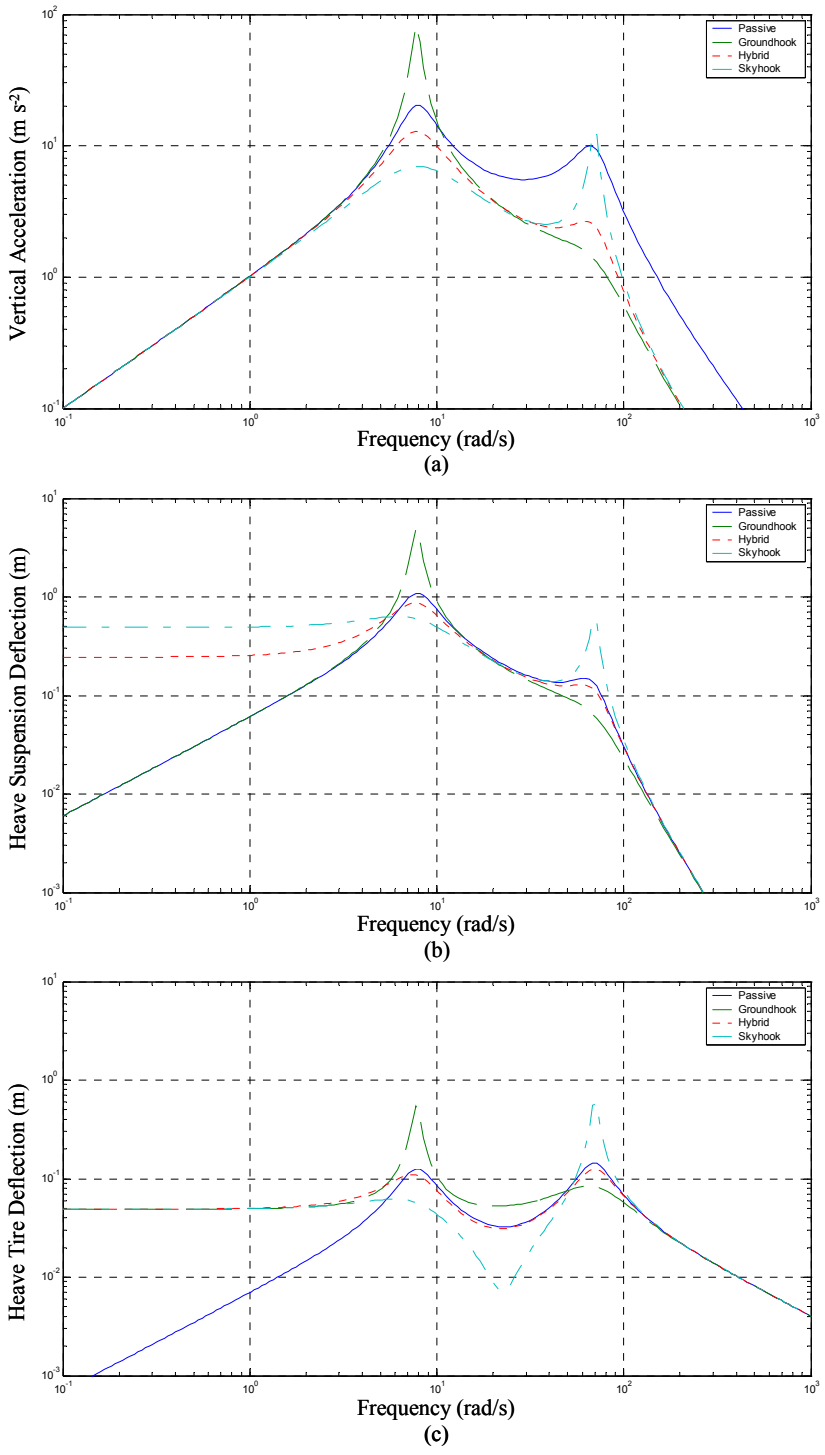

Figure 4.2: Heave Response to Heave Input of 1 m/s Amplitude Using Quarter Car Approximation: (a) Vertical Acceleration; (b) Suspension Deflection; (c) Tire Deflection

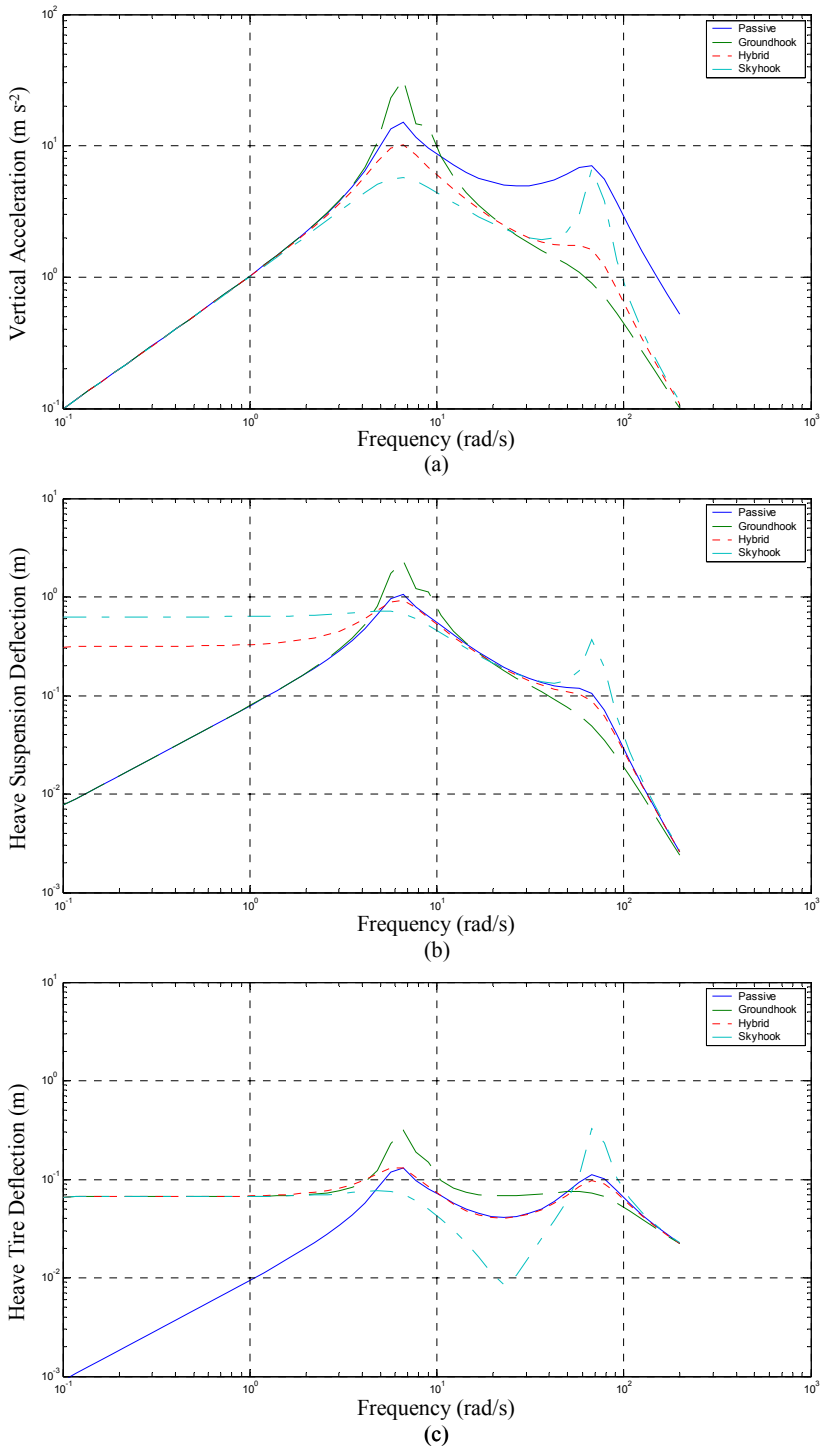

Figure 4.3: Heave Response to Heave Input of 1 m/s Amplitude at Each Corner:

(a) Vertical Acceleration; (b) Suspension Deflection; (c) Tire Deflection

Figures 4.2 and 4.3 show that the exact same conclusions can be drawn for the full-vehicle model as for the quarter-car model. The quarter-car model is therefore a very good approximation for studying the heave response of a full vehicle subjected to a heave input. The main difference is that the peaks obtained near the sprung mass natural frequency and the unsprung mass natural frequency are lower for the full vehicle model. The four 'quarter cars' of the full vehicle behave differently and do not vibrate at the exact same frequency, which creates an averaging effect.

The hybrid configuration is clearly the best one in order to minimize the vertical acceleration of the sprung mass for overall frequencies. It is also a good compromise for minimizing the suspension deflection and the tire displacement. The skyhook configuration yields low transmibilities near the sprung mass natural frequency at the cost of higher transmibilities near the unsprung mass natural frequency. The groundhook configuration yields low transmibilities near the unsprung mass natural frequency at the cost of much higher transmibilities near the sprung mass natural frequency. It can be noted that the groundhook configuration yields much lower suspension deflections at low frequencies than both the skyhook and hybrid configurations.

The passive suspension has one advantage over the hybrid semiactive suspension: it yields lower suspension deflections and tire deflections at low frequencies. However, the hybrid semiactive suspension is the configuration that yields the best results when the objective is to minimize the rms vertical acceleration of the sprung mass, the rms tire deflection and the rms suspension travel. It yields by far the lowest rms vertical acceleration of the sprung mass.

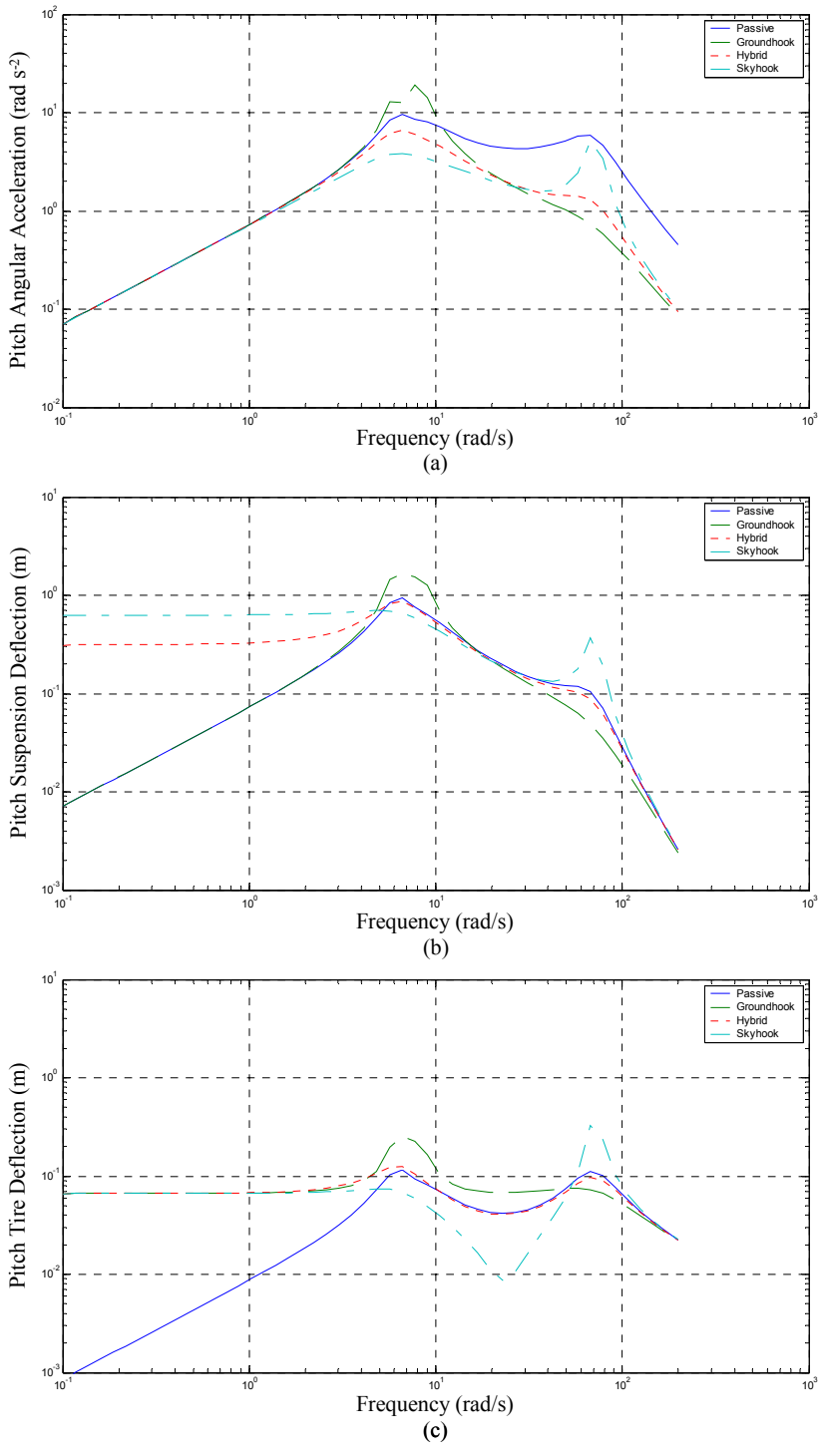

Figure 4.4: Pitch Response to Pitch Input of 1 m/s Amplitude at Each Corner:

(a) Angular Acceleration; (b) Suspension Deflection; (c) Tire Deflection

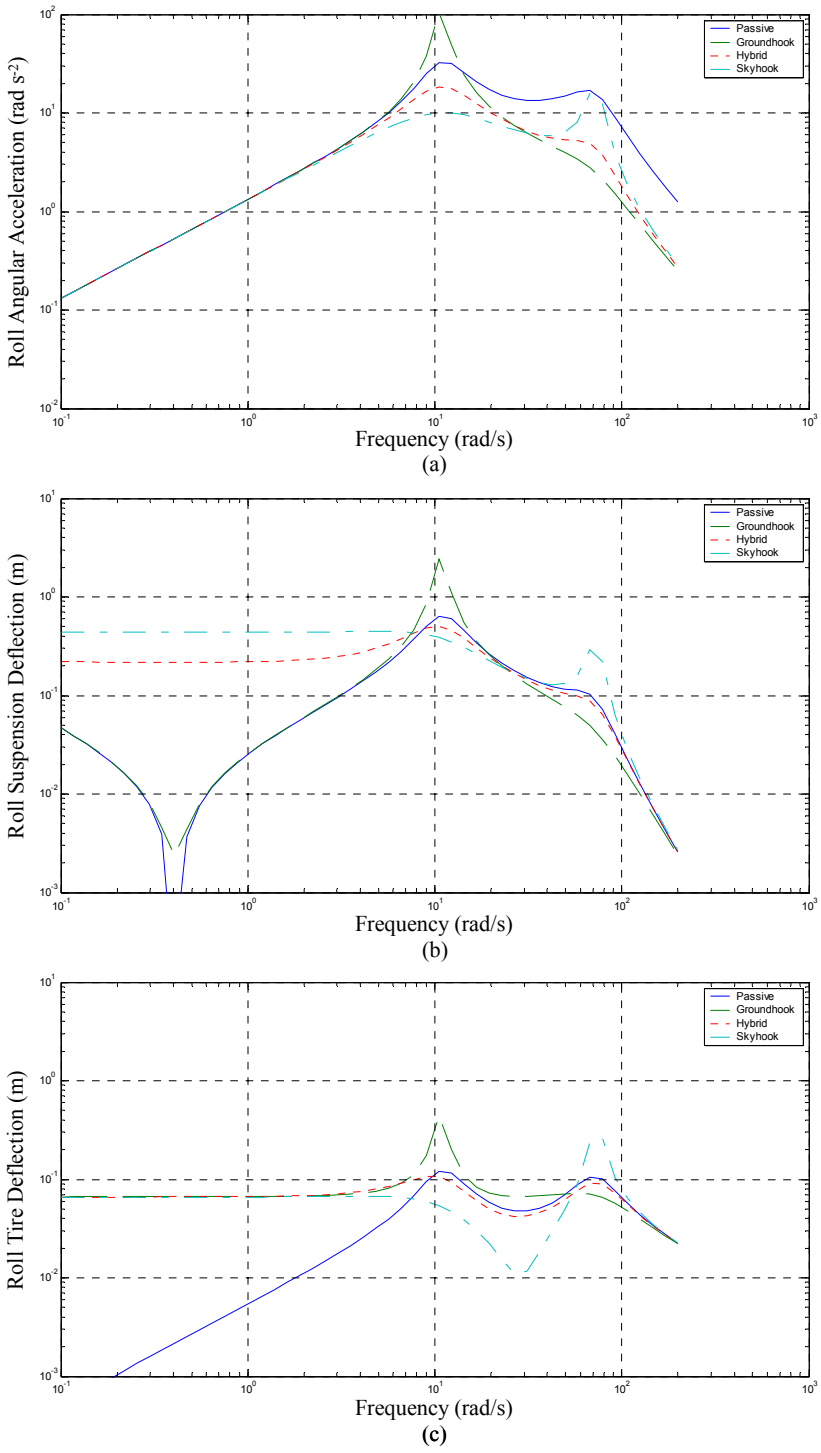

Figure 4.5: Roll Response to Roll Input of 1 m/s Amplitude at Each Corner:

(a) Angular Acceleration; (b) Suspension Deflection; (c) Tire Deflection

Figure 4.4 and Figure 4.5 show that the pitch response to a pitch input and the roll response to a roll input are both similar to the heave response to a heave input, for each configuration (passive, groundhook, hybrid, skyhook). Therefore, working on a simplified quarter-car model not only provides a good way to estimate the behavior of a full-vehicle subjected to a heave input, but also gives a good idea of how the full-vehicle would behave when subjected to a pitch or roll input.

The pitch response to the heave input and the heave response to the pitch input are shown in Figures 4.6 and 4.7 below. The trends mentioned earlier still hold true. Once again, the hybrid configuration yields better overall results, i.e., less coupling between heave and pitch motions in this case.

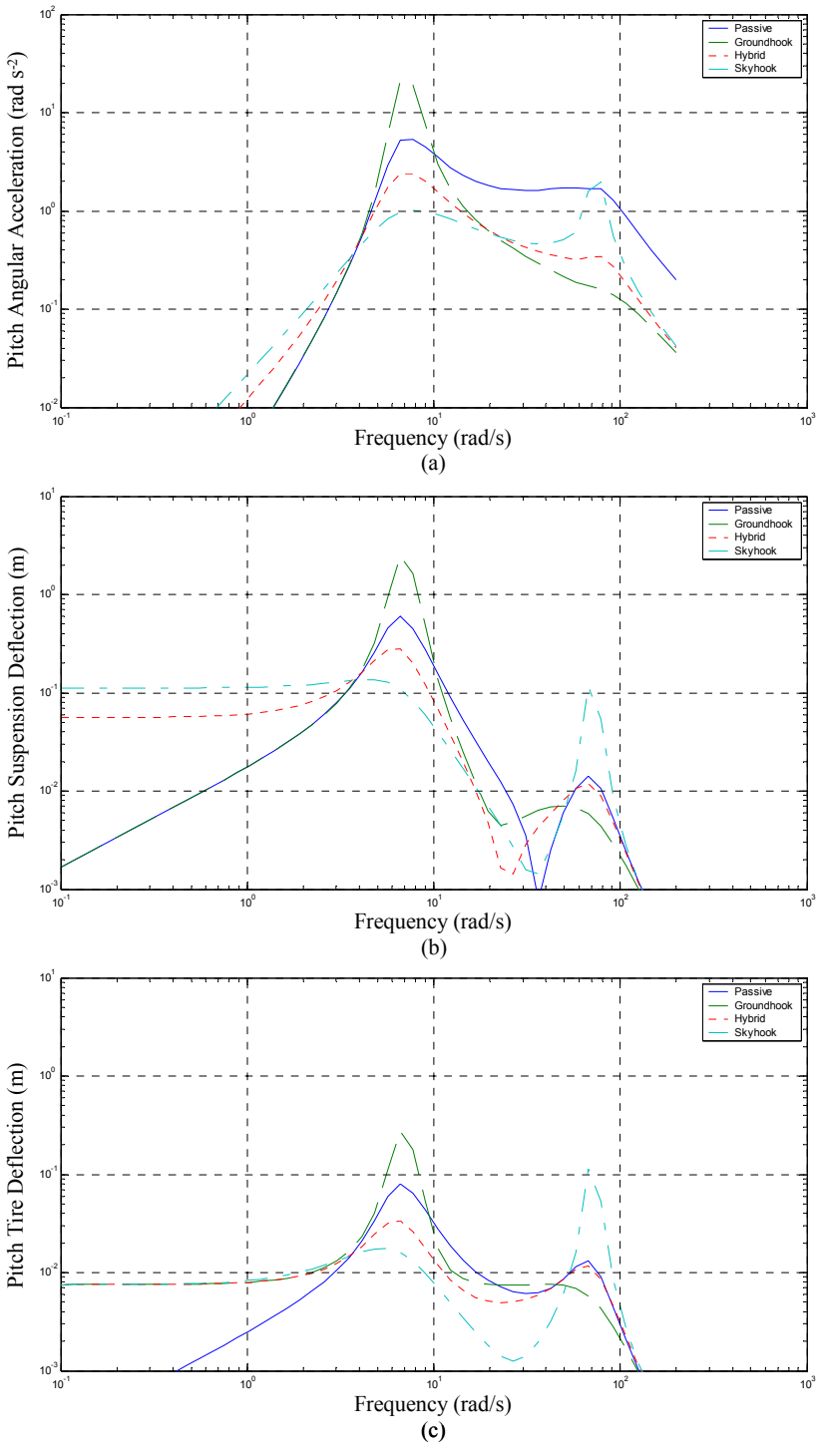

Figure 4.6: Pitch Response to Heave Input of 1 m/s Amplitude at Each Corner:

(a) Angular Acceleration; (b) Suspension Deflection; (c) Tire Deflection

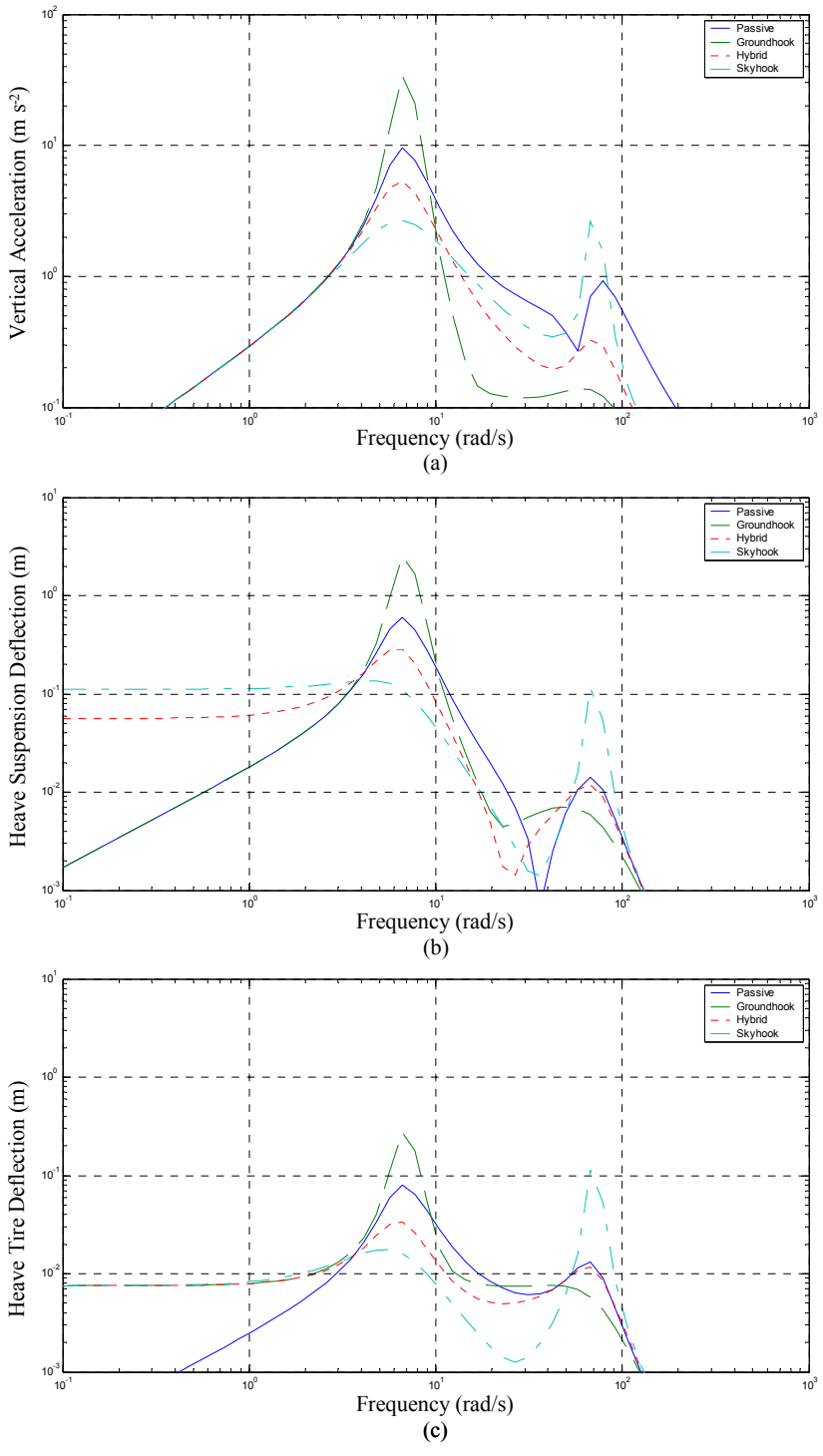

Figure 4.7: Heave Response to Pitch Input of 1 m/s Amplitude at Each Corner:

(a) Vertical Acceleration; (b) Suspension Deflection; (c) Tire Deflection

4.3 Vehicle Ride Response to Discrete Road Inputs

The road disturbance used for this simulation analysis is the "chuck hole" used in [2]. The height of the road drops linearly by 5 cm over a longitudinal distance of 76 cm, stays at that level over a longitudinal distance of 76 cm, and goes back to the original height linearly over a longitudinal distance of 76 cm. This road profile is shown in Figure 4.8.

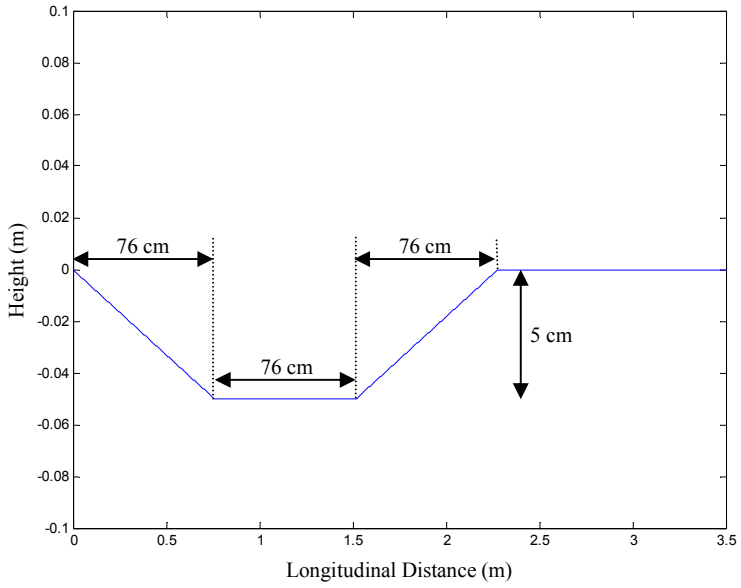

Figure 4.8: Road Profile Used to Compute the Response of the Vehicle

The response of the vehicle will be computed for a vehicle speed of 40 km/h (i.e., approximately 25 mph), and assuming that only the right side of the vehicle is subjected to the "chuck hole" road disturbance, so that both pitch and roll motions are produced at the same time. The pitch response is shown in Figure 4.9, and the roll response is shown in Figure 4.10.

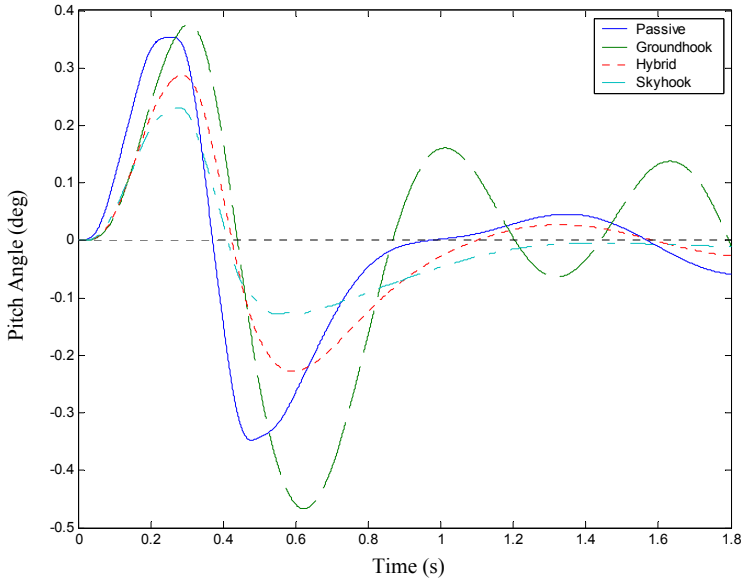

Figure 4.9: Pitch Response of the Vehicle When Subjected to the "Chuck Hole" Road Disturbance

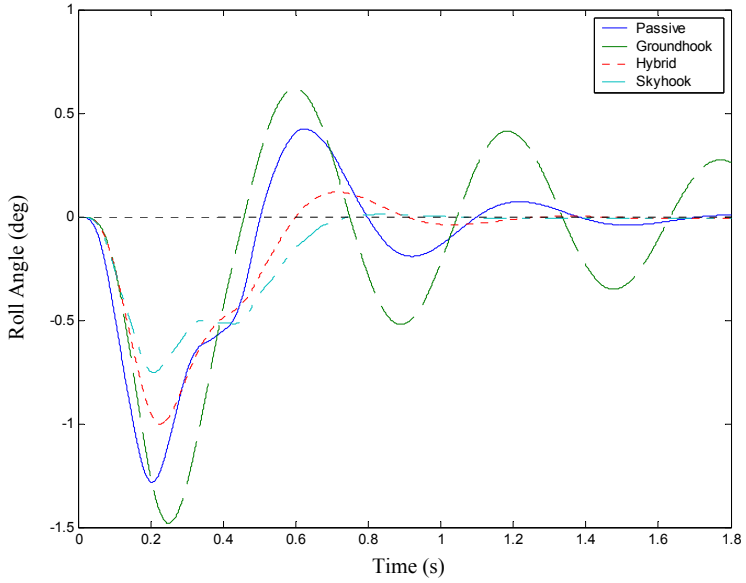

Figure 4.10: Roll Response of the Vehicle When Subjected to the "Chuck Hole" Road Disturbance

At $t = 0$, the right front wheel enters the chuck hole. The vehicle therefore pitches forward and rolls to the right. Then, at $t = 0.21\,s$, the right front wheel emerges from the chuck hole, and right after, at $t = 0.25\,s$, the rear right wheel enters the chuck hole. The pitch angle therefore starts to decrease and eventually oscillates, while the roll angle starts to increase and eventually oscillates, except for the skyhook configuration, which results in a fast attenuation of the pitch and roll motions.

The skyhook configuration yields the best results: it yields the smaller peak pitch angle, the smaller roll peak angle, and the fastest time to eliminate both the pitch and roll motions. For those criteria, the hybrid configuration comes second, and the passive configuration third. Clearly, the groundhook configuration yields very poor results for both the pitch and roll angles.

The skyhook configuration yields a peak pitch angle approximately 35% smaller than the peak pitch angle obtained with the passive configuration, while the hybrid configuration yields a reduction in peak pitch angle of approximately 20%.

The skyhook configuration yields a peak roll angle approximately 40% smaller than the peak roll angle obtained with the passive configuration, while the hybrid configuration yields a reduction in peak roll angle of approximately 20%.

The vertical acceleration at the right front seat, i.e., the passenger seat, is shown in Figure 4.11. The three semiactive configurations all yield smaller peak accelerations. However, the vertical acceleration does not die out quickly with the groundhook configuration. Also, the skyhook configuration yields fast oscillations of the vertical acceleration. The hybrid configuration clearly yields the best results. It yields the smallest peak acceleration for instance: the reduction of peak acceleration is approximately 50% compared with the passive case.

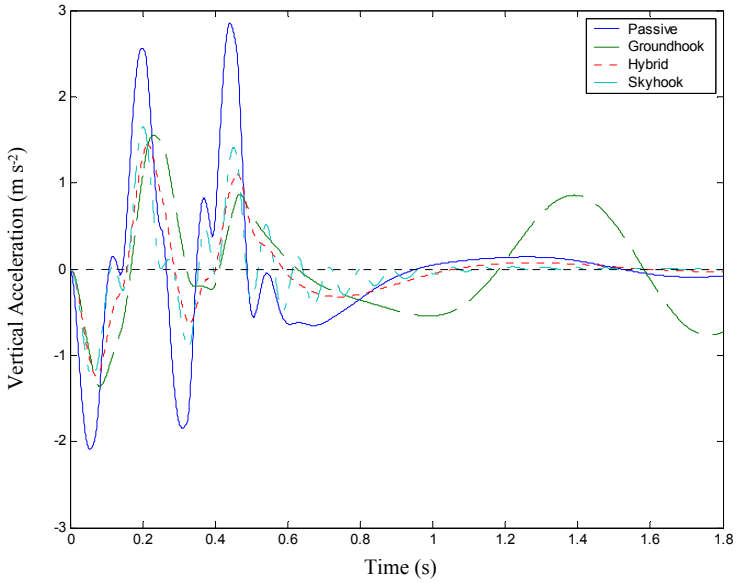

Figure 4.11: Vertical Acceleration at the Right Front Seat Due to the "Chuck Hole" Road Disturbance

The deflection of the right rear suspension is shown in Figure 4.12. The only semiactive configuration that yields a smaller peak deflection than the passive suspension is the groundhook configuration. However, the deflection of the right rear suspension does not die out quickly with the groundhook configuration. The skyhook configuration yields a high deflection peak. Among the semiactive configurations, the hybrid configuration yields the best results. Compared to the passive suspension, it yields a slightly higher peak deflection in rebound (extension) than for a passive suspension, and a smaller peak deflection in jounce (compression).

The deflection of the right rear tire is shown in Figure 4.13. The hybrid configuration yields better results than the skyhook and the groundhook configurations. It yields approximately the same peak deflection in extension than a passive suspension, but a slightly smaller peak in compression.

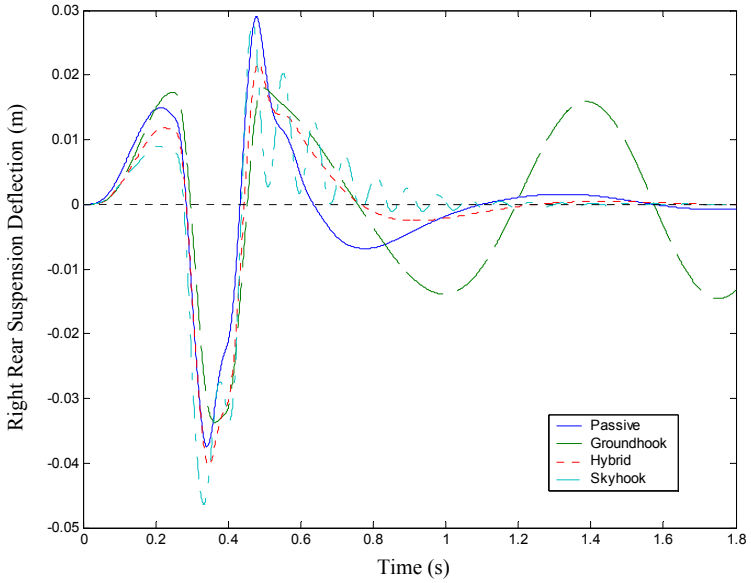

Figure 4.12: Deflection of the Right Rear Suspension Due to the "Chuck Hole" Road Disturbance

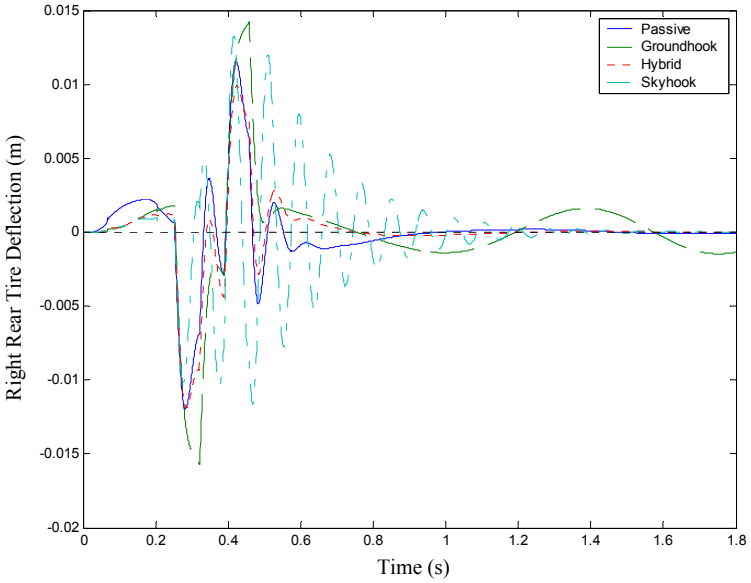

Figure 4.13: Deflection of the Right Rear Tire Due to the "Chuck Hole" Road Disturbance

5 H2 optimization

The objective of H_2 optimization is to reduce the total vibration energy of the system for overall frequencies [9], which is equivalent to reducing the appropriate mean square responses to a white noise input, like the ones described in Chapter 3. For fixed values of masses and springs, closed form solutions for the optimal damping coefficients will be derived for a quarter-car model, using a procedure similar to the one used in [9]. Finally, the algebraic expressions will be replaced by a set of numerical values in order to study how the behavior of the suspension system is affected by the choice of the damping coefficients.

5.1 Model Formulation

The model of the quarter–car passive suspension system used in this analysis is shown in Figure 5.1, and the model parameters are shown in Table 5.1.

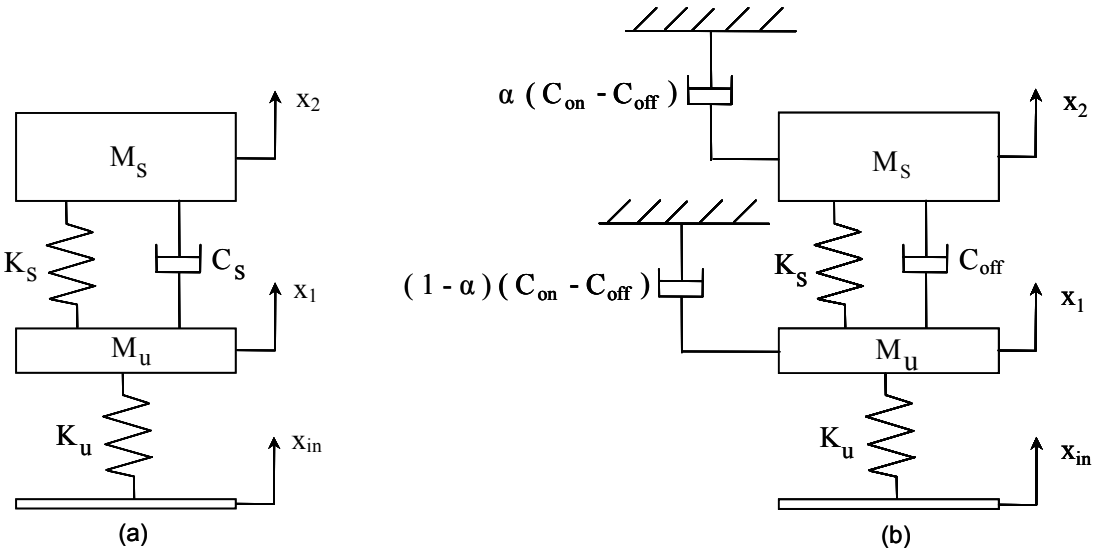

Figure 5.1: Quarter - Car Model: (a) Passive Suspension; (b) Semiactive Suspension

In Chapter 3, the mean square responses to a white noise input were computed for three motion variables. In this chapter, the values of the masses and the springs will be fixed. The role of the springs is to balance the static load of the vehicle, and the dampers are often the only parts of the suspension system one would like to change in order to modify its behavior. Also, being able to make another parameter varying would yield trivial solutions that are not possible to use in real life, as explained in § 2.5. The model parameters are shown in Table 5.1. They are the same ones as the model parameters that were shown in Table 3.1.

Table 5.1: Model Parameters

Parameter	Value
Sprung Body Weight (M_S)	240 Kg
Unsprung Body Weight (M_u)	36Kg
Suspension Stiffness (K_S)	16000 N / m
Tire Stiffness (K_U)	160000 N / m

The value of the suspension stiffness being fixed based on the weight of the vehicle, the damping coefficient C_S is the only variable of the system for the passive suspension. For the semiactive suspension, α, C_{off}, and C_{on} are the variables of the system.

5.2 Definition of the Performance Indices

The objective of this chapter is to reduce the total vibration energy of the system for overall frequencies. The total area under the frequency response curve needs to be minimized. It is equivalent to minimizing the square root of that area, which is called the H_2 norm: this is the origin of the name "H_2 optimization" [9]. The objective is therefore

to find the expressions of C_S for the passive suspension model (α, C_{off}, and C_{on} for the semiactive suspension model) minimizing the integrals shown below.

The first three integrals to be minimized will be:

- $\int_{-\infty}^{\infty} \left| \frac{\ddot{x}_2}{\dot{x}_{in}} \right|^2 d\omega$, used as a measure of the vibration level
- $\int_{-\infty}^{\infty} \left| \frac{x_2 - x_1}{\dot{x}_{in}} \right|^2 d\omega$, used as a measure of the rattlespace requirement
- $\int_{-\infty}^{\infty} \left| \frac{x_1 - x_{in}}{\dot{x}_{in}} \right|^2 d\omega$, used as a measure of the road-holding quality

Minimizing the three integrals shown above is equivalent to minimizing the three mean square responses that were computed in Chapter 3 using the relationship $E[y^2] = S_0 \int_{-\infty}^{\infty} \left| H_y(\omega) \right|^2 d\omega$, where S_0 was the spectral density of the white-noise velocity input. A white noise velocity input was used because the road profile can be approximated by an integrated white-noise input [1].

Other integrals will be minimized as well. For instance, if the objective is to minimize the velocity of the sprung mass for overall frequencies, $\int_{-\infty}^{\infty} \left| \frac{\dot{x}_2}{\dot{x}_{in}} \right|^2 d\omega$ needs to be minimized. If the objective is to minimize the velocity of the unsprung mass for overall frequencies, $\int_{-\infty}^{\infty} \left| \frac{\dot{x}_1}{\dot{x}_{in}} \right|^2 d\omega$ needs to be minimized. However, isolating one mass is at the expense of having the other one vibrating more. It is therefore interesting to minimize the integral $\int_{-\infty}^{\infty} \left((1-\beta) \left| \frac{\dot{x}_1}{\dot{x}_{in}} \right|^2 + \beta \left| \frac{\dot{x}_2}{\dot{x}_{in}} \right|^2 \right) d\omega$ for $0 \le \beta \le 1$. When the weighting

coefficient β gets close to 0, the unsprung mass is well isolated, while when β gets close to 0, the sprung mass is well isolated. Weighting coefficients will also be used for other pairs of integrals.

5.3 Optimization for Passive Suspensions

5.3.1 Procedure for H_2 Optimization

This procedure is similar to the one used by [9]. For the passive suspension system shown in Figure 5.1, the equations of motion of the system are:

$$M_S \ddot{x}_2 + C_S (\dot{x}_2 - \dot{x}_1) + K_S (x_2 - x_1) = 0 \tag{5.1}$$

$$M_U \ddot{x}_1 + C_S (\dot{x}_1 - \dot{x}_2) + K_S (x_1 - x_2) + K_U (x_1 - x_{in}) = 0 \tag{5.2}$$

Using the Laplace transform yields:

$$(M_S s^2 + C_S s + K_S) X_2 = (C_S s + K_S) X_1 \tag{5.3}$$

$$(M_U s^2 + C_S s + (K_S + K_U)) X_1 = (C_S s + K_S) X_2 + K_U X_{in} \tag{5.4}$$

Finally, substituting *s* by $j\omega$ yields the equations of motion in the frequency domain:

$$(M_S \omega^2 + C_S j\omega + K_S) X_2 = (C_S j\omega + K_S) X_1 \tag{5.5}$$

$$(M_U \omega^2 + C_S j\omega + (K_S + K_U)) X_1 = (C_S j\omega + K_S) X_2 + K_U X_{in} \tag{5.6}$$

Now, the objective is to minimize the integral $\int_{-\infty}^{\infty} T(\omega)\, d\omega$, which can be any integral mentioned earlier in 5.2. For instance, when the objective is to minimize the total

vibration energy of the system felt by the driver and the passengers for overall frequencies, the integral $\int_{-\infty}^{\infty} T(\omega)\,d\omega$ will be $\int_{-\infty}^{\infty} \left| \frac{\ddot{x}_2}{\dot{x}_{in}} \right|^2 d\omega$.

The first important step is to write the integral using the form shown below in (5.7):

$$T(\omega) = \frac{a_1 \omega^6 + a_2 \omega^4 + a_3 \omega^2 + a_4}{(\omega^4 - b_2 \omega^2 + b_4)^2 + (b_1 \omega^3 - b_3 \omega)^2} \tag{5.7}$$

It should be noted that $\int_{-\infty}^{\infty} T(\omega)\,d\omega$ is always defined when $T(\omega)$ has the form shown in (5.7) and $b_4 \neq 0$. However, $\int_{-\infty}^{\infty} T(\omega)\,d\omega$ is not always defined. For instance, $\int_{-\infty}^{\infty} \left| \frac{x_1}{\dot{x}_{in}} \right|^2 d\omega$ and $\int_{-\infty}^{\infty} \left| \frac{x_2}{\dot{x}_{in}} \right|^2 d\omega$ are not defined.

The expression to be integrated has to be written using the form shown in (5.7) in order to be able to follow the next steps of the calculation. Then, after separating the denominator into two factors, as shown in Equation (5.8), the expression can be expressed as a function of its 4 pairs of complex conjugate poles ($\pm j\omega_1$, $\pm j\omega_2$, $\pm j\omega_3$, and $\pm j\omega_4$), as shown in Equation (5.9).

$$T(\omega) = \frac{a_1 \omega^6 + a_2 \omega^4 + a_3 \omega^2 + a_4}{(\omega^4 + j b_1 \omega^3 - b_2 \omega^2 - j b_3 \omega + b_4)\ (\omega^4 - j b_1 \omega^3 - b_2 \omega^2 + j b_3 \omega + b_4)} \tag{5.8}$$

$$T(\omega) = \frac{a_1 \omega^6 + a_2 \omega^4 + a_3 \omega^2 + a_4}{(\omega + j\omega_1)(\omega - j\omega_1)(\omega + j\omega_2)(\omega - j\omega_2)(\omega + j\omega_3)(\omega - j\omega_3)(\omega + j\omega_4)(\omega - j\omega_4)} \tag{5.9}$$

The coefficients b_1, b_2, b_3, and b_4 can be expressed as a function of ω_1, ω_2, ω_3, and ω_4, as shown in Equations (5.10) to (5.13). They are obtained by equating the denominator in Equation (5.8) and the denominator in Equation (5.9).

$$b_1 = \omega_1 + \omega_2 + \omega_3 + \omega_4 \tag{5.10}$$

$$b_2 = \omega_1\,\omega_2 + \omega_1\,\omega_3 + \omega_1\,\omega_4 + \omega_2\,\omega_3 + \omega_2\,\omega_4 + \omega_3\,\omega_4 \tag{5.11}$$

$$b_3 = \omega_1\,\omega_2\,\omega_3 + \omega_1\,\omega_2\,\omega_4 + \omega_1\,\omega_3\,\omega_4 + \omega_2\,\omega_3\,\omega_4 \tag{5.12}$$

$$b_4 = \omega_1\,\omega_2\,\omega_3\,\omega_4 \tag{5.13}$$

The integral $\int_{-\infty}^{\infty} T(\omega)\,d\omega$ can be expressed as a function of ω_1, ω_2, ω_3, and ω_4 by using the residue integration formula (5.14):

$$\int_{-\infty}^{\infty} T(\omega)\,d\omega = 2\pi\,j\ \sum \mathrm{Res}[T(\omega)] \tag{5.14}$$

where $\mathrm{Res}[T(\omega)]$ denotes a residue of $T(\omega)$ corresponding to a pole of $T(\omega)$ located in the upper-half of the complex plane [9].

Also, ω_1, ω_2, ω_3, and ω_4 are positive numbers because the coefficients b_1, b_2, b_3 and b_4 that are obtained when deriving Equation (5.7) are always positive.

Therefore,

$$\int_{-\infty}^{\infty} T(\omega)\,d\omega = 2\pi\,j\ \sum_{k=1}^{4} \lim(\omega - j\,\omega_k)\,T(\omega) \tag{5.15}$$

When applying the formula shown above in (5.15), the expression used for $T(\omega)$ should be the one shown in (5.9). It is possible, though long and difficult, to rearrange the terms in order to express the integral in function of b_1, b_2, b_3, and b_4. The result is shown in Equation (5.16).

$$\int_{-\infty}^{\infty} T(\omega)\,d\omega = \pi\,\frac{a_1\,b_4\,(b_2\,b_3 - b_1\,b_4) + a_2\,(b_3\,b_4) + a_3\,(b_1\,b_4) + a_4\,(b_1\,b_2 - b_3)}{b_4\,(-b_1^{\,2}\,b_4 - b_3^{\,2} + b_1\,b_2\,b_3)} \qquad (5.16)$$

Substituting the coefficients a_0, a_1, a_2, a_3, a_4, b_1, b_2, b_3, b_4 by their algebraic expressions yields:

$$\int_{-\infty}^{\infty} T(\omega)\,d\omega = f(M_S, M_U, K_S, K_U, C_S) \qquad (5.17)$$

The objective is to find the optimal value C_{opt}, i.e., the value of C_S that minimizes the integral $\int_{-\infty}^{\infty} T(\omega)\,d\omega$. This value is obtained by taking the derivative versus C_S of the expression on the right in (5.17) and set it equal to zero.

It finally yields:

$$C_{opt} = f(M_S, M_U, K_S, K_U) \qquad (5.18)$$

5.3.2 Optimized Performance Indices

The expressions of C_S optimizing the performance indices that do not use weighting coefficients are shown in Table 5.2. The corresponding numerical values for C_S and the damping ratios $\zeta_S = \dfrac{C_S}{2\sqrt{K_S\,M_S}}$ are also shown in Table 4.2, using the set of numerical values of Table 5.1.

Table 5.2: Optimized Performance Indices

$T(\omega)$	Value of C_S minimizing $\int_{-\infty}^{\infty} T(\omega)\,d\omega$ with: $M_S = 240\,\text{Kg}$, $M_U = 36\,\text{Kg}$, $K_S = 16000\,\text{N/m}$, $K_U = 160000\,\text{N/m}$
$\left\lvert \frac{\ddot{x}_2}{\dot{x}_{in}} \right\rvert^2$	$C_S = K_S \sqrt{\frac{M_S + M_U}{K_U}}$ $C_S = 664.53\ \text{N}\cdot\text{s/m}$, i.e., $\zeta_S = 0.170$
$\left\lvert \frac{x_2 - x_1}{\dot{x}_{in}} \right\rvert^2$	$C_S = \infty$
$\left\lvert \frac{x_1 - x_{in}}{\dot{x}_{in}} \right\rvert^2$	$C_S = \sqrt{\frac{K_U^{\,2} M_S^{\,2} M_U - 2 K_S K_U M_S M_U (M_S + M_U) + K_S^{\,2} (M_S + M_U)^3}{K_U (M_S + M_U)^2}}$ $C_S = 1948.14\ \text{N}\cdot\text{s/m}$, i.e., $\zeta_S = 0.497$
$\left\lvert \frac{\dot{x}_2}{\dot{x}_{in}} \right\rvert^2$	$C_S = \sqrt{\frac{K_S \left(K_U M_S^{\,2} + K_S (M_S + M_U)^2\right)}{K_U (M_S + M_U)}}$ $C_S = 1944.41\ \text{N}\cdot\text{s/m}$, i.e., $\zeta_S = 0.496$
$\left\lvert \frac{\dot{x}_1}{\dot{x}_{in}} \right\rvert^2$	$C_S = \sqrt{\frac{K_S^{\,2} (M_S + M_U)^2 + K_U M_S \left(K_U M_S - K_S (M_S + 2 M_U)\right)}{K_U (M_S + M_U)}}$ $C_S = 5430.66\ \text{N}\cdot\text{s/m}$, i.e., $\zeta_S = 1.386$
$\left\lvert \frac{\ddot{x}_1}{\dot{x}_{in}} \right\rvert^2$	$C_S = \sqrt{\frac{K_S^{\,2} M_U (M_S + M_U) + K_U^{\,2} M_S^{\,2} - 2 K_S K_U M_S M_U}{K_U M_U}}$ $C_S = 15772.2\ \text{N}\cdot\text{s/m}$, i.e., $\zeta_S = 4.024$

The results shown in Table 5.2 illustrate the classic trade off between ride comfort and vehicle stability for passive suspensions mentioned in Chapter 2. Minimizing the vibration level index yields a low damping ratio ($\zeta_S = 0.170$), whereas minimizing the road-holding quality index yields a much higher damping ratio ($\zeta_S = 0.497$). The choice of the value for ζ_S is always a compromise between ride comfort and road holding quality. For instance, taking $C_S = 980\ \mathrm{N \cdot s/m}$ yields $\zeta_S = 0.250$, which is between 0.170 and 0.497.

The expressions of C_S optimizing the performance indices that use weighting factors are shown below:

- Minimizing $(1-\beta)\left|\frac{x_1 - x_{in}}{\dot{x}_{in}}\right|^2 + \beta\left|\frac{x_2 - x_1}{\dot{x}_{in}}\right|^2$ yields:

$$C_S = \sqrt{\frac{K_U^{\,2} M_S^{\,2} (M_U + M_S \beta) + K_S^{\,2}(M_S + M_U)^3 (1-\beta) - 2 K_S K_U M_S M_U (M_S + M_U)(1-\beta)}{K_U (M_S + M_U)^2 (1-\beta)}}$$

- Minimizing $(1-\beta)\left|\frac{\ddot{x}_1}{\dot{x}_{in}}\right|^2 + \beta\left|\frac{\ddot{x}_2}{\dot{x}_{in}}\right|^2$ yields:

$$C_S = \sqrt{\frac{K_S^{\,2} M_U (M_S + M_U) + K_U^{\,2} M_S^{\,2} (1-\beta) - 2 K_S K_U M_S M_U (1-\beta)}{K_U M_U}}$$

- Minimizing $\int_{-\infty}^{\infty}\left((1-\beta)\left|\frac{\dot{x}_1}{\dot{x}_{in}}\right|^2 + \beta\left|\frac{\dot{x}_2}{\dot{x}_{in}}\right|^2\right)d\omega$ yields:

$$C_S = \left(\begin{array}{l} \beta\ \dfrac{K_S\left(K_U M_S^{\,2} + K_S(M_S + M_U)^2\right)}{K_U (M_S + M_U)} \\ +(1-\beta)\ \dfrac{K_S^{\,2}(M_S + M_U)^2 + K_U M_S \left(K_U M_S - K_S (M_S + 2 M_U)\right)}{K_U (M_S + M_U)} \end{array}\right)^{\frac{1}{2}}$$

5.3.3 Effects of Optimizing the Performance Indices

The expressions $\left|\frac{\ddot{x}_2}{\dot{x}_{in}}\right|(\omega)$, $\left|\frac{x_2 - x_1}{\dot{x}_{in}}\right|(\omega)$, and $\left|\frac{x_1 - x_{in}}{\dot{x}_{in}}\right|(\omega)$ are plotted in Figure 5.2, Figure 5.3, and Figure 5.4 respectively. Each of the three figures uses the same four values for C_S:

- The value minimizing $\int_{-\infty}^{\infty}\left|\frac{\ddot{x}_2}{\dot{x}_{in}}\right|^2 d\omega$: $C_S = 664.53\ N\cdot s/m$ (i.e., $\zeta_S = 0.170$)
- The value minimizing $\int_{-\infty}^{\infty}\left|\frac{x_1 - x_{in}}{\dot{x}_{in}}\right|^2 d\omega$: $C_S = 1948.14\ N\cdot s/m$ (i.e., $\zeta_S = 0.497$)
- The value minimizing $\int_{-\infty}^{\infty}\left|\frac{x_2 - x_1}{\dot{x}_{in}}\right|^2 d\omega$: $C_S = \infty$ (i.e., $\zeta_S = \infty$)
- A value resulting in a compromise between comfort and stability: $C_S = 980\ N\cdot s/m$ (i.e., $\zeta_S = 0.250$)

The objective of plotting these three figures is to see how minimizing each of the three performance indices actually affects the corresponding integrated transmibility depending on the frequency. Minimizing the total area under the frequency response curve does not necessarily mean that the corresponding integrated expression is minimized at every frequency.

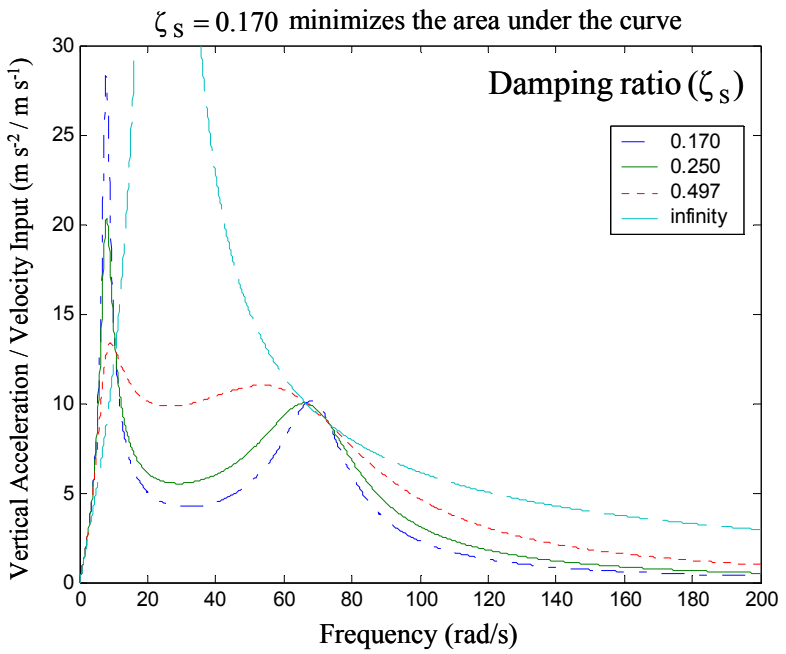

Figure 5.2: Effect of Damping on the Vertical Acceleration of the Sprung Mass

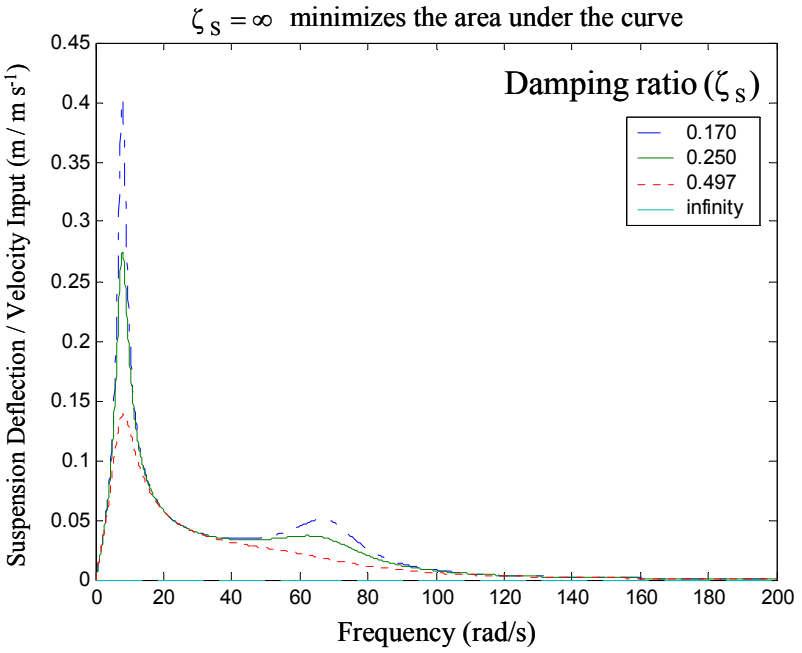

Figure 5.3: Effect of Damping on Suspension Displacement

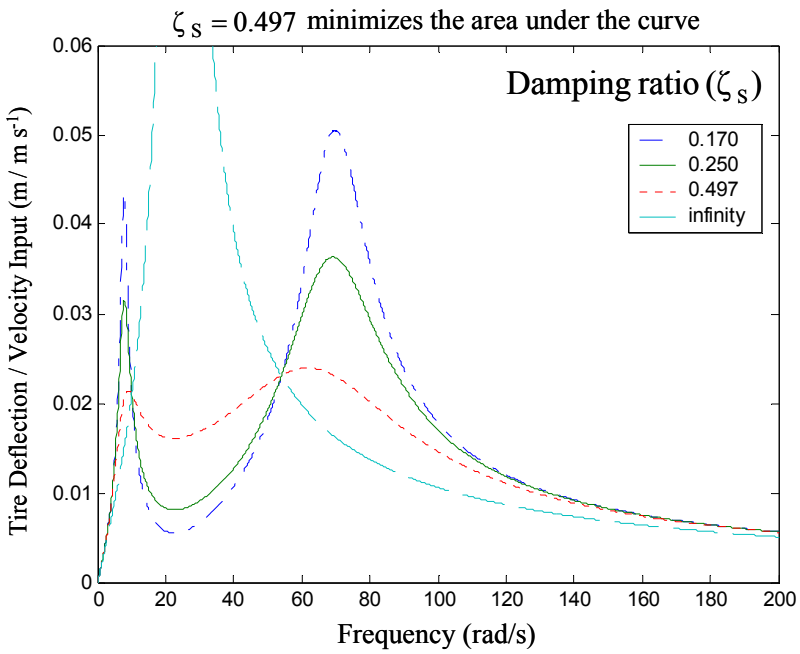

Figure 5.4: Effect of Damping on Tire Displacement

Figure 5.4 shows that minimizing $\int_{-\infty}^{\infty} \left| \frac{x_1 - x_{in}}{\dot{x}_{in}} \right|^2 d\omega$ (i.e., taking $\zeta_S = 0.497$) yields a lower peak tire displacement than the other damping ratios, near both the sprung mass natural frequency (ω_s = 8.165 rad/s, i.e., 1.30 Hz) and the unsprung mass natural frequency (ω_u = 66.666 rad/s, i.e., 10.61 Hz). However, taking $\zeta_S = 0.497$ yields higher values than the ones obtained with $\zeta_S = 0.170$ only for a range of frequencies comprised between ω_s and ω_u, but these values are lower than the peak values obtained near ω_s and ω_u. The road-holding quality index $\int_{-\infty}^{\infty} \left| \frac{x_1 - x_{in}}{\dot{x}_{in}} \right|^2 d\omega$ therefore appears to be a good index.

Figure 5.2 shows that minimizing $\int_{-\infty}^{\infty} \left| \frac{\ddot{x}_2}{\dot{x}_{in}} \right|^2 d\omega$ (i.e., taking $\zeta_S = 0.170$) is actually achieved at the cost of a higher peak near the sprung mass natural frequency ω_s. The maximum acceleration of the sprung mass is twice the maximum acceleration obtained with $\zeta_S = 0.497$. The comfort index $\int_{-\infty}^{\infty} \left| \frac{\ddot{x}_2}{\dot{x}_{in}} \right|^2 d\omega$ is therefore far from being perfect. When the index is optimized, the acceleration felt by the driver and the passengers can actually become very strong when the frequency gets close to ω_{ns}. When using this index, the average comfort is therefore increased at the cost of a worst case scenario. Taking a damping ratio higher than 0.170 not only improves the road-holding quality, but also guarantees that the maximum acceleration will not reach values as great as the peak acceleration that can be reached when minimizing $\int_{-\infty}^{\infty} \left| \frac{\ddot{x}_2}{\dot{x}_{in}} \right|^2 d\omega$. Before using the comfort index $\int_{-\infty}^{\infty} \left| \frac{\ddot{x}_2}{\dot{x}_{in}} \right|^2 d\omega$, a maximum acceptable value of $\left| \frac{\ddot{x}_2}{\dot{x}_{in}} \right|(\omega)$ should be specified. Then, the optimal damping ratio should be increased enough so that the maximum acceptable value can never be reached for any frequency.

Figure 5.3 shows that taking $\zeta_S = \infty$ reduces the suspension displacement to zero at every frequency. For every frequency, the suspension displacement can always be reduced by increasing damping. However, taking a high damping ratio makes the ride very harsh and even yields a very poor stability when the damping gets very high, as shown for $\zeta_S = \infty$ in Figure 5.4. An extremely high damping results in a very unsafe vehicle.

Achieving a good compromise between comfort and stability should be the first consideration. It usually yields a damping ratio bigger than the value minimizing the comfort index but smaller than the value for minimizing the road-holding stability index.

Then, if this compromise yields too much suspension displacement, the damping should be increased until the suspension displacement meets the predefined requirements.

5.4 Optimization for Semiactive Suspensions

5.4.1 Optimized Performance Indices

For the semiactive suspension system shown in Figure 5.1, the equations of motion of the system are:

$$M_S\,\ddot{x}_2 + \alpha\,(C_{on} - C_{off})\,\dot{x}_2 + C_{off}\,(\dot{x}_2 - \dot{x}_1) + K_S\,(x_2 - x_1) = 0 \tag{5.19}$$

$$M_U\,\ddot{x}_1 + (1-\alpha)\,(C_{on} - C_{off})\,\dot{x}_1 + C_{off}\,(\dot{x}_1 - \dot{x}_2) + K_S\,(x_1 - x_2) + K_U\,(x_1 - x_{in}) = 0 \tag{5.20}$$

In the Laplace domain, the equations of motion are:

$$\left(M_S\,s^2 + \left(\alpha\,(C_{on} - C_{off}) + C_{off}\right)s + K_S\right)X_2 = (C_{off}\,s + K_S)\,X_1 \tag{5.21}$$

$$\left(M_U\,s^2 + \left((1-\alpha)\,(C_{on} - C_{off}) + C_{off}\right)s + (K_S + K_U)\right)X_1 = (C_{off}\,s + K_S)\,X_2 + K_U\,X_{in} \tag{5.22}$$

The expressions $\int_{-\infty}^{\infty}\left|\frac{\ddot{x}_2}{\dot{x}_{in}}\right|^2 d\omega$, $\int_{-\infty}^{\infty}\left|\frac{x_1 - x_{in}}{\dot{x}_{in}}\right|^2 d\omega$, and $\int_{-\infty}^{\infty}\left|\frac{x_2 - x_1}{\dot{x}_{in}}\right|^2 d\omega$ are shown in Appendix 1 (with the notations of Chapter 3).

Closed form solutions to the H_2 optimization problem depending on α, C_{on} and C_{off} are not possible to derive with such a powerful software tool as *Mathematica* when using the procedure explained in § 5.3.1. However, looking at Figure 5.1 is enough to see that H_2 optimization for semiactive suspensions yields trivial solutions.

For instance, taking $C_{on} = \infty$ yields $\int_{-\infty}^{\infty} \left| \frac{\ddot{x}_2}{\dot{x}_{in}} \right|^2 d\omega = 0$ for every configuration (i.e., skyhook, groundhook, and hybrid), which minimizes the comfort index.

Also, taking $C_{off} = \infty$ yields $\int_{-\infty}^{\infty} \left| \frac{x_2 - x_1}{\dot{x}_{in}} \right|^2 d\omega = 0$ for every configuration, which minimizes the rattlespace requirement index.

For the road-holding quality index, no straightforward conclusion can be drawn by looking at the semiactive suspension system in Figure 5.1. However, contour plots tend to show that it probably yields either very high or infinite, damping values.

Since damping coefficients cannot take any desired value, like infinite values, contour plots are used to show the effect of changing $C_{on} - C_{off}$ and C_{off} (which is equivalent to show the effect of changing $\zeta_{on} - \zeta_{off}$ and ζ_{off}) on the value of:

- $\int_{-\infty}^{\infty} \left| \frac{\ddot{x}_2}{\dot{x}_{in}} \right|^2 d\omega$ for Figure 5.5
- $\int_{-\infty}^{\infty} \left| \frac{x_2 - x_1}{\dot{x}_{in}} \right|^2 d\omega$ for Figure 5.6
- $\int_{-\infty}^{\infty} \left| \frac{x_1 - x_{in}}{\dot{x}_{in}} \right|^2 d\omega$ for Figure 5.7

The values of ζ_{off} used for the contour plots are between 0.01 and 0.1, and the values of $\zeta_{on} - \zeta_{off}$ used for the contour plots are between 0.1 and 0.6. Other values would not be

realistic. Each figure uses three configurations for the contour plots: skyhook, groundhook, and hybrid with $\alpha = 0.5$.

The on-state damping ratio is given by:

$$\zeta_{on} = \frac{C_{on}}{2\sqrt{K_S M_S}} \tag{5.23}$$

The off-state damping ratio is given by:

$$\zeta_{off} = \frac{C_{off}}{2\sqrt{K_S M_S}} \tag{5.24}$$

The numbers displayed in the colorbars are:

- $\log_{10}\left(\int_{-\infty}^{\infty}\left|\frac{\ddot{x}_2}{\dot{x}_{in}}\right|^2 d\omega\right)$ for Figure 5.5
- $\log_{10}\left(\int_{-\infty}^{\infty}\left|\frac{x_2 - x_1}{\dot{x}_{in}}\right|^2 d\omega\right)$ for Figure 5.6
- $\log_{10}\left(\int_{-\infty}^{\infty}\left|\frac{x_1 - x_{in}}{\dot{x}_{in}}\right|^2 d\omega\right)$ for Figure 5.7

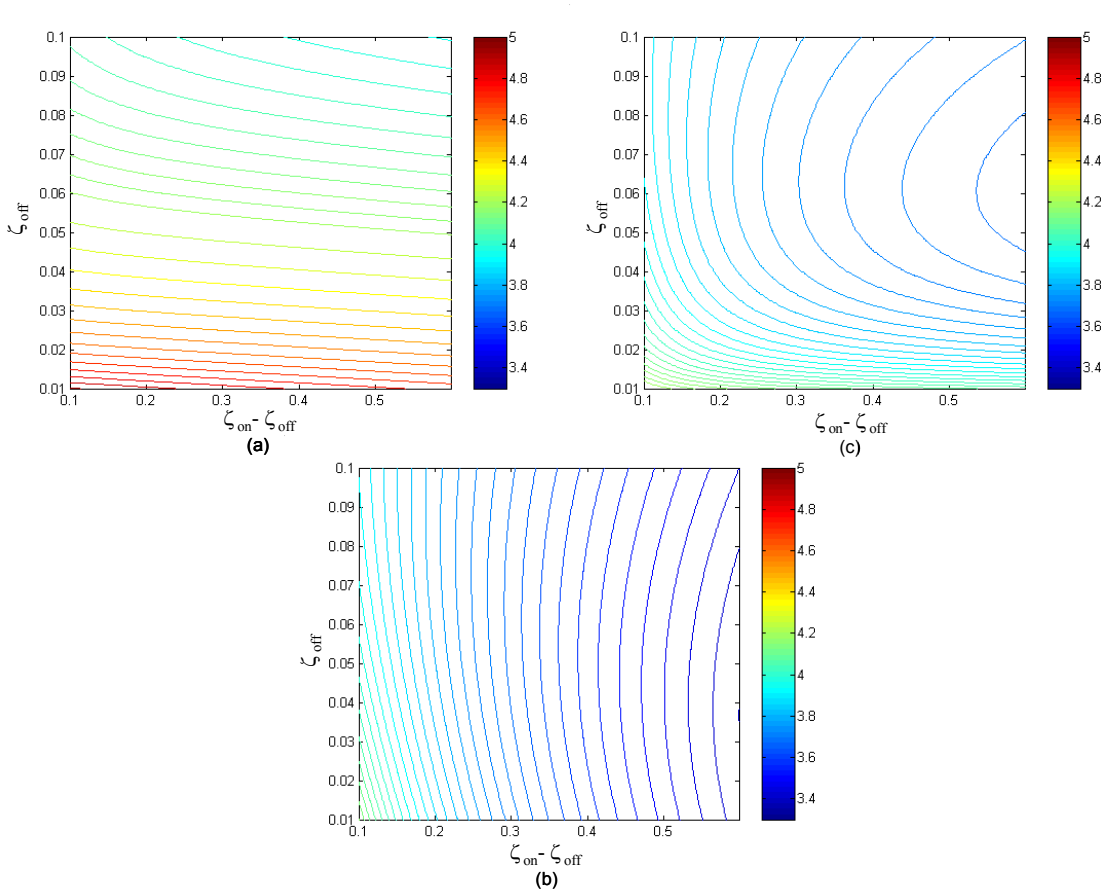

Figure 5.5: Effect of Damping on the Comfort Performance Index for the Semiactive Suspension: (a) Groundhook; (b) Hybrid with $\alpha = 0.5$; (c) Skyhook

Figure 5.5 shows that the hybrid configuration is the best one when the objective is to minimize the comfort index. The damping ratio ζ_{off} is desired to be small, and increasing $\zeta_{on} - \zeta_{off}$ for small values of ζ_{off} quickly reduces the comfort performance index. The groundhook configuration is clearly the worst for minimizing the comfort performance index: it yields high values even when both $\zeta_{on} - \zeta_{off}$ and ζ_{off} are taken as high as possible.

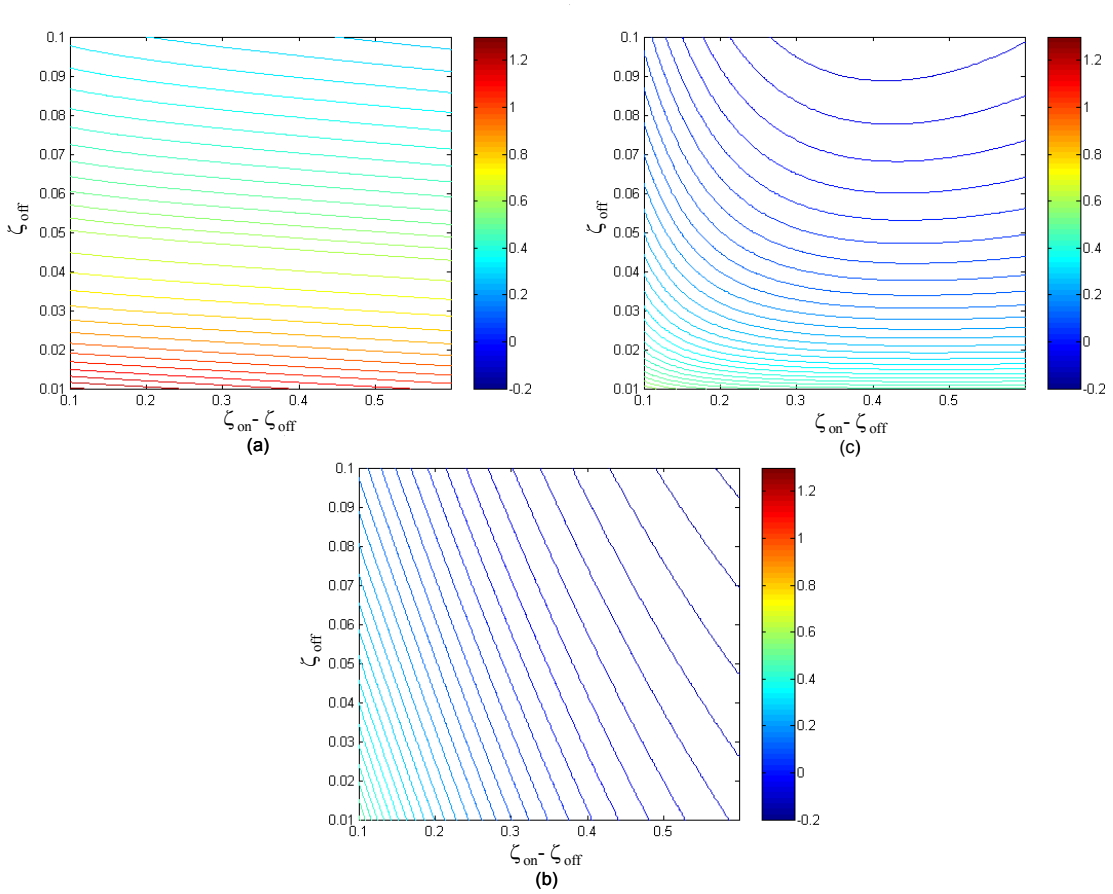

Figure 5.6: Effect of Damping on the Suspension Displacement Index for the Semiactive Suspension: (a) Groundhook; (b) Hybrid with $\alpha = 0.5$; (c) Skyhook

Figure 5.6 shows that the hybrid configuration is the best one when the objective is to minimize the suspension displacement index. The damping ratio ζ_{off} is desired to be small, and increasing $\zeta_{on} - \zeta_{off}$ for small values of ζ_{off} quickly reduces the suspension displacement index. The groundhook configuration is the worst for minimizing the suspension displacement index, even though it would eventually be a better one than skyhook if ζ_{off} could take extremely high values: suppressing the vibrations of the unsprung mass would also eliminate the suspension displacement.

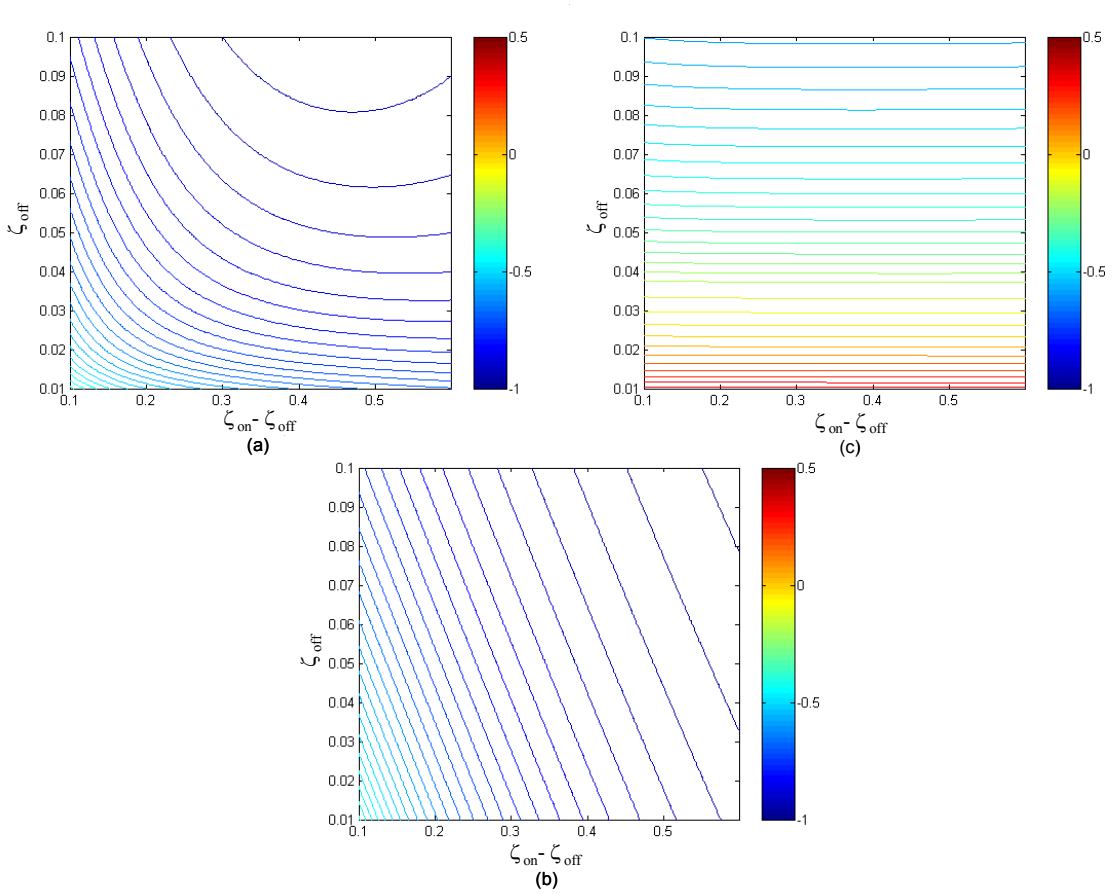

Figure 5.7: Effect of Damping on the Road Holding Quality Index for the Semiactive Suspension: (a) Groundhook; (b) Hybrid with $\alpha = 0.5$; (c) Skyhook

Figure 5.7 shows that the hybrid configuration is the best one when the objective is to minimize the road-holding quality index. Not surprisingly, the groundhook configuration is better than the skyhook configuration: controlling the movement of the unsprung mass yields more stability than controlling the movement of the sprung mass, which results in more comfort.

Figures 5.5 - 5.7 show that the hybrid configuration with $\alpha = 0.5$ is always better than both groundhook and skyhook configurations when the objective is to minimize any of the three performance indices with the use of realistic damping ratios.

5.4.2 Effect of Alpha on Performance Indices

The hybrid configuration with $\alpha = 0.5$ is always better than both groundhook and skyhook configurations when the objective is to minimize any of the three performance indices with the use of realistic damping ratios. However, it does not mean that $\alpha = 0.5$ is an optimal coefficient. When the groundhook configuration yields better results than the skyhook configuration, an optimal value of α would seem to be smaller than 0.5. When the skyhook configuration yields better results than the groundhook configuration, an optimal value of α would seem to be bigger than 0.5.

It is possible to find the optimal value of α for each performance index when the values of ζ_{on} and ζ_{off} are fixed. Typical values of C_{on} and C_{off} are chosen by taking $C_{on} = 2.2\,C_S$ and $C_{off} = 0.2\,C_S$ where C_S is the damping coefficient chosen for the passive suspension. For $C_S = 980\ \mathrm{N\cdot s/m}$ (i.e., $\zeta_S = 0.250$), it yields:

$$C_{on} = 2156\ \mathrm{N\cdot s/m}\ (\text{i.e., } \zeta_{on} = 0.550) \tag{5.25}$$

$$C_{off} = 196\ \mathrm{N\cdot s/m}\ (\text{i.e., } \zeta_{off} = 0.050) \tag{5.26}$$

Combining the numerical values of Table 5.1 and of Equations (5.25) and (5.26) yields the following results:

- Minimizing $\int_{-\infty}^{\infty} \left| \frac{\ddot{x}_2}{\dot{x}_{in}} \right|^2 d\omega$ yields $\alpha = 0.698$
- Minimizing $\int_{-\infty}^{\infty} \left| \frac{x_2 - x_1}{\dot{x}_{in}} \right|^2 d\omega$ yields $\alpha = 0.655$
- Minimizing $\int_{-\infty}^{\infty} \left| \frac{x_1 - x_{in}}{\dot{x}_{in}} \right|^2 d\omega$ yields $\alpha = 0.255$

As expected after looking at the contour plots, optimizing the comfort index or the suspension displacement index yields $\alpha > 0.5$, while optimizing the tire displacement index yields $\alpha < 0.5$.

The expressions $\left|\frac{\ddot{x}_2}{\dot{x}_{in}}\right|(\omega)$, $\left|\frac{x_2 - x_1}{\dot{x}_{in}}\right|(\omega)$, and $\left|\frac{x_1 - x_{in}}{\dot{x}_{in}}\right|(\omega)$ are plotted in Figure 5.8, Figure 5.9, and Figure 5.10 respectively, for $\zeta_{on} = 0.550$ and $\zeta_{off} = 0.050$. The results obtained with the optimal values of α that were just derived are compared with the results obtained with the value of α used in Chapter 3, i.e., $\alpha = 0.5$, and with the passive case, using $\zeta_S = 0.250$. A non-logarithmic scale is used in order to give another perspective than the figures shown in Chapter 3. Since $\alpha = 0.698$ and $\alpha = 0.655$ yield very similar results, $\alpha = 0.655$ is used only when it is the optimal value, i.e., in Figure 5.9.

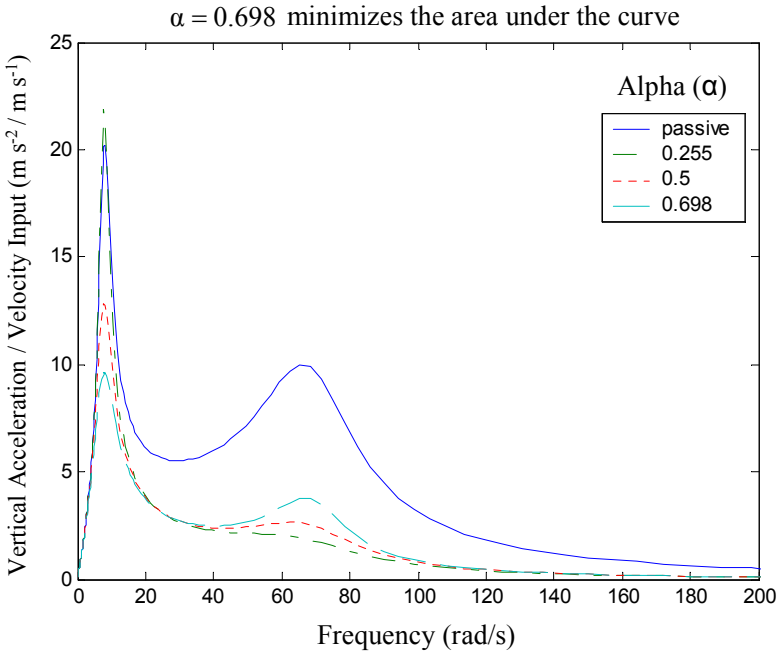

Figure 5.8: Effect of Alpha on the Vertical Acceleration of the Sprung Mass

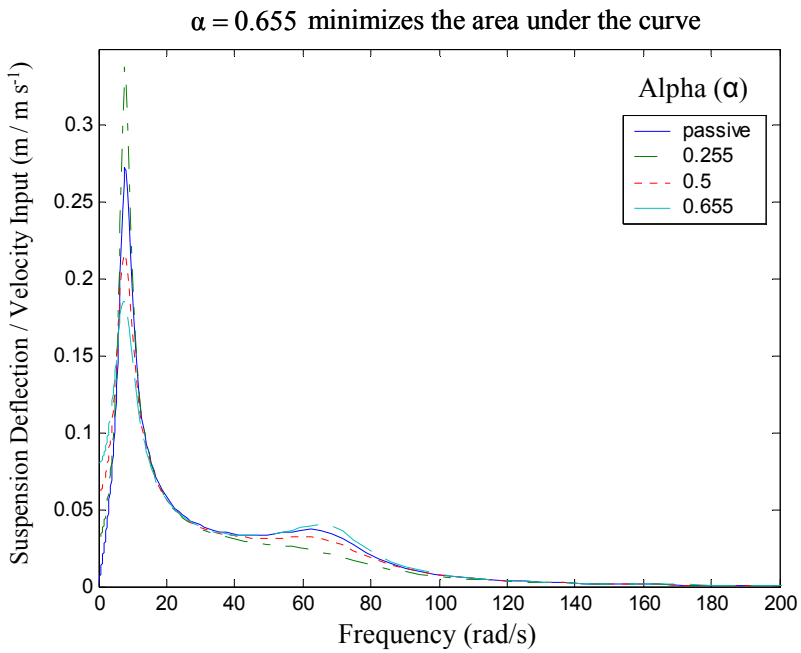

Figure 5.9: Effect of Alpha on Suspension Displacement

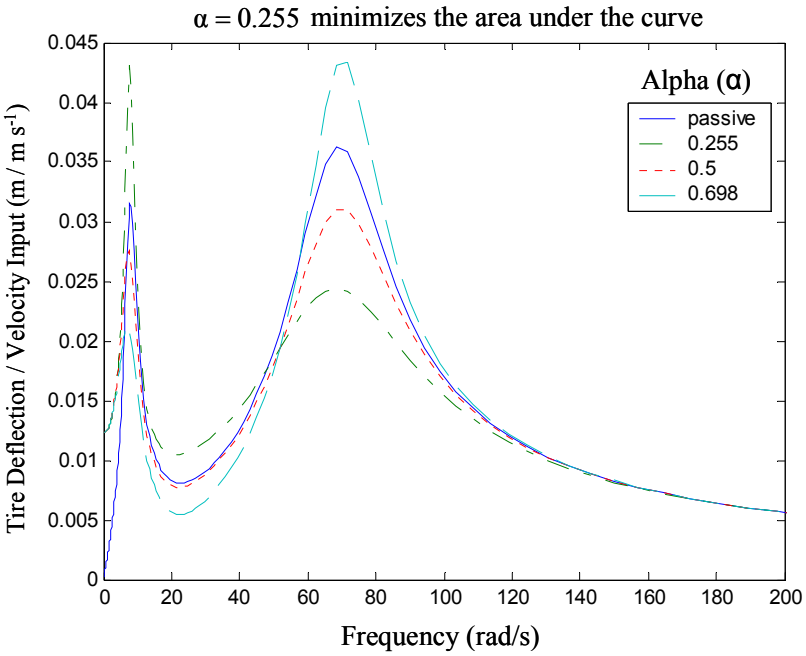

Figure 5.10: Effect of Alpha on Tire Displacement

Figure 5.8 shows that taking the optimal value of α for the comfort index, i.e., $\alpha = 0.698$ results in a better comfort except for frequencies near the unsprung mass natural frequency ω_u. Not only it is optimal for overall frequencies, it also reduces the peak value.

Figure 5.9 shows that taking the optimal value of α for the suspension displacement index, i.e., $\alpha = 0.655$, results in less suspension displacement except for frequencies near the unsprung mass natural frequency ω_u. This optimal value $\alpha = 0.655$ yields a lower suspension displacement peak.

Figure 5.10 shows that the optimal value of α for the tire displacement (i.e., $\alpha = 0.255$) reduces the vibration energy in the tire for overall frequencies, but at the cost of a higher peak value near the sprung mass natural frequency ω_s. It is still a much better value than $\alpha = 0.698$ for instance, which yields an even higher transmibility peak obtained near ω_u. It is not obviously better than taking $\alpha = 0.5$ though.

As a conclusion, the three figures clearly show that the value of α used in Chapter 3 (i.e., $\alpha = 0.5$) was a very good compromise: it is the only value displayed in the figures that clearly yields better results than the passive case for each of the three performance indices. It is also the only value that yields lower transmibilities than the passive case at any frequency, for each of the three transmibilities used for computing our indices.

6 Conclusion and Recommendations

This chapter provides a summary of the research presented in the previous chapters and the significant results that were obtained. It further includes several recommendations for future work that should be pursued in this area of research.

6.1 Summary

Skyhook, groundhook, and hybrid control techniques are semiactive control techniques that can be effectively applied to automobile suspensions. The behavior of a semi-actively-suspended vehicle using these three control policies has been evaluated analytically and compared to the behavior of a passively-suspended vehicle.

In this research, a passive representation of the semi-active suspensions has been used. This representation takes in account the fact that it is not possible to completely eliminate any amount of damping in the suspension. With this linear approximation, it has been possible to work in the frequency domain and optimize performance indices related to different transmibilities for a two-degree-of-freedom 'quarter-car' model, assuming random road disturbances. Three main performance indices were derived. They were used as a measure of vibration isolation (which can be seen as a comfort index), suspension travel requirements, and road-holding quality. After briefly studying the frequency responses in order to have a better understanding of how the performance indices are affected by every frequency component, the relationship between vibration isolation, suspension travel, and road-holing quality has been evaluated through different parametric studies for each configuration (passive, skyhook, groundhook, and hybrid). The hybrid configuration yields the best results. For typical values associated to passenger cars, the results indicate that the hybrid configuration yields a better comfort than a passive suspension, without reducing the road-holding quality or increasing the suspension displacement for most passenger cars.

The quarter-car model could only be used to study the heave motion. Therefore, a seven-degree-of-freedom numerical model of a full-vehicle has been developed to study the heave, pitch, and roll motions of vehicle, for periodic and discrete road inputs. The results obtained for the periodic road inputs showed that the motion of the quarter-car model was not only a good approximation of the heave motion of a full-vehicle model, but also of the pitch and roll motions since both are similar to the heave motion.

Finally, H_2 optimization techniques have been used in order to find closed-form solutions minimizing the performance indices defined for the quarter-car. Closed forms solutions were found for a passively-suspended car. For the semi-active configuration, the optimizations yield infinite damping ratios. Therefore, contour plots have been used to show the effect of damping on the different performance indices. Finally, numerical simulations have shown that the relative ratio between the skyhook and groundhook control that was used for the hybrid configuration all along this study, i.e., $\alpha = 0.5$, results in a very good compromise between comfort, road-holding and suspension travel requirements, compared to other values of α. It indicates that the results obtained during this study with the hybrid configuration are probably good results for a semi-active suspension, at least for typical passenger cars.

6.2 Recommendations for Future Research

Minimizing the H_2 norm is sometimes done at the cost of a higher peak, especially for the comfort index. Minimizing the H_2 norm for the comfort index results in a worst case scenario. Generally, the comfort is improved, but if the frequency input gets too close to the sprung mass frequency for too long, the ride becomes extremely harsh. The peak value is also called the H_∞ norm. An extension of this work would be to develop mixed H_2/H_∞ techniques. The best approach would probably be to specify a maximum acceptable peak, and minimize the H_2 norm without reaching the value that was specified at any frequency.

The model used for the semi-active suspension configurations was a linear approximation. An extension of this work would be to compare the contour plots showing the effect of damping on the three performance indices with experimental contour plots obtained with he same numerical values.

Appendix 1: Detailed Expressions of the Mean Square Responses

The dimensionless expressions shown in Equations (3.12) through (3.14) are detailed below: (conoff represents $C_{on} - C_{off}$)

$$
\begin{aligned}
&E[x_1^2] = \\
&\Big(ku\,\pi\,S0\,\big(-coff\,ks\,ku\,ms^3 - conoff\,ks\,ku\,ms^3 - coff\,ks\,ku\,ms^2\,mu + conoff\,ks\,ku\,ms^3\,\alpha - \\
&\quad conoff\,ks\,ku\,ms^2\,mu\,\alpha - coff^2\,conoff^3\,ms\,\alpha^2 - coff\,conoff^4\,ms\,\alpha^2 - coff\,conoff^2\,ks\,ms^2\,\alpha^2 - \\
&\quad conoff^3\,ks\,ms^2\,\alpha^2 - coff\,conoff^2\,ku\,ms^2\,\alpha^2 - conoff^3\,ku\,ms^2\,\alpha^2 - coff^2\,conoff^3\,mu\,\alpha^2 - \\
&\quad 2\,coff\,conoff^2\,ks\,ms\,mu\,\alpha^2 - coff\,conoff^2\,ks\,mu^2\,\alpha^2 - conoff^5\,ms\,\alpha^3 + conoff^3\,ks\,ms^2\,\alpha^3 + \\
&\quad conoff^3\,ku\,ms^2\,\alpha^3 - 2\,coff\,conoff^4\,mu\,\alpha^3 - conoff^3\,ks\,mu^2\,\alpha^3 + coff\,conoff^4\,ms\,\alpha^4 + \\
&\quad 2\,conoff^5\,ms\,\alpha^4 + coff\,conoff^4\,mu\,\alpha^4 - conoff^5\,mu\,\alpha^4 - conoff^5\,ms\,\alpha^5 + conoff^5\,mu\,\alpha^5\big)\Big) / \\
&\Big(ks\,\big(-coff^2\,conoff^2\,ks\,ms - coff\,conoff^3\,ks\,ms - coff^3\,conoff\,ku\,ms - coff^2\,conoff^2\,ku\,ms - \\
&\quad coff\,conoff\,ks^2\,ms^2 - conoff^2\,ks^2\,ms^2 - coff^2\,ku^2\,ms^2 - coff\,conoff\,ku^2\,ms^2 - \\
&\quad coff^2\,conoff^2\,ks\,mu - coff^3\,conoff\,ku\,mu - 2\,coff\,conoff\,ks^2\,ms\,mu + \\
&\quad 2\,coff\,conoff\,ks\,ku\,ms\,mu - coff\,conoff\,ks^2\,mu^2 - conoff^4\,ks\,ms\,\alpha - coff^2\,conoff^2\,ku\,ms\,\alpha - \\
&\quad 2\,coff\,conoff^3\,ku\,ms\,\alpha + conoff^2\,ks^2\,ms^2\,\alpha - 2\,coff\,conoff\,ks\,ku\,ms^2\,\alpha - \\
&\quad 2\,conoff^2\,ks\,ku\,ms^2\,\alpha - conoff^2\,ku^2\,ms^2\,\alpha - 2\,coff\,conoff^3\,ks\,mu\,\alpha - 3\,coff^2\,conoff^2\,ku\,mu\,\alpha - \\
&\quad 2\,coff\,conoff\,ks\,ku\,ms\,mu\,\alpha + 2\,conoff^2\,ks\,ku\,ms\,mu\,\alpha - conoff^2\,ks^2\,mu^2\,\alpha + \\
&\quad coff\,conoff^3\,ks\,ms\,\alpha^2 + 2\,conoff^4\,ks\,ms\,\alpha^2 + coff^2\,conoff^2\,ku\,ms\,\alpha^2 + 2\,coff\,conoff^3\,ku\,ms\,\alpha^2 - \\
&\quad conoff^4\,ku\,ms\,\alpha^2 + 2\,conoff^2\,ks\,ku\,ms^2\,\alpha^2 + conoff^2\,ku^2\,ms^2\,\alpha^2 + coff\,conoff^3\,ks\,mu\,\alpha^2 - \\
&\quad conoff^4\,ks\,mu\,\alpha^2 + coff^2\,conoff^2\,ku\,mu\,\alpha^2 - 3\,coff\,conoff^3\,ku\,mu\,\alpha^2 - \\
&\quad 2\,conoff^2\,ks\,ku\,ms\,mu\,\alpha^2 - conoff^4\,ks\,ms\,\alpha^3 + 2\,conoff^4\,ku\,ms\,\alpha^3 + conoff^4\,ks\,mu\,\alpha^3 + \\
&\quad 2\,coff\,conoff^3\,ku\,mu\,\alpha^3 - conoff^4\,ku\,mu\,\alpha^3 - conoff^4\,ku\,ms\,\alpha^4 + conoff^4\,ku\,mu\,\alpha^4\big)\Big)
\end{aligned}
$$

$$
\begin{aligned}
&E[\dot{x}_2^2] = \\
&\Big(ku^2\,\pi\,S0\,\big(coff^2\,conoff\,ks + coff^3\,ku + coff\,ks^2\,ms + conoff\,ks^2\,ms + coff\,ks^2\,mu + \\
&\quad coff^2\,conoff\,ku\,\alpha - conoff\,ks^2\,ms\,\alpha + conoff\,ks^2\,mu\,\alpha\big)\Big) / \\
&\Big(coff^2\,conoff^2\,ks\,ms + coff\,conoff^3\,ks\,ms + coff^3\,conoff\,ku\,ms + coff^2\,conoff^2\,ku\,ms + \\
&\quad coff\,conoff\,ks^2\,ms^2 + conoff^2\,ks^2\,ms^2 + coff^2\,ku^2\,ms^2 + coff\,conoff\,ku^2\,ms^2 + \\
&\quad coff^2\,conoff^2\,ks\,mu + coff^3\,conoff\,ku\,mu + 2\,coff\,conoff\,ks^2\,ms\,mu - 2\,coff\,conoff\,ks\,ku\,ms\,mu + \\
&\quad coff\,conoff\,ks^2\,mu^2 + conoff^4\,ks\,ms\,\alpha + coff^2\,conoff^2\,ku\,ms\,\alpha + 2\,coff\,conoff^3\,ku\,ms\,\alpha - \\
&\quad conoff^2\,ks^2\,ms^2\,\alpha + 2\,coff\,conoff\,ks\,ku\,ms^2\,\alpha + 2\,conoff^2\,ks\,ku\,ms^2\,\alpha + conoff^2\,ku^2\,ms^2\,\alpha + \\
&\quad 2\,coff\,conoff^3\,ks\,mu\,\alpha + 3\,coff^2\,conoff^2\,ku\,mu\,\alpha + 2\,coff\,conoff\,ks\,ku\,ms\,mu\,\alpha - \\
&\quad 2\,conoff^2\,ks\,ku\,ms\,mu\,\alpha + conoff^2\,ks^2\,mu^2\,\alpha - coff\,conoff^3\,ks\,ms\,\alpha^2 - 2\,conoff^4\,ks\,ms\,\alpha^2 - \\
&\quad coff^2\,conoff^2\,ku\,ms\,\alpha^2 - 2\,coff\,conoff^3\,ku\,ms\,\alpha^2 + conoff^4\,ku\,ms\,\alpha^2 - 2\,conoff^2\,ks\,ku\,ms^2\,\alpha^2 - \\
&\quad conoff^2\,ku^2\,ms^2\,\alpha^2 - coff\,conoff^3\,ks\,mu\,\alpha^2 + conoff^4\,ks\,mu\,\alpha^2 - coff^2\,conoff^2\,ku\,mu\,\alpha^2 + \\
&\quad 3\,coff\,conoff^3\,ku\,mu\,\alpha^2 + 2\,conoff^2\,ks\,ku\,ms\,mu\,\alpha^2 + conoff^4\,ks\,ms\,\alpha^3 - 2\,conoff^4\,ku\,ms\,\alpha^3 - \\
&\quad conoff^4\,ks\,mu\,\alpha^3 - 2\,coff\,conoff^3\,ku\,mu\,\alpha^3 + conoff^4\,ku\,mu\,\alpha^3 + conoff^4\,ku\,ms\,\alpha^4 - conoff^4\,ku\,mu\,\alpha^4\big)
\end{aligned}
$$

$$E\left[x_3^2\right] =$$

$$\left(\pi\, S0\, \left(-coff^2\, conoff^3\, ks\, ms - coff\, conoff^4\, ks\, ms - coff^3\, conoff^2\, ku\, ms - coff^2\, conoff^3\, ku\, ms - coff\, conoff^2\, ks^2\, ms^2 - conoff^3\, ks^2\, ms^2 - coff^2\, conoff\, ks\, ku\, ms^2 - coff\, conoff^2\, ks\, ku\, ms^2 - coff^3\, ku^2\, ms^2 - 2\, coff^2\, conoff\, ku^2\, ms^2 - coff\, conoff^2\, ku^2\, ms^2 - coff\, ks^2\, ku\, ms^3 - conoff\, ks^2\, ku\, ms^3 - coff^2\, conoff^3\, ks\, mu - coff^3\, conoff^2\, ku\, mu - 2\, coff\, conoff^2\, ks^2\, ms\, mu - 2\, coff^2\, conoff\, ks\, ku\, ms\, mu + coff\, conoff^2\, ks\, ku\, ms\, mu - 2\, coff^3\, ku^2\, ms\, mu - coff^2\, conoff\, ku^2\, ms\, mu - 3\, coff\, ks^2\, ku\, ms^2\, mu - conoff\, ks^2\, ku\, ms^2\, mu + 2\, coff\, ks\, ku^2\, ms^2\, mu - coff\, ku^3\, ms^2\, mu - coff\, conoff^2\, ks^2\, mu^2 - coff^2\, conoff\, ks\, ku\, mu^2 - coff^3\, ku^2\, mu^2 - 3\, coff\, ks^2\, ku\, ms\, mu^2 + 2\, coff\, ks\, ku^2\, ms\, mu^2 - coff\, ks^2\, ku\, mu^3 - conoff^5\, ks\, ms\, \alpha - coff^2\, conoff^3\, ku\, ms\, \alpha - 2\, coff\, conoff^4\, ku\, ms\, \alpha + conoff^3\, ks^2\, ms^2\, \alpha - 2\, coff\, conoff^2\, ks\, ku\, ms^2\, \alpha - 3\, conoff^3\, ks\, ku\, ms^2\, \alpha + coff^2\, conoff\, ku^2\, ms^2\, \alpha - conoff^3\, ku^2\, ms^2\, \alpha + conoff\, ks^2\, ku\, ms^3\, \alpha - 2\, coff\, conoff^4\, ks\, mu\, \alpha - 3\, coff^2\, conoff^3\, ku\, mu\, \alpha - 4\, coff\, conoff^2\, ks\, ku\, ms\, mu\, \alpha + conoff^3\, ks\, ku\, ms\, mu\, \alpha - 2\, coff^2\, conoff\, ku^2\, ms\, mu\, \alpha - 2\, coff\, conoff^2\, ku^2\, ms\, mu\, \alpha + conoff\, ks^2\, ku\, ms^2\, mu\, \alpha - conoff\, ku^3\, ms^2\, mu\, \alpha - conoff^3\, ks^2\, mu^2\, \alpha - 2\, coff\, conoff^2\, ks\, ku\, mu^2\, \alpha - 3\, coff^2\, conoff\, ku^2\, mu^2\, \alpha - conoff\, ks^2\, ku\, ms\, mu^2\, \alpha + 2\, conoff\, ks\, ku^2\, ms\, mu^2\, \alpha - conoff\, ks^2\, ku\, mu^3\, \alpha + coff\, conoff^4\, ks\, ms\, \alpha^2 + 2\, conoff^5\, ks\, ms\, \alpha^2 + 2\, coff^2\, conoff^3\, ku\, ms\, \alpha^2 + 3\, coff\, conoff^4\, ku\, ms\, \alpha^2 - conoff^5\, ku\, ms\, \alpha^2 + 2\, coff\, conoff^2\, ks\, ku\, ms^2\, \alpha^2 + 5\, conoff^3\, ks\, ku\, ms^2\, \alpha^2 + coff\, conoff^2\, ku^2\, ms^2\, \alpha^2 + 2\, conoff^3\, ku^2\, ms^2\, \alpha^2 + coff\, conoff^4\, ks\, mu\, \alpha^2 - conoff^5\, ks\, mu\, \alpha^2 + 2\, coff^2\, conoff^3\, ku\, mu\, \alpha^2 - 3\, coff\, conoff^4\, ku\, mu\, \alpha^2 + 4\, coff\, conoff^2\, ks\, ku\, ms\, mu\, \alpha^2 - conoff^3\, ks\, ku\, ms\, mu\, \alpha^2 + coff\, conoff^2\, ku^2\, ms\, mu\, \alpha^2 - conoff^3\, ku^2\, ms\, mu\, \alpha^2 + 2\, coff\, conoff^2\, ks\, ku\, mu^2\, \alpha^2 - conoff^3\, ks\, ku\, mu^2\, \alpha^2 - 3\, coff\, conoff^2\, ku^2\, mu^2\, \alpha^2 - conoff^5\, ks\, ms\, \alpha^3 + 3\, conoff^5\, ku\, ms\, \alpha^3 - 2\, conoff^3\, ks\, ku\, ms^2\, \alpha^3 - conoff^3\, ku^2\, ms^2\, \alpha^3 + conoff^5\, ks\, mu\, \alpha^3 + 4\, coff\, conoff^4\, ku\, mu\, \alpha^3 - conoff^5\, ku\, mu\, \alpha^3 + conoff^3\, ku^2\, ms\, mu\, \alpha^3 + 2\, conoff^3\, ks\, ku\, mu^2\, \alpha^3 - conoff^3\, ku^2\, mu^2\, \alpha^3 - coff\, conoff^4\, ku\, ms\, \alpha^4 - 3\, conoff^5\, ku\, ms\, \alpha^4 - coff\, conoff^4\, ku\, mu\, \alpha^4 + 2\, conoff^5\, ku\, mu\, \alpha^4 + conoff^5\, ku\, ms\, \alpha^5 - conoff^5\, ku\, mu\, \alpha^5\right)\right) /$$

$$\left(ku\, \left(-coff^2\, conoff^2\, ks\, ms - coff\, conoff^3\, ks\, ms - coff^3\, conoff\, ku\, ms - coff^2\, conoff^2\, ku\, ms - coff\, conoff\, ks^2\, ms^2 - conoff^2\, ks^2\, ms^2 - coff^2\, ku^2\, ms^2 - coff\, conoff\, ku^2\, ms^2 - coff^2\, conoff^2\, ks\, mu - coff^3\, conoff\, ku\, mu - 2\, coff\, conoff\, ks^2\, ms\, mu + 2\, coff\, conoff\, ks\, ku\, ms\, mu - coff\, conoff\, ks^2\, mu^2 - conoff^4\, ks\, ms\, \alpha - coff^2\, conoff^2\, ku\, ms\, \alpha - 2\, coff\, conoff^3\, ku\, ms\, \alpha + conoff^2\, ks^2\, ms^2\, \alpha - 2\, coff\, conoff\, ks\, ku\, ms^2\, \alpha - 2\, conoff^2\, ks\, ku\, ms^2\, \alpha - conoff^2\, ku^2\, ms^2\, \alpha - 2\, coff\, conoff^3\, ks\, mu\, \alpha - 3\, coff^2\, conoff^2\, ku\, mu\, \alpha - 2\, coff\, conoff\, ks\, ku\, ms\, mu\, \alpha + 2\, conoff^2\, ks\, ku\, ms\, mu\, \alpha - conoff^2\, ks^2\, mu^2\, \alpha + coff\, conoff^3\, ks\, ms\, \alpha^2 + 2\, conoff^4\, ks\, ms\, \alpha^2 + coff^2\, conoff^2\, ku\, ms\, \alpha^2 + 2\, coff\, conoff^3\, ku\, ms\, \alpha^2 - conoff^4\, ku\, ms\, \alpha^2 + 2\, conoff^2\, ks\, ku\, ms^2\, \alpha^2 + conoff^2\, ku^2\, ms^2\, \alpha^2 + coff\, conoff^3\, ks\, mu\, \alpha^2 - conoff^4\, ks\, mu\, \alpha^2 + coff^2\, conoff^2\, ku\, mu\, \alpha^2 - 3\, coff\, conoff^3\, ku\, mu\, \alpha^2 - 2\, conoff^2\, ks\, ku\, ms\, mu\, \alpha^2 - conoff^4\, ks\, ms\, \alpha^3 + 2\, conoff^4\, ku\, ms\, \alpha^3 + conoff^4\, ks\, mu\, \alpha^3 + 2\, coff\, conoff^3\, ku\, mu\, \alpha^3 - conoff^4\, ku\, mu\, \alpha^3 - conoff^4\, ku\, ms\, \alpha^4 + conoff^4\, ku\, mu\, \alpha^4\right)\right)$$

The dimensionless expressions shown in Equations (3.20) through (3.22) are detailed below: (Zonoff represents $\zeta_{on} - \zeta_{off}$, and Zoff represents ζ_{off})

$$\left(\frac{E[x_1^2]}{\pi\, S0}\, wu\right) =$$
$$\left(\left(rk^2\left(rk\, Zoff + rk\, rm\, Zoff + rk\, Zonoff - rk\, Zonoff\,\alpha + rk\, rm\, Zonoff\,\alpha + 4\, Zoff\, Zonoff^2\,\alpha^2 + 4\, rk\, Zoff\, Zonoff^2\,\alpha^2 + 8\, rm\, Zoff\, Zonoff^2\,\alpha^2 + 4\, rm^2\, Zoff\, Zonoff^2\,\alpha^2 + 4\, Zonoff^3\,\alpha^2 + 4\, rk\, Zonoff^3\,\alpha^2 + 16\, Zoff^2\, Zonoff^3\,\alpha^2 + 16\, rm\, Zoff^2\, Zonoff^3\,\alpha^2 + 16\, Zoff\, Zonoff^4\,\alpha^2 - 4\, Zonoff^3\,\alpha^3 - 4\, rk\, Zonoff^3\,\alpha^3 + 4\, rm^2\, Zonoff^3\,\alpha^3 + 32\, rm\, Zoff\, Zonoff^4\,\alpha^3 + 16\, Zonoff^5\,\alpha^3 - 16\, Zoff\, Zonoff^4\,\alpha^4 - 16\, rm\, Zoff\, Zonoff^4\,\alpha^4 - 32\, Zonoff^5\,\alpha^4 + 16\, rm\, Zonoff^5\,\alpha^4 + 16\, Zonoff^5\,\alpha^5 - 16\, rm\, Zonoff^5\,\alpha^5\right)\right) \Big/$$
$$\left(2\sqrt{rk\, rm}\,\left(rk^2\, Zoff^2 + Zoff\, Zonoff + rk^2\, Zoff\, Zonoff + 2\, rm\, Zoff\, Zonoff - 2\, rk\, rm\, Zoff\, Zonoff + rm^2\, Zoff\, Zonoff + 4\, rk\, Zoff^3\, Zonoff + 4\, rk\, rm\, Zoff^3\, Zonoff + Zonoff^2 + 4\, Zoff^2\, Zonoff^2 + 4\, rk\, Zoff^2\, Zonoff^2 + 4\, rm\, Zoff^2\, Zonoff^2 + 4\, Zoff\, Zonoff^3 + 2\, rk\, Zoff\, Zonoff\,\alpha + 2\, rk\, rm\, Zoff\, Zonoff\,\alpha - Zonoff^2\,\alpha + 2\, rk\, Zonoff^2\,\alpha + rk^2\, Zonoff^2\,\alpha - 2\, rk\, rm\, Zonoff^2\,\alpha + rm^2\, Zonoff^2\,\alpha + 4\, rk\, Zoff^2\, Zonoff^2\,\alpha + 12\, rk\, rm\, Zoff^2\, Zonoff^2\,\alpha + 8\, rk\, Zoff\, Zonoff^3\,\alpha + 8\, rm\, Zoff\, Zonoff^3\,\alpha + 4\, Zonoff^4\,\alpha - 2\, rk\, Zonoff^2\,\alpha^2 - rk^2\, Zonoff^2\,\alpha^2 + 2\, rk\, rm\, Zonoff^2\,\alpha^2 - 4\, rk\, Zoff^2\, Zonoff^2\,\alpha^2 - 4\, rk\, rm\, Zoff^2\, Zonoff^2\,\alpha^2 - 4\, Zoff\, Zonoff^3\,\alpha^2 - 8\, rk\, Zoff\, Zonoff^3\,\alpha^2 - 4\, rm\, Zoff\, Zonoff^3\,\alpha^2 + 12\, rk\, rm\, Zoff\, Zonoff^3\,\alpha^2 - 8\, Zonoff^4\,\alpha^2 + 4\, rk\, Zonoff^4\,\alpha^2 + 4\, rm\, Zonoff^4\,\alpha^2 - 8\, rk\, rm\, Zoff\, Zonoff^3\,\alpha^3 + 4\, Zonoff^4\,\alpha^3 - 8\, rk\, Zonoff^4\,\alpha^3 - 4\, rm\, Zonoff^4\,\alpha^3 + 4\, rk\, rm\, Zonoff^4\,\alpha^3 + 4\, rk\, Zonoff^4\,\alpha^4 - 4\, rk\, rm\, Zonoff^4\,\alpha^4\right)\right)$$

$$\left(\frac{E[\dot{x}_2^2]}{\pi\, S0\, wu^3}\right) =$$
$$\left(rk\, rm^2\left(Zoff + rm\, Zoff + 4\, rk\, Zoff^3 + Zonoff + 4\, Zoff^2\, Zonoff - Zonoff\,\alpha + rm\, Zonoff\,\alpha + 4\, rk\, Zoff^2\, Zonoff\,\alpha\right)\right) \Big/$$
$$\left(2\sqrt{rk\, rm}\,\left(rk^2\, Zoff^2 + Zoff\, Zonoff + rk^2\, Zoff\, Zonoff + 2\, rm\, Zoff\, Zonoff - 2\, rk\, rm\, Zoff\, Zonoff + rm^2\, Zoff\, Zonoff + 4\, rk\, Zoff^3\, Zonoff + 4\, rk\, rm\, Zoff^3\, Zonoff + Zonoff^2 + 4\, Zoff^2\, Zonoff^2 + 4\, rk\, Zoff^2\, Zonoff^2 + 4\, rm\, Zoff^2\, Zonoff^2 + 4\, Zoff\, Zonoff^3 + 2\, rk\, Zoff\, Zonoff\,\alpha + 2\, rk\, rm\, Zoff\, Zonoff\,\alpha - Zonoff^2\,\alpha + 2\, rk\, Zonoff^2\,\alpha + rk^2\, Zonoff^2\,\alpha - 2\, rk\, rm\, Zonoff^2\,\alpha + rm^2\, Zonoff^2\,\alpha + 4\, rk\, Zoff^2\, Zonoff^2\,\alpha + 12\, rk\, rm\, Zoff^2\, Zonoff^2\,\alpha + 8\, rk\, Zoff\, Zonoff^3\,\alpha + 8\, rm\, Zoff\, Zonoff^3\,\alpha + 4\, Zonoff^4\,\alpha - 2\, rk\, Zonoff^2\,\alpha^2 - rk^2\, Zonoff^2\,\alpha^2 + 2\, rk\, rm\, Zonoff^2\,\alpha^2 - 4\, rk\, Zoff^2\, Zonoff^2\,\alpha^2 - 4\, rk\, rm\, Zoff^2\, Zonoff^2\,\alpha^2 - 4\, Zoff\, Zonoff^3\,\alpha^2 - 8\, rk\, Zoff\, Zonoff^3\,\alpha^2 - 4\, rm\, Zoff\, Zonoff^3\,\alpha^2 + 12\, rk\, rm\, Zoff\, Zonoff^3\,\alpha^2 - 8\, Zonoff^4\,\alpha^2 + 4\, rk\, Zonoff^4\,\alpha^2 + 4\, rm\, Zonoff^4\,\alpha^2 - 8\, rk\, rm\, Zoff\, Zonoff^3\,\alpha^3 + 4\, Zonoff^4\,\alpha^3 - 8\, rk\, Zonoff^4\,\alpha^3 - 4\, rm\, Zonoff^4\,\alpha^3 + 4\, rk\, rm\, Zonoff^4\,\alpha^3 + 4\, rk\, Zonoff^4\,\alpha^4 - 4\, rk\, rm\, Zonoff^4\,\alpha^4\right)\right)$$

$$\left(\frac{E[x_3^2]}{\pi\, S0}\ wu\right) =$$

$$\Big(\big(rk\ Zoff + 3\ rk\ rm\ Zoff - 2\ rk^2\ rm\ Zoff + rk^3\ rm\ Zoff + 3\ rk\ rm^2\ Zoff - 2\ rk^2\ rm^2\ Zoff +$$
$$rk\ rm^3\ Zoff + 4\ rk^2\ Zoff^3 + 8\ rk^2\ rm\ Zoff^3 + 4\ rk^2\ rm^2\ Zoff^3 + rk\ Zonoff + rk\ rm\ Zonoff +$$
$$4\ rk\ Zoff^2\ Zonoff + 8\ rk^2\ Zoff^2\ Zonoff + 8\ rk\ rm\ Zoff^2\ Zonoff + 4\ rk^2\ rm\ Zoff^2\ Zonoff +$$
$$4\ rk\ rm^2\ Zoff^2\ Zonoff + 4\ Zoff\ Zonoff^2 + 4\ rk\ Zoff\ Zonoff^2 + 4\ rk^2\ Zoff\ Zonoff^2 +$$
$$8\ rm\ Zoff\ Zonoff^2 - 4\ rk\ rm\ Zoff\ Zonoff^2 + 4\ rm^2\ Zoff\ Zonoff^2 + 16\ rk\ Zoff^3\ Zonoff^2 +$$
$$16\ rk\ rm\ Zoff^3\ Zonoff^2 + 4\ Zonoff^3 + 16\ Zoff^2\ Zonoff^3 + 16\ rk\ Zoff^2\ Zonoff^3 +$$
$$16\ rm\ Zoff^2\ Zonoff^3 + 16\ Zoff\ Zonoff^4 - rk\ Zonoff\ \alpha - rk\ rm\ Zonoff\ \alpha + rk^3\ rm\ Zonoff\ \alpha +$$
$$rk\ rm^2\ Zonoff\ \alpha - 2\ rk^2\ rm^2\ Zonoff\ \alpha + rk\ rm^3\ Zonoff\ \alpha - 4\ rk^2\ Zoff^2\ Zonoff\ \alpha +$$
$$8\ rk^2\ rm\ Zoff^2\ Zonoff\ \alpha + 12\ rk^2\ rm^2\ Zoff^2\ Zonoff\ \alpha + 8\ rk\ Zoff\ Zonoff^2\ \alpha +$$
$$16\ rk\ rm\ Zoff\ Zonoff^2\ \alpha + 8\ rk^2\ rm\ Zoff\ Zonoff^2\ \alpha + 8\ rk\ rm^2\ Zoff\ Zonoff^2\ \alpha -$$
$$4\ Zonoff^3\ \alpha + 12\ rk\ Zonoff^3\ \alpha + 4\ rk^2\ Zonoff^3\ \alpha - 4\ rk\ rm\ Zonoff^3\ \alpha + 4\ rm^2\ Zonoff^3\ \alpha +$$
$$16\ rk\ Zoff^2\ Zonoff^3\ \alpha + 48\ rk\ rm\ Zoff^2\ Zonoff^3\ \alpha + 32\ rk\ Zoff\ Zonoff^4\ \alpha +$$
$$32\ rm\ Zoff\ Zonoff^4\ \alpha + 16\ Zonoff^5\ \alpha - 8\ rk\ Zoff\ Zonoff^2\ \alpha^2 - 4\ rk^2\ Zoff\ Zonoff^2\ \alpha^2 -$$
$$16\ rk\ rm\ Zoff\ Zonoff^2\ \alpha^2 - 4\ rk^2\ rm\ Zoff\ Zonoff^2\ \alpha^2 - 8\ rk\ rm^2\ Zoff\ Zonoff^2\ \alpha^2 +$$
$$12\ rk^2\ rm^2\ Zoff\ Zonoff^2\ \alpha^2 - 20\ rk\ Zonoff^3\ \alpha^2 - 8\ rk^2\ Zonoff^3\ \alpha^2 + 4\ rk\ rm\ Zonoff^3\ \alpha^2 +$$
$$4\ rk^2\ rm\ Zonoff^3\ \alpha^2 + 4\ rk\ rm^2\ Zonoff^3\ \alpha^2 - 32\ rk\ Zoff^2\ Zonoff^3\ \alpha^2 - 32\ rk\ rm\ Zoff^2\ Zonoff^3\ \alpha^2 -$$
$$16\ Zoff\ Zonoff^4\ \alpha^2 - 48\ rk\ Zoff\ Zonoff^4\ \alpha^2 - 16\ rm\ Zoff\ Zonoff^4\ \alpha^2 + 48\ rk\ rm\ Zoff\ Zonoff^4\ \alpha^2 -$$
$$32\ Zonoff^5\ \alpha^2 + 16\ rk\ Zonoff^5\ \alpha^2 + 16\ rm\ Zonoff^5\ \alpha^2 + 8\ rk\ Zonoff^3\ \alpha^3 + 4\ rk^2\ Zonoff^3\ \alpha^3 -$$
$$4\ rk^2\ rm\ Zonoff^3\ \alpha^3 - 8\ rk\ rm^2\ Zonoff^3\ \alpha^3 + 4\ rk^2\ rm^2\ Zonoff^3\ \alpha^3 - 64\ rk\ rm\ Zoff\ Zonoff^4\ \alpha^3 +$$
$$16\ Zonoff^5\ \alpha^3 - 48\ rk\ Zonoff^5\ \alpha^3 - 16\ rm\ Zonoff^5\ \alpha^3 + 16\ rk\ rm\ Zonoff^5\ \alpha^3 +$$
$$16\ rk\ Zoff\ Zonoff^4\ \alpha^4 + 16\ rk\ rm\ Zoff\ Zonoff^4\ \alpha^4 + 48\ rk\ Zonoff^5\ \alpha^4 - 32\ rk\ rm\ Zonoff^5\ \alpha^4 -$$
$$16\ rk\ Zonoff^5\ \alpha^5 + 16\ rk\ rm\ Zonoff^5\ \alpha^5\big)\Big) \Big/$$
$$\Big(2\sqrt{rk\ rm}\ \big(rk^2\ Zoff^2 + Zoff\ Zonoff + rk^2\ Zoff\ Zonoff + 2\ rm\ Zoff\ Zonoff -$$
$$2\ rk\ rm\ Zoff\ Zonoff + rm^2\ Zoff\ Zonoff + 4\ rk\ Zoff^3\ Zonoff + 4\ rk\ rm\ Zoff^3\ Zonoff +$$
$$Zonoff^2 + 4\ Zoff^2\ Zonoff^2 + 4\ rk\ Zoff^2\ Zonoff^2 + 4\ rm\ Zoff^2\ Zonoff^2 + 4\ Zoff\ Zonoff^3 +$$
$$2\ rk\ Zoff\ Zonoff\ \alpha + 2\ rk\ rm\ Zoff\ Zonoff\ \alpha - Zonoff^2\ \alpha + 2\ rk\ Zonoff^2\ \alpha + rk^2\ Zonoff^2\ \alpha -$$
$$2\ rk\ rm\ Zonoff^2\ \alpha + rm^2\ Zonoff^2\ \alpha + 4\ rk\ Zoff^2\ Zonoff^2\ \alpha + 12\ rk\ rm\ Zoff^2\ Zonoff^2\ \alpha +$$
$$8\ rk\ Zoff\ Zonoff^3\ \alpha + 8\ rm\ Zoff\ Zonoff^3\ \alpha + 4\ Zonoff^4\ \alpha - 2\ rk\ Zonoff^2\ \alpha^2 -$$
$$rk^2\ Zonoff^2\ \alpha^2 + 2\ rk\ rm\ Zonoff^2\ \alpha^2 - 4\ rk\ Zoff^2\ Zonoff^2\ \alpha^2 - 4\ rk\ rm\ Zoff^2\ Zonoff^2\ \alpha^2 -$$
$$4\ Zoff\ Zonoff^3\ \alpha^2 - 8\ rk\ Zoff\ Zonoff^3\ \alpha^2 - 4\ rm\ Zoff\ Zonoff^3\ \alpha^2 + 12\ rk\ rm\ Zoff\ Zonoff^3\ \alpha^2 -$$
$$8\ Zonoff^4\ \alpha^2 + 4\ rk\ Zonoff^4\ \alpha^2 + 4\ rm\ Zonoff^4\ \alpha^2 - 8\ rk\ rm\ Zoff\ Zonoff^3\ \alpha^3 +$$
$$4\ Zonoff^4\ \alpha^3 - 8\ rk\ Zonoff^4\ \alpha^3 - 4\ rm\ Zonoff^4\ \alpha^3 + 4\ rk\ rm\ Zonoff^4\ \alpha^3 + 4\ rk\ Zonoff^4\ \alpha^4 -$$
$$4\ rk\ rm\ Zonoff^4\ \alpha^4\big)\Big)$$

Appendix 2: Equations of Motion for the Full Car Model

The 14 equations of motion obtained for the actual passive representation of the semi active suspension are shown below. Replacing α by 0 yields the equations of motion for the ideal groundhook configuration. Replacing α by 1 yields the equations of motion for the ideal skyhook configuration. Replacing $C_{off,i}$ by $C_{S,i}$ and $(C_{on,i} - C_{off,i})$ by 0 (with $i = 1,\ 2,\ \ldots 4$) yields the equations for the passive system used in [2].

$$\begin{aligned} &M_S\ \dot{x}_1 + K_{S1}\ x_4 + K_{S2}\ x_5 + K_{S3}\ x_6 + K_{S4}\ x_7 \\ &+ \alpha\,(c_{on1} - c_{off1})\,(\dot{x}_4 + x_8) + c_{off1}\ \dot{x}_4 + \alpha\,(c_{on2} - c_{off2})\,(\dot{x}_5 + x_9) + c_{off2}\ \dot{x}_5 \\ &+ \alpha\,(c_{on3} - c_{off3})\,(\dot{x}_6 + x_{10}) + c_{off3}\ \dot{x}_6 + \alpha\,(c_{on4} - c_{off4})\,(\dot{x}_7 + x_{11}) + c_{off4}\ \dot{x}_7 = 0 \end{aligned} \tag{A2.1}$$

$$\begin{aligned} &I_{YY}\ \dot{x}_2 + l_r\,(K_{S2}\ x_5 + K_{S3}\ x_6) - l_f\,(K_{S1}\ x_4 + K_{S4}\ x_7) \\ &- l_f\,[\,\alpha\,(c_{on1} - c_{off1})\,(\dot{x}_4 + x_8) + c_{off1}\ \dot{x}_4\,] \\ &+ l_r\,[\,\alpha\,(c_{on2} - c_{off2})\,(\dot{x}_5 + x_9) + c_{off2}\ \dot{x}_5\,] \\ &+ l_r\,[\,\alpha\,(c_{on3} - c_{off3})\,(\dot{x}_6 + x_{10}) + c_{off3}\ \dot{x}_6\,] \\ &- l_f\,[\,\alpha\,(c_{on4} - c_{off4})\,(\dot{x}_7 + x_{11}) + c_{off4}\ \dot{x}_7\,] = 0 \end{aligned} \tag{A2.2}$$

$$\begin{aligned} &I_{XX}\ \dot{x}_3 + \frac{t_f}{2} K_{S4}\ x_7 + \frac{t_r}{2} K_{S3}\ x_6 - \frac{t_f}{2} K_{S1}\ x_4 - \frac{t_r}{2} K_{S2}\ x_5 \\ &\quad - \frac{t_f}{2}\,[\,\alpha\,(c_{on1} - c_{off1})\,(\dot{x}_4 + x_8) + c_{off1}\ \dot{x}_4\,] \\ &\quad - \frac{t_r}{2}\,[\,\alpha\,(c_{on2} - c_{off2})\,(\dot{x}_5 + x_9) + c_{off2}\ \dot{x}_5\,] \\ &\quad + \frac{t_r}{2}\,[\,\alpha\,(c_{on3} - c_{off3})\,(\dot{x}_6 + x_{10}) + c_{off3}\ \dot{x}_6\,] \\ &\quad + \frac{t_f}{2}\,[\,\alpha\,(c_{on4} - c_{off4})\,(\dot{x}_7 + x_{11}) + c_{off4}\ \dot{x}_7\,] \\ &\quad\quad - \frac{K_r}{t_r}(x_5 - x_6) - \frac{K_f}{t_f}(x_4 - x_7) = 0 \end{aligned} \tag{A2.3}$$

$$\dot{x}_4 = x_1 - x_2\, l_f - x_3\, \frac{t_f}{2} - x_8 \tag{A2.4}$$

$$\dot{x}_5 = x_1 + x_2\, l_r - x_3\, \frac{t_r}{2} - x_9 \tag{A2.5}$$

$$\dot{x}_6 = x_1 + x_2\, l_r + x_3\, \frac{t_r}{2} - x_{10} \tag{A2.6}$$

$$\dot{x}_7 = x_1 - x_2\, l_f + x_3\, \frac{t_f}{2} - x_{11} \tag{A2.7}$$

$$\begin{aligned} &M_{U1}\, \dot{x}_8 + K_{U1}\left[x_{12} - \frac{t_f}{4}\left(\frac{(x_{\xi 1} - x_{\xi 4})}{t_f} - \frac{(x_{\xi 2} - x_{\xi 3})}{t_r}\right)\right] - K_{S1}\, x_4 \\ &- c_{off1}\, \dot{x}_4 + (1-\alpha)\,(c_{on1} - c_{off1})\, x_8 - \frac{K_f}{t_f^2}(x_4 - x_7) + c_{U1}\,(x_8 - v_{\xi 1}) = 0 \end{aligned} \tag{A2.8}$$

$$\begin{aligned} &M_{U2}\, \dot{x}_9 + K_{U2}\left[x_{13} + \frac{t_r}{4}\left(\frac{(x_{\xi 1} - x_{\xi 4})}{t_f} - \frac{(x_{\xi 2} - x_{\xi 3})}{t_r}\right)\right] - K_{S2}\, x_5 \\ &- c_{off2}\, \dot{x}_5 + (1-\alpha)\,\, (c_{on2} - c_{off2})\, x_9 - \frac{K_r}{t_r^2}(x_5 - x_6) + c_{U2}\,(x_9 - v_{\xi 2}) = 0 \end{aligned} \tag{A2.9}$$

$$\begin{aligned} &M_{U3}\, \dot{x}_{10} + K_{U3}\left[x_{14} - \frac{t_r}{4}\left(\frac{(x_{\xi 1} - x_{\xi 4})}{t_f} - \frac{(x_{\xi 2} - x_{\xi 3})}{t_r}\right)\right] - K_{S3}\, x_6 \\ &- c_{off3}\, \dot{x}_6 + (1-\alpha)\,(c_{on3} - c_{off3})\, x_{10} + \frac{K_r}{t_r^2}(x_5 - x_6) + c_{U3}\,(x_{10} - v_{\xi 3}) = 0 \end{aligned} \tag{A2.10}$$

$$M_{U4}\,\dot{x}_{11} + K_{U4}\left[(x_4 + x_{12} - x_7) - \left[(x_5 + x_{13}) - (x_6 + x_{14})\right]\frac{t_f}{t_r} + \ldots \right.$$
$$\left. \frac{t_f}{4}\left(\frac{(x_{\xi 1} - x_{\xi 4})}{t_f} - \frac{(x_{\xi 2} - x_{\xi 3})}{t_r}\right)\right] \qquad \text{(A2.11)}$$
$$- K_{S4}\,x_7 - c_{off4}\,\dot{x}_7 + (1-\alpha)\,(c_{on4} - c_{off4})\,x_{11} + \frac{K_f}{t_f^2}(x_4 - x_7) + c_{U4}\,(x_{11} - v_{\xi 4}) = 0$$

$$\dot{x}_{12} = x_8 - \frac{1}{4}\left(3\,v_{\xi 1} + v_{\xi 4} + \frac{(v_{\xi 2} - v_{\xi 3})\,t_f}{t_r}\right) \qquad \text{(A2.12)}$$

$$\dot{x}_{13} = x_9 - \frac{1}{4}\left(3\,v_{\xi 2} + v_{\xi 3} + \frac{(v_{\xi 1} - v_{\xi 4})\,t_r}{t_f}\right) \qquad \text{(A2.13)}$$

$$\dot{x}_{14} = x_{10} - \frac{1}{4}\left(3\,v_{\xi 3} + v_{\xi 2} - \frac{(v_{\xi 1} - v_{\xi 4})\,t_r}{t_f}\right) \qquad \text{(A2.14)}$$

These equations were obtained using a force-balance analysis and kinematic relations. In equations (A2.8) through (A2.11), the original variables x'_{12}, x'_{13}, x'_{14} and x'_{15} described in Table 4.2 have been substituted by the variables x_{12}, x_{13} and x_{14}, using equations (4.1) through (4.4). Equations (A2.8) through (A2.11) are simply derived using the vertical equilibrium of the four unsprung masses. Equations (A2.12) through (A2.14) are actually very simple kinematic relations that can also be written $\dot{x}'_{12} = x_8 - v_{\xi 1}$, $\dot{x}'_{13} = x_9 - v_{\xi 2}$, and $\dot{x}'_{14} = x_{10} - v_{\xi 3}$. The fifteenth equation, $\dot{x}'_{15} = x_{11} - v_{\xi 4}$, does not need to be included to fully describe the system because the deflection of the front right tire can be related to the deflection of the three other tires and the four suspension deflections, as shown by equations (4.1) through (4.4).

Appendix 3: System Matrix A and Disturbance Matrix L

The 14×14 system matrix A and of the he 14×8 disturbance matrix L are shown below for the hybrid configuration. Replacing α by 0 yields the matrices A and L for the ideal groundhook configuration. Replacing α by 1 yields the matrices A and for the ideal skyhook configuration. Replacing $C_{off,i}$ by $C_{S,i}$ and $(C_{on,i} - C_{off,i})$ by 0 (with $i = 1,\ 2,\ \ldots 4$) yields the matrices A and L for the passive system used in [2].

conoff1, conoff2, conoff3, and conoff4 represent $(C_{on1} - C_{off1})$, $(C_{on2} - C_{off2})$, $(C_{on3} - C_{off3})$, and $(C_{on4} - C_{off4})$ respectively.

The system matrix A is given by:

```
A = [a0101 a0102 a0103 a0104 a0105 a0106 a0107 a0108 a0109 a0110 a0111 a0112 a0113 a0114;
a0201 a0202 a0203 a0204 a0205 a0206 a0207 a0208 a0209 a0210 a0211 a0212 a0213 a0214;...
a0301 a0302 a0303 a0304 a0305 a0306 a0307 a0308 a0309 a0310 a0311 a0312 a0313 a0314;...
a0401 a0402 a0403 a0404 a0405 a0406 a0407 a0408 a0409 a0410 a0411 a0412 a0413 a0414;...
a0501 a0502 a0503 a0504 a0505 a0506 a0507 a0508 a0509 a0510 a0511 a0512 a0513 a0514;...
a0601 a0602 a0603 a0604 a0605 a0606 a0607 a0608 a0609 a0610 a0611 a0612 a0613 a0614;...
a0701 a0702 a0703 a0704 a0705 a0706 a0707 a0708 a0709 a0710 a0711 a0712 a0713 a0714;...
a0801 a0802 a0803 a0804 a0805 a0806 a0807 a0808 a0809 a0810 a0811 a0812 a0813 a0814;...
a0901 a0902 a0903 a0904 a0905 a0906 a0907 a0908 a0909 a0910 a0911 a0912 a0913 a0914;...
a1001 a1002 a1003 a1004 a1005 a1006 a1007 a1008 a1009 a1010 a1011 a1012 a1013 a1014;...
a1101 a1102 a1103 a1104 a1105 a1106 a1107 a1108 a1109 a1110 a1111 a1112 a1113 a1114;...
a1201 a1202 a1203 a1204 a1205 a1206 a1207 a1208 a1209 a1210 a1211 a1212 a1213 a1214;...
a1301 a1302 a1303 a1304 a1305 a1306 a1307 a1308 a1309 a1310 a1311 a1312 a1313 a1314;...
a1401 a1402 a1403 a1404 a1405 a1406 a1407 a1408 a1409 a1410 a1411 a1412 a1413 a1414];
```

with:

```
a0101 = -(coff1 + coff2 + coff3 + coff4 + conoff1*Alpha + conoff2*Alpha + conoff3*Alpha +
conoff4*Alpha)/ms ;
a0102 = (coff1*lf + coff4*lf - coff2*lr - coff3*lr + conoff1*lf*Alpha + conoff4*lf*Alpha -
conoff2*lr*Alpha - conoff3*lr*Alpha)/ms;
a0103 = (coff1*tf - coff4*tf + coff2*tr - coff3*tr + conoff1*tf*Alpha - conoff4*tf*Alpha +
conoff2*tr*Alpha - conoff3*tr*Alpha)/(2*ms);
a0104 = -ks1/ms;
a0105 = -ks2/ms;
a0106 = -ks3/ms;
a0107 = -ks4/ms;
```

```
a0108 = coff1/ms;
a0109 = coff2/ms;
a0110 = coff3/ms;
a0111 = coff4/ms;
a0112 = 0;
a0113 = 0;
a0114 = 0;
a0201 = (coff1*lf + coff4*lf - coff2*lr - coff3*lr + conoff1*lf*Alpha + conoff4*lf*Alpha -
conoff2*lr*Alpha - conoff3*lr*Alpha)/Iyy;
a0202 = -(coff1*lf^2 + coff4*lf^2 + coff2*lr^2 + coff3*lr^2 + conoff1*lf^2*Alpha + conoff4*lf^2*Alpha +
conoff2*lr^2*Alpha + conoff3*lr^2*Alpha)/Iyy;
a0203 = -(coff1*lf*tf - coff4*lf*tf - coff2*lr*tr + coff3*lr*tr + conoff1*lf*tf*Alpha - conoff4*lf*tf*Alpha -
conoff2*lr*tr*Alpha + conoff3*lr*tr*Alpha)/(2*Iyy);
a0204 = (ks1*lf)/Iyy;
a0205 = -(ks2*lr)/Iyy;
a0206 = -(ks3*lr)/Iyy;
a0207 = (ks4*lf)/Iyy;
a0208 =  -(coff1*lf)/Iyy;
a0209 = (coff2*lr)/Iyy;
a0210 = (coff3*lr)/Iyy;
a0211 = -(coff4*lf)/Iyy;
a0212 = 0;
a0213 = 0;
a0214 = 0;
a0301 = (coff1*tf - coff4*tf + coff2*tr - coff3*tr + conoff1*tf*Alpha - conoff4*tf*Alpha +
conoff2*tr*Alpha - conoff3*tr*Alpha)/(2*Ixx);
a0302 = -(coff1*lf*tf - coff4*lf*tf - coff2*lr*tr + coff3*lr*tr + conoff1*lf*tf*Alpha - conoff4*lf*tf*Alpha -
conoff2*lr*tr*Alpha + conoff3*lr*tr*Alpha)/(2*Ixx) ;
a0303 = -(coff1*tf^2 + coff4*tf^2 + coff2*tr^2 + coff3*tr^2 + conoff1*tf^2*Alpha + conoff4*tf^2*Alpha +
conoff2*tr^2*Alpha + conoff3*tr^2*Alpha)/(4*Ixx);
a0304 = (2*kf + ks1*tf^2)/(2*Ixx*tf);
a0305 = (2*kr + ks2*tr^2)/(2*Ixx*tr);
a0306 = -(2*kr + ks3*tr^2)/(2*Ixx*tr);
a0307 = -(2*kf + ks4*tf^2)/(2*Ixx*tf);
a0308 = -(coff1*tf)/(2*Ixx);
a0309 = -(coff2*tr)/(2*Ixx);
a0310 = (coff3*tr)/(2*Ixx);
a0311 = (coff4*tf)/(2*Ixx);
a0312 = 0;
a0313 = 0;
a0314 = 0;
a0401 = 1;
a0402 = -lf;
a0403 = -tf/2;
a0404 = 0;
a0405 = 0;
a0406 = 0;
a0407 = 0;
a0408 = -1;
a0409 = 0;
a0410 = 0;
a0411 = 0;
a0412 = 0;
a0413 = 0;
a0414 = 0;
a0501 = 1;
```

```
a0502 = lr;
a0503 = -tr/2;
a0504 = 0;
a0505 = 0;
a0506 = 0;
a0507 = 0;
a0508 = 0;
a0509 = -1;
a0510 = 0;
a0511 = 0;
a0512 = 0;
a0513 = 0;
a0514 = 0;
a0601 = 1;
a0602 = lr;
a0603 = tr/2;
a0604 = 0;
a0605 = 0;
a0606 = 0;
a0607 = 0;
a0608 = 0;
a0609 = 0;
a0610 = -1;
a0611 = 0;
a0612 = 0;
a0613 = 0;
a0614 = 0;
a0701 = 1;
a0702 = -lf;
a0703 = tf/2;
a0704 = 0;
a0705 = 0;
a0706 = 0;
a0707 = 0;
a0708 = 0;
a0709 = 0;
a0710 = 0;
a0711 = -1;
a0712 = 0;
a0713 = 0;
a0714 = 0;
a0801 = coff1/mu1;
a0802 = -(coff1*lf)/mu1 ;
a0803 = -(coff1*tf)/(2*mu1) ;
a0804 = (kf + ks1*tf^2)/(mu1*tf^2);
a0805 = 0;
a0806 = 0;
a0807 = -kf/(mu1*tf^2);
a0808 = -(coff1 + conoff1 + cu1 - conoff1*Alpha)/mu1 ;
a0809 = 0;
a0810 = 0;
a0811 = 0;
a0812 = -ku1/mu1;
a0813 = 0;
a0814 = 0;
a0901 = coff2/mu2;
```

```
a0902 = (coff2*lr)/mu2;
a0903 = -(coff2*tr)/(2*mu2);
a0904 = 0;
a0905 = (kr + ks2*tr^2)/(mu2*tr^2);
a0906 = -kr/(mu2*tr^2);
a0907 = 0;
a0908 = 0;
a0909 = -(coff2 + conoff2 + cu2 - conoff2*Alpha)/mu2 ;
a0910 = 0;
a0911 = 0;
a0912 = 0;
a0913 = -ku2/mu2;
a0914 = 0;
a1001 = coff3/mu3;
a1002 = (coff3*lr)/mu3;
a1003 = (coff3*tr)/(2*mu3);
a1004 = 0;
a1005 = - kr/(mu3*tr^2);
a1006 = (kr + ks3*tr^2)/(mu3*tr^2);
a1007 = 0;
a1008 = 0;
a1009 = 0;
a1010 = -(coff3 + conoff3 + cu3 - conoff3*Alpha)/mu3;
a1011 = 0;
a1012 = 0;
a1013 = 0;
a1014 = -ku3/mu3;
a1101 = coff4/mu4;
a1102 = -(coff4*lf)/mu4;
a1103 = (coff4*tf)/(2*mu4);
a1104 = -(kf + ku4*tf^2)/(mu4*tf^2) ;
a1105 = (ku4*tf)/(mu4*tr);
a1106 = -(ku4*tf)/(mu4*tr);
a1107 = (kf + ks4*tf^2 + ku4*tf^2)/(mu4*tf^2);
a1108 = 0;
a1109 = 0;
a1110 = 0;
a1111 = -(coff4 + conoff4 + cu4 - conoff4*Alpha)/mu4;
a1112 = -ku4/mu4;
a1113 = (ku4*tf)/(mu4*tr);
a1114 = -(ku4*tf)/(mu4*tr);
a1201 = 0; a1202 = 0; a1203 = 0; a1204 = 0; a1205 = 0; a1206 = 0; a1207 = 0;
a1208 = 1; a1209 = 0; a1210 = 0; a1211 = 0; a1212 = 0; a1213 = 0; a1214 = 0;
a1301 = 0; a1302 = 0; a1303 = 0; a1304 = 0; a1305 = 0; a1306 = 0; a1307 = 0;
a1308 = 0; a1309 = 1; a1310 = 0; a1311 = 0; a1312 = 0; a1313 = 0; a1314 = 0;
a1401 = 0; a1402 = 0; a1403 = 0; a1404 = 0; a1405 = 0; a1406 = 0; a1407 = 0;
a1408 = 0; a1409 = 0; a1410 = 1; a1411 = 0; a1412 = 0; a1413 = 0; a1414 = 0;
```

The disturbance matrix L is given by:

```
L = [L0101 L0102 L0103 L0104 L0105 L0106 L0107 L0108;
L0201 L0202 L0203 L0204 L0205 L0206 L0207 L0208;...
L0301 L0302 L0303 L0304 L0305 L0306 L0307 L0308;...
L0401 L0402 L0403 L0404 L0405 L0406 L0407 L0408;...
L0501 L0502 L0503 L0504 L0505 L0506 L0507 L0508;...
L0601 L0602 L0603 L0604 L0605 L0606 L0607 L0608;...
L0701 L0702 L0703 L0704 L0705 L0706 L0707 L0708;...
L0801 L0802 L0803 L0804 L0805 L0806 L0807 L0808;...
L0901 L0902 L0903 L0904 L0905 L0906 L0907 L0908;...
L1001 L1002 L1003 L1004 L1005 L1006 L1007 L1008;...
L1101 L1102 L1103 L1104 L1105 L1106 L1107 L1108;...
L1201 L1202 L1203 L1204 L1205 L1206 L1207 L1208;...
L1301 L1302 L1303 L1304 L1305 L1306 L1307 L1308;...
L1401 L1402 L1403 L1404 L1405 L1406 L1407 L1408];
```

with:

```
L0101 = 0; L0102 = 0; L0103 = 0; L0104 = 0; L0105 = 0; L0106 = 0; L0107 = 0; L0108 = 0;
L0201 = 0; L0202 = 0; L0203 = 0; L0204 = 0; L0205 = 0; L0206 = 0; L0207 = 0; L0208 = 0;
L0301 = 0; L0302 = 0; L0303 = 0; L0304 = 0; L0305 = 0; L0306 = 0; L0307 = 0; L0308 = 0;
L0401 = 0; L0402 = 0; L0403 = 0; L0404 = 0; L0405 = 0; L0406 = 0; L0407 = 0; L0408 = 0;
L0501 = 0; L0502 = 0; L0503 = 0; L0504 = 0; L0505 = 0; L0506 = 0; L0507 = 0; L0508 = 0;
L0601 = 0; L0602 = 0; L0603 = 0; L0604 = 0; L0605 = 0; L0606 = 0; L0607 = 0; L0608 = 0;
L0701 = 0; L0702 = 0; L0703 = 0; L0704 = 0; L0705 = 0; L0706 = 0; L0707 = 0; L0708 = 0;
L0801 = ku1/(4*mu1);
L0802 = -(ku1*tf)/(4*mu1*tr);
L0803 = (ku1*tf)/(4*mu1*tr);
L0804 = -ku1/(4*mu1);
L0805 = cu1/mu1;
L0806 = 0;
L0807 = 0;
L0808 = 0;
L0901 = -(ku2*tr)/(4*mu2*tf);
L0902 = ku2/(4*mu2);
L0903 = -ku2/(4*mu2);
L0904 = (ku2*tr)/(4*mu2*tf);
L0905 = 0;
L0906 = cu2/mu2;
L0907 = 0;
L0908 = 0;
L1001 = (ku3*tr)/(4*mu3*tf);
L1002 = -ku3/(4*mu3);
L1003 = ku3/(4*mu3);
L1004 = -(ku3*tr)/(4*mu3*tf);
L1005 = 0;
L1006 = 0;
L1007 = cu3/mu3;
L1008 = 0;
L1101 = -ku4/(4*mu4);
L1102 = (ku4*tf)/(4*mu4*tr);
L1103 = -(ku4*tf)/(4*mu4*tr);
L1104 = ku4/(4*mu4);
```

```
L1105 = 0;
L1106 = 0;
L1107 = 0;
L1108 = cu4/mu4;
L1201 = 0;
L1202 = 0;
L1203 = 0;
L1204 = 0;
L1205 = -3/4;
L1206 = -tf/(4*tr);
L1207 = tf/(4*tr);
L1208 = -1/4;
L1301 = 0;
L1302 = 0;
L1303 = 0;
L1304 = 0;
L1305 = -tr/(4*tf);
L1306 = -3/4;
L1307 = -1/4;
L1308 = tr/(4*tf);
L1401 = 0;
L1402 = 0;
L1403 = 0;
L1404 = 0;
L1405 = tr/(4*tf);
L1406 = -1/4;
L1407 = -3/4;
L1408 = -tr/(4*tf);
```

References

1. Chalasani, R.M., “Ride Performance Potential of Active Suspension Systems - Part I: Simplified Analysis Based on a Quarter-Car Model,” *ASME Symposium on Simulation and Control of Ground Vehicles and Transportation Systems*, AMD-vol. 80, DSC-vol. 2, pp. 187-204, 1986.

2. Chalasani, R.M., “Ride Performance Potential of Active Suspension Systems-Part II: Comprehensive Analysis Based on a Full-Car Model,” *ASME Symposium on Simulation and Control of Ground Vehicles and Transportation Systems*, AMD-vol. 80, DSC-vol. 2, pp. 205-234, 1986.

3. Crosby, M. J., Karnopp, D. C., “The Active Damper,” The Shock and Vibrations Bulletin 43, Naval Research Laboratory, Washington, DC, 1973.

4. Karnopp, D. C., Crosby, M. J., “System for Controlling the Transmission of Energy Between Spaced Members,” U.S. Patent 3,807,678.

5. Miller, L. R., "An Introduction to Semiactive Suspension Systems," *Lord Library of Technical Articles*, Document LL-1204, 1986.

6. Karnopp, D., "Active and Semiactive Vibration Isolation," *Journal of Vibrations and Acoustics*, vol. 117, No. 3B, pp. 177-185, June 1995.

7. Ahmadian, M., "A Hybrid Semiactive Control for Secondary Suspension Applications," *Proceedings of the Sixth ASME Symposium on Advanced Automotive Technologies*, 1997 ASME International Congress and Exposition, November 1997.

8. Ahmadian, M., "On the Isolation Properties of Semiactive Dampers" *Journal of Vibrations and Control*, vol. 5, pp. 217-232, 1999.

9. Asami, T., Nishihara, O., "H_2 Optimization to Semiactive of the Three-Element Type Dynamic Vibration Absorbers," *Journal of Vibration and Acoustics*, vol. 124, No. 4, pp. 583-592, October 2002.

10. Griffin, M.J., *Handbook of Human Vibrations*, Academic Press, New York, 1996.

11. Ikenaga, S., Lewis, F. L., Campos, J., Davis, L., "Active Suspension Control of Ground Vehicle Based on Full-Vehicle Model," *Proceedings of the 2000 IEEE American Control Conference*, vol. 6, Piscataway, NJ, pp. 4019-4024, 2000.

12. Ahmadian, M., Pare, C A., "A Quarter-Car Experimental Analysis of Alternative Semiactive Control Methods," *Journal of Intelligent Material Systems & Structures,* vol. 11, No. 8, pp. 604-612, August 2001.

13. Lieh, J., Li, W. J., "Adaptive Fuzzy Control of Vehicle Semi-Active Suspensions," *ASME Dynamic Systems and Control Division, DSC*, vol. 61, Fairfield, NJ, pp. 293-297, 1997.

14. Jalili, N., "A Comparative Study and Analyis of Semi-Active Vibration-Control Systems," *Journal of Vibration and Acoustics*, vol. 124, pp. 593-605, October 2002.

15. Asami, T., Nishihara, O., Baz, A. M., "Analytical Solution to H_∞ and H_2 Optimization of Dynamic Vibration Absorbers Attached to Damped Linear Systems," *Journal of Vibration and Acoustics*, vol. 124, No. 2, pp. 284-295, April 2002.

16. Jeong, S. G., Kim, I. S., Yoon, K. S., Lee, J. N., Bae, J. I., Lee, M. H., "Robust H_∞ Controller Design for Performance Improvement of a Semi-Active Suspension System," *IEEE International Symposium on Industrial Electronics,* vol. 2, pp. 706-709, 2000.

17. Ohsaku, S., Nakayama, T., Kamimura, I.., Motozono, Y., "Nonlinear H infinity Control for Semi-Active Suspension," *Japanese society of Automotive Engineers,* vol. 20, No. 4, pp. 447-452, 1999.

18. Haddad, W. M., Razavi, A., "H2, Mixed H2/H infinity and H2/L1 Optimally Tuned Passive Isolators and Absorbers," *Proceedings of the 1997 IEEE American Control Conference*, vol. 5, Piscataway, NJ, pp. 3120-3124, 1997.

Vita

Emmanuel D. Blanchard joined the Advanced Vehicle Dynamics Lab (AVDL) of Virginia Tech in the fall of 2001 to pursue his interest in controls and dynamics. After completing his M.S. in Mechanical Engineering in the summer of 2003, he will move to Columbus, IN to work for Cummins, Inc. as a systems / controls engineer.